

**CLONING, EXPRESSION and PURIFICATION of DURUM WHEAT
METALLOTHIONEIN DOMAINS**

and

STRUCTURAL MODELLING

By

FILIZ KISAAYAK COLLAK

Submitted to the Graduate School of Engineering and Natural Sciences
in partial fulfillment of
the requirements for the degree of
Doctor of Philosophy

Sabanci University
January 2009

CLONING, EXPRESSION and PURIFICATION of DURUM WHEAT
METALLOTHIONEIN DOMAINS and STRUCTURAL MODELLING

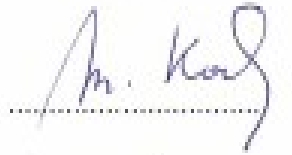
APPROVED BY:

Prof. Dr. Zehra Sayers Gökhan

(Dissertation Supervisor)



Prof. Dr. Michel Koch



Prof. Dr. Ahmet Koman



Prof. Dr. Selim Çetiner



Assoc. Prof. Dr. Uğur Sezerman



DATE OF APPROVAL:

21.01.2009

© FILIZ KISAAYAK COLLAK 2009

All rights reserved.

CLONING, EXPRESSION and PURIFICATION of DURUM WHEAT METALLOTHIONEIN DOMAINS and STRUCTURAL MODELLING

Filiz KISAAYAK COLLAK

Ph.D. Thesis, 2009

Thesis supervisor, Prof. Dr. Zehra SAYERS

Key words: Durum wheat metallothionein, domains, Cd, SAXS

ABSTRACT

Metallothioneins (MTs) are small proteins with high cysteine content and high binding capacity for metals including Zn, Cu and Cd. They exist in a wide range of organisms and are classified in one super-family according to the distribution of cysteine motifs in their sequences. Type I plant MTs, similar to mammalian MTs, have the cysteine motifs clustered in the N- and C-termini constituting the β - and α -domains, respectively. In type I plant MTs the two domains are connected by a long (about 42 amino acids) hinge region whose structural and functional properties are unclear.

A *mt* gene in Cd resistant durum wheat coding for a type I MT (dMT) was identified and the recombinant protein (dMT) was overexpressed in *E. coli* as GST fusion (GSTdMT) (Bilecen *et al.*, 2005). In the present study, for detailed structural investigations; GST-fusion constructs of β -hinge, α -hinge and the isolated hinge domains of dMT were overexpressed in *E. coli*. Proteins were purified and were characterized by size exclusion chromatography, SDS- and native-PAGE, limited trypsinolysis, inductively coupled plasma optical emission spectroscopy (ICP-OES), UV-vis absorption spectroscopy, dynamic light scattering (DLS) and small-angle solution X-ray scattering (SAXS).

GSTdMT fusion constructs were purified as stable dimeric forms in solution. Cd^{2+} /protein ratio were found to be 1.53 ± 0.6 for GST β -hingedMT and 1.5 ± 0.8 for GST α -hingedMT. GSThingedMT and GST α -hingedMT were easily cleaved from the hinge region confirming its susceptibility to proteolytic attack. Hinge region in the GST β -hingedMT construct, on the other hand, was protected. Cleavage was not observed in the constructs within the β - and α -domains which strongly indicated their compact structure with the bound Cd^{2+} ions.

SAXS measurement results indicated that GSThingedMT, GST β -hingedMT and GST α -hingedMT have symmetric, elongated shapes. *ab initio* models revealed structures with GST molecules forming electron dense regions at the center of mass and the partner dMT domains extending from this region. Evidence from Cd-binding, tryptic cleavage and SAXS models suggest that hingedMT, β -hingedMT and α -hingedMT structures fold independently of GST in the fusion constructs. The combination of SAXS results with biochemical data indicated extended structures for the dMT domains and supports the dumbbell model previously proposed for durum wheat MT (Bilecen *et al.*, 2005).

DURUM BUĞDAYI METALLOTİONİN BÖLGELERİNİN KLONLANMASI, SENTEZLETTİRİLMESİ, SAFLAŞTIRILMASI VE YAPISAL MODELLENMESİ

Filiz KISAAYAK COLLAK

Ph.D. Thesis, 2009

Tez danışmanı, Prof. Dr. Zehra SAYERS

Anahtar kelimeler: Durum buğdayı metallothioneini, bölgeler, Cd, SAXS

ÖZET

Metallothioneinler (MT'ler), küçük molekül ağırlıklı, sistince zengin, Zn, Cu ve Cd gibi metallere yüksek bağlanma kapasitesi olan proteinlerdir. MT'ler hemen hemen bütün organizmalarda bulunurlar ve amino acid dizilimlerindeki sistin motiflerinin dağılımına göre tek bir süper familya içerisinde sınıflandırılırlar. Tip I bitki MT'leri, memeli MT'lerine benzer bir şekilde, N- ve C- uçlarında sistin motifleri içerirler ve bu bölgeler β - ve α - bölgeleri olarak adlandırılır. Tip I bitki MT'lerinde, β - ve α - bölgeleri uzun (yaklaşık 42 amino asit) bir köprü bölgesi ile bağlanırlar. Köprü bölgesinin yapısal ve işlevsel özellikleri henüz açıklık kazanmamıştır.

Cd'a dirençli durum buğdayında Tip I bitki MT geni tesbit edilmiş ve *E.coli* bakterisinde GST füzyon proteini (GSTdMT) şeklinde sentezlettirilmiştir (Bilecen, 2005). Bu tezdeki çalışmada, detaylı yapısal ve işlevsel incelemeler yapmak amacıyla, dMT'nin β - köprü, α -köprü ve köprü bölgeleri ayrı ayrı GST füzyon proteini olarak *E.coli*'de sentezlettirilmiştir. Proteinler saflaştırılmış ve özellikleri moleküler elek kromatografisi (SEC), SDS ve natif PAGE, tiripsin ile limitli kırılma, UV-vis absorpsiyon spektrofotometresi, ICP-OES spektrofotometresi, dinamik ışık saçılması (DLS) ve X-ışınları küçük açı saçılma (SAXS) yöntemleri kullanılarak incelenmiştir.

Proteinler çözeltide dimer halinde bulunmaktadır. Cd²⁺ bağlanma oranı GST β -hingedMT için 1.53 ± 0.6 ve GST α -hingedMT için 1.5 ± 0.8 olarak hesaplanmıştır. Tiripsin ile kırılma çalışmaları GSTköprüdMT ve GST α -köprüdMT proteinlerinin köprü bölgesinden kesildiğini göstermiştir. Bu durum köprü bölgesinin proteolitik hücumlara hassas olduğunu kanıtlamaktadır. GST β -köprüdMT and GST α -köprüdMT proteinlerinde tiripsinle kırılma β - ve α - bölgeleri içinde görülmemektedir ki bu da bu bölgerin bağladıkları Cd²⁺ ile katlanarak kapalı bir yapıya sahip olduklarını göstermektedir. .

SAXS ölçümleri GSTköprüdMT, GST β -köprüdMT ve GST α -köprüdMT'nin uzun simetrik şekle sahip olduklarını göstermiştir. *ab initio* modelleri merkezde GST dimerinin oluşturduğu bir elektron yoğun bölge ve bu bölgeden iki ayrı yönde uzanan köprüdMT, β -köprüdMT ve α -köprüdMT moleküllerinden oluşan bir yapı göstermektedir. Cd bağlama özellikleri, tiriptik kırılma analizi sonuçları ve SAXS sonuçları köprüdMT, β -köprüdMT ve α -köprüdMT yapılarının GST'den bağımsız oluştuğuna işaret etmektedir. SAXS sonuçları ve biyokimya verileri dMT bölgeleri için uzun bir yapı vermekte ve sonuçlar dMT yapısının daha önce önerilen (Bilecen, 2005) halter benzeri bir şekle sahip olduğunu desteklemektedir.

To my family,

For their limitless support and love...

ACKNOWLEDGEMENTS

The support of many people were crucial for my achievements in the graduate program at Sabanci University. Without their help, I would not have completed it.

I was very lucky to have Prof. Dr. Zehra Sayers as my research advisor. She is an excellent mentor with guidance and support as well as a perfect teacher with a unique way of scientific thinking. Faculty members at Biological Sciences and Bioengineering Program, namely Prof. Dr. Selim Cetiner, Assist. Prof. Drs. Ugur Sezerman and Hikmet Budak were always supportive during my graduate studies, whom I dearly appreciate. I am grateful to Assist. Prof. Dr. Alpay Taralp for reshaping my thinking of protein chemistry. Kind patience and guidance of Prof. Dr. Ahmet Koman of Bogazici University was invaluable. Prof. Dr. Michel Koch provided valuable comments on written part of thesis, particularly on discussion points.

I received generous help from Veli Bayir during the analyses of samples with ICP-OES. Filiz Yesilirmak is a best friend beyond being a co-worker in the lab. She was always there when help needed without hesitation. Gizem Dinler provided support and expertise in a variety of forms. My lab mates Onur, Burcu and Ceren collaborated throughout my research. My friends Damla, Neslihan, Ozge, Zeynep, Ceyda, Bahar, Gozde always shared hard times and fun times throughout my presence at Sabanci University.

My parents believed in my decions and provided invaluable support and love. Other members of my family, especially my husband, anxiously awaited completion of my studies.

Many thanks to you all of you.

Filiz K1saayak Collak
Istanbul, January 2009

TABLE OF CONTENTS

1. INTRODUCTION.....	1
2. OVERVIEW	4
2.1 Metallothioneins (MTs)	4
2.2 Plant MTs.....	9
2.2.1 Classification of Plant MTs	10
2.2.2 Function of plant MTs	13
2.2.3 Structure and Metal Binding Properties of plant MTs.....	14
2.3 Vertebrate and Invertebrate MTs	17
2.3.1 Structure and Metal Binding Properties of Vertebrate and Invertebrate MTs.....	17
2.3.2 Structure and Metal Binding Properties of Vertebrate β - and α -domains	21
3. MATERIALS and METHODS.....	23
3.1 MATERIALS.....	23
3.1.1 Chemicals	23
3.1.2 Primers.....	23
3.1.3 Enzymes.....	24
3.1.4 Vectors.....	24
3.1.5 Cells	24
3.1.6 Buffers and Solutions	24
3.1.7 Commercial Kits.....	25
3.1.8 Culture Media	25
3.1.8.1 Liquid medium	25
3.1.8.2 Solid medium.....	25
3.1.9 Equipments	25
3.2 METHODS	25
3.2.1 Nucleic acid methods.....	25
3.2.1.1 PCR.....	26
3.2.1.2 Subcloning of hdMT	26
3.2.1.3 Ligation.....	27
3.2.1.4 Transformation	27
3.2.1.5 Colony selection	27
3.2.1.6 Plasmid isolation.....	27
3.2.1.7 Restriction enzyme analysis	28
3.2.1.8 Sequence verification	28
3.2.1.9 Cloning into expression vector	28

3.2.2	Protein expression.....	29
3.2.2.1	Monitoring expression of the recombinant fusion proteins.....	29
3.2.2.2	Culture growth for purification.....	29
3.2.3	Purification and analysis.....	30
3.2.3.1	Affinity Chromatography	30
3.2.3.2	Size exclusion chromatography.....	31
3.2.4	SDS polyacrylamide gel electrophoresis (PAGE).....	31
3.2.5	Native polyacrylamide gel electrophoresis (PAGE).....	31
3.2.6	Coomassie blue staining.....	32
3.2.7	Western blotting.....	32
3.2.8	Thrombin cleavage	32
3.2.8.1	Small scale cleavage.....	32
3.2.8.2	Large scale cleavage and purification of the cleaved protein.....	33
3.2.9	Protein concentration determination.....	34
3.2.10	Dynamic light scattering.....	34
3.2.11	Limited proteolytic cleavage with trypsin	35
3.2.12	Small angle X-ray scattering (SAXS).....	35
3.2.13	Inductively coupled plasma optical emission spectroscopy (ICP-OES).....	37
4.	RESULTS	38
4.1	Cloning of constructs for domains of dMT.....	38
4.1.1	Amplification of hinge dMT, β -hinge dMT and α -hinge dMT cDNAs.....	38
4.1.3	Cloning of β hdMT and α hdMT	41
4.2	Expression of the recombinant GSThdMT, GST β hdMT and GST α hdMT in E. coli.....	42
4.2.1	Monitoring growth of transformed E. coli cells.....	42
4.2.2	Monitoring expression of the recombinant fusion proteins	45
4.3	Purification of recombinant GSThdMT, GST β hdMT and GST α hdMT	47
4.3.1	Affinity Chromatography	49
4.3.2	Size Exclusion Chromatography	51
4.3.2.1	Purification of GSThdMT by size exclusion chromatography.....	51
4.3.2.1.1	Optimization of the expression conditions for GSThdMT.....	53
4.3.2.1.2	Determination of storage conditions for GSThdMT	54
4.3.2.1.3	Western blot analysis of GSThdMT	60
4.3.2.1.4	Thrombin cleavage of GSThdMT.....	61
4.3.2.2	Purification of GST β hdMT and GST α hdMT by size exclusion chromatography	63
4.3.2.2.1	Optimization of expression condition for GST α hdMT.....	66

4.4 Determination of Cd ²⁺ /Protein ratio for GSTβhdMT and GSTαhdMT	67
4.5 UV-Vis Spectrophotometric Characterization of GSTβhdMT and GSTαhdMT	72
4.6 Structural Analysis of GST and GSTdMT constructs.....	73
4.6.1 Native Gel Analysis of GST and GSTdMT constructs.....	73
4.6.2 Structural Characterization of GSTdMT constructs by limited proteolytic cleavage.	73
4.6.3 Structural Characterization of GSTdMT constructs using SAXS	76
5. DISCUSSION	97
5.1 Cloning, Expression and Purification of dMT constructs	97
5.2 Biophysical Characterization of GSTdMT constructs	102
5.3 Structural Analysis of GSTdMT constructs.....	103
6. CONCLUSION	108
7. REFERENCES.....	111
APPENDIX A	125
APPENDIX B	127
APPENDIX C	128
APPENDIX D	129

ABBREVIATIONS

Ag	Silver
Al	Aluminium
Ar	Argon
As	Arsenic
Au	Gold
Bi	Bismuth
bp	Base pair
BSA	Bovine serum albumin
Cd	Cadmium
CD	Circular dichroism
cDNA	Complementary DNA
Co	Cobalt
Cu	Copper
Cys	Cystein
DLS	Dynamic light scattering
dMT	Durum wheat metallothionein
dNTP	Deoxyribonucleotide triphosphate
DTT	Dithiothreitol
EtBr	Ethidium bromide
ESI-MS	electrospray ionization mass spectrometry
Fe	Iron
FPLC	Fast perfusion liquid chromatography
GST	Glutathione S-transferase
GSTαhdMT	Glutathione S transferase alpha hinge durum wheat metallothionein
GSTβhdMT	Glutathione S transferase beta hinge durum wheat metallothionein
GSTdMT	Glutathione S transferase durum wheat metallothionein
GSThdMT	Glutathione S transferase hinge durum wheat metallothionein
HEPES	4-(2-hydroxyethyl)-1-piperazineethanesulfonicacid
Hg	Mercury

Hmw	High molecular weight
ICP-OES	Inductively coupled plasma optical emission spectroscopy
IPTG	Isopropyl- β -D-thiogalactoside
$I(0)$	Forward scattering
kDa	Kilodalton
Lmw	Low molecular weight
Lys	Lysine
Mg	Milligram
ml	Milliliter
μl	Micro liter
Ni	Nickel
nm	Nanometer
PBS	Phosphate Buffered Saline
PCR	Polymerase chain reaction
PMSF	Phenylmethanesulphonylfluoride
$P(r)$	Distance distribution function
Pt	Platinum
Rg	Radius of gyration
SAXS	Small angle X-ray scattering
α	Alfa
β	Beta
Zn	Zinc

LIST OF FIGURES

Figure 2.1:	Amino acid sequences, spacer region length and Cys-motifs in different types of plant MTs.	10
Figure 2.2:	(A) Schematic representation of the dumbbell model (B) Predicted structure of dMT.	15
Figure 2.3:	(A) Schematic representation of hairpin structure of MTs (B) Proposed hairpin structure for pea MT, PsMT _A	16
Figure 2.4:	Schematic representation of mammalian MT-2 with its N- and C-terminal with 20 cysteines (blue squares) and with S- atoms.	18
Figure 2.5:	Molecular mode structure of Cd ₇ -mammalian MT with the N terminal β-domain on the left and the C terminal α-domain on the right (A) Space filling (B) Ball and stick representation with the domains in space filling form.	18
Figure 2.6:	Ribbon presentation of NMR solution structure of NcMT.	20
Figure 2.7:	Comparison of the X-ray crystal structure of Cu ₈ -MT (cyan) with Ag ₇ -MT NMR model (green) (Peterson <i>et al.</i> , 1996) (A) and Cu ₇ -MT NMR model (red) (Bertini <i>et al.</i> , 2000) (B).	21
Figure 4.1:	2 % Agarose gel analysis of PCR amplified domains of dMT.	38
Figure 4.2:	cDNA and amino acid sequences of GSTdMT constructs. (A) hdMT (B) βhdMT and (C) αhdMT.	39
Figure 4.3:	2% Agarose gel analysis of double digested pGEM®-T Easy hdMT construct.	40
Figure 4.4:	1.5% Agarose gel analysis of PCR from pGEXhdMT construct positive colony.	41
Figure 4.5:	2% Agarose gel analysis of (A) colony PCR (B) double digestion of pGEXβhdMT constructs.	42
Figure 4.6:	2% Agarose gel analysis of (A) colony PCR (B) double digestion of pGEXαhdMT constructs.	42
Figure 4.7:	Growth curves of 0.75 mM IPTG induced BL21(DE3) bacterial cells containing (A) pGEXhdMT (B) pGEXβhdMT and (C) pGEXαhdMT.	43
Figure 4.8:	Growth curves of noninduced BL21(DE3).	44
Figure 4.9:	Growth curves of induced BLβhdMT and BLαhdMT grown in the	45

	presence of 0.1 mM CdCl ₂ .	
Figure 4.10:	Time course of expression of (A) GSThdmt (B) GST monitored by 12 % SDS PAGE analysis.	46
Figure 4.11:	Expression of (A) GSTβhdMT (B) GSTαhdMT analyzed by 12 % SDS PAGE.	46
Figure 4.12:	Schematic representation of the purification procedure of recombinant proteins.	48
Figure 4.13:	Elution profiles of (A)GSThdMT (B)GSTβhdMT and (C)GSTαhdMT from GSTrap® FF affinity column.	49
Figure 4.14:	12% SDS PAGE analysis of purified samples of (A) GSThdMT (B) GSTβhdMT (C) GSTαhdMT.	50
Figure 4.15:	Native-PAGE analysis of (A) GSThdMT (B) GSTβhdMT (C) GSTαhdMT purified from GST affinity column.	51
Figure 4.16:	Elution profile of GSThdMT from Hiload™ 16/60 Superdex™ 75 gel filtration column.	52
Figure 4.17:	SDS-PAGE analysis of fractions from purification of GSThdMT.	52
Figure 4.18:	Native-PAGE analysis of fractions after purification of GSThdMT.	53
Figure 4.19:	Size distribution by intensity DLS measurements of GSThdMT eluted from size exclusion chromatography.	53
Figure 4.20:	12% SDS PAGE analysis of GSThdMT fractions stored for (A) two days (B) five days at different temperatures and with/without additives.	55
Figure 4.21:	8% Native PAGE analysis of GSThdMT fractions stored for (A) two days (B) five days at different temperatures and with/without additives.	56
Figure 4.22:	Size distribution by intensity profile of GSThdMT (A) without additive (B) with 50% glycerol (C) with 0.5 mM PMSF stored at 4 °C for two days.	57
Figure 4.23:	Size distribution by intensity profile of GSThdMT (A) without additive (B) with 50% glycerol (C) with 0.5 mM PMSF stored at -20 °C for two days.	58
Figure 4.24:	Size distribution by intensity profile of GSThdMT (A) without additive (B) with 50% glycerol (C) with 0.5 mM PMSF stored at -80 °C for two days.	59
Figure	Western blot analysis of GSThdMT fractions eluted from Sephadex	60

4.25:	G-75 16/60 column.	
Figure 4.26:	16% Tris-tricine PAGE analysis of thrombin cleavage of GSThdMT.	61
Figure 4.27:	Elution profile of cleaved GSThdMT on Hiload TM 16/60 Superdex TM 75 gel filtration column.	62
Figure 4.28:	16% Tris-tricine PAGE analysis of GSThdMT thrombin cleavage products.	62
Figure 4.29:	Elution profiles of GSTβhdMT (A) 11 mg and (B) 8.25 mg loaded to Hiload TM 16/60 Superdex TM 75 gel filtration column.	63
Figure 4.30:	Elution profiles of GSTαhdMTt (A) 11 mg and (B) 8 mg loaded to Hiload TM 16/60 Superdex TM 75 gel filtration column.	64
Figure 4.31:	SDS-PAGE analysis of purified fractions of GSTdMT constructs. (A) GSTβhdMT and (B) GSTαhdMT.	65
Figure 4.32:	Native-PAGE analysis of fractions of purified GSTdMT constructs. (A) GSTβhdMT and (B) GSTαhdMT.	65
Figure 4.33:	Size distribution by intensity DLS measurements of GSTdMT constructs.	66
Figure 4.34:	Dynamic light scattering (DLS) measurements of purified GSTαhdMT.	67
Figure 4.35:	Absorbance spectrum of GSTβhdMT (○) GSTαhdMT (●) and GSThdMT (▼).	72
Figure 4.36:	8% Native page gel analysis of GSTdMT constructs.	73
Figure 4.37:	dMT amino acid sequence.	74
Figure 4.38:	14 % Tris-tricine PAGE analysis of GSThdMT and GST.	74
Figure 4.39:	16 % Tris tricine PAGE analysis of GSTβhdMT and GST.	75
Figure 4.40:	14 % Tris tricine PAGE analysis of GSTαhdMT.	75
Figure 4.41:	SAXS curves of GST and GSTdMT constructs.	76
Figure 4.42:	Superposition of scattering curves of GST and GSThdMT in the range $0 < s < 1.5 \text{ (nm}^{-1}\text{)}$.	78

Figure 4.43:	Superposition of the scattering curves of GST and GSTdMT constructs in the range $0 < s < 1.0$ (nm^{-1}).	79
Figure 4.44:	Guinier plots for GST and GSTdMT constructs.	80
Figure 4.45:	Correlation between R_g and GSTdMT constructs.	83
Figure 4.46:	Analysis of SAXS data using GNOM algorithm.	85
Figure 4.47:	Shape models for GSThdMT, GST β hdMT and GST α hdMT with P1 symmetry; (A1), (B1) and (C1) and with P2 symmetry; (A2), (B2) and (C2) developed by DAMMIF.	90
Figure 4.48:	Shape models (DAMFILT) for (A1) GSThdMT, (B1) GST β hdMT and (C1) GST α hdMT developed by DAMMIF with P2 symmetry, prolate and across.	92
Figure 4.49:	Shape models for (A) GSThdMT (B) GST β hdMT (C) GST α hdMT developed by BUNCH.	95
Figure 5.1:	Superposition of GST model with (A) GSThdMT (B) GST β hdMT (C) GST α hdMT ab initio shape models.	105

LIST OF TABLES

Table 2.1:	Metallothionein families and subfamilies.	5
Table 2.2:	Amino acid sequences of different MTs.	8
Table 2.3:	Four types of plant MTs.	12
Table 2.4:	Amino acid sequences of rat MT2 and sea urchin MTA.	19
Table 3.1:	Primers used in the PCR amplification of GSTdMT constructs.	24
Table 3.2:	PCR conditions used for amplification of hdMT, β hdMT and α hdMT	26
Table 4.1:	ICP-OES results of samples with known concentrations.	69
Table 4.2:	Cd/Protein binding ratio for (A) GST β hdMT and (B) GST α hdMT.	71
Table 4.3:	Structural parameters of GSTdMT and mutants calculated from SAXS measurements.	82

Chapter 1

1. INTRODUCTION

Metallothioneins (MTs) are low molecular weight (6-10 kDa), cysteine (Cys) rich proteins that are synthesized almost ubiquitously in fungi, plant and animal species. MTs have the ability to bind a series of transition IB and IIB metals via the thiol groups of their Cys-residues (Hamer, 1986, Kägi and Kojima, 1987, Vasak and Hasler, 2000). Although, they were previously grouped into three classes according to their primary structure similarities with mammalian counterparts, latest classification based on the distribution of Cys residues and phylogenetic relationships resulted in the identification of 15 families with several subfamilies (Binz and Kägi, 1999). Plant MTs belong to Family 15 and have been further classified into four subtypes according to the type and distribution of Cys-motifs in their amino acid sequences (Fowler *et al.*, 1987, Binz and Kägi, 1999, Cobett and Goldsbrough, 2002).

The precise physiological roles of MTs have not yet been established. In the light of the metal binding properties, heavy metal detoxification (cadmium and mercury) and involvement in the homeostasis of essential metals (zinc and copper) have been proposed for mammalian MTs. Free radical scavenging, protection against reactive oxygen species (ROS), adaptation to stress and antiapoptotic effects are some of the other proposed functions of mammalian MTs (Vasak, 2005). Plant MTs are thought to function in micronutrient homeostasis, heavy metal detoxification, senescence, protection against oxidative stress and developmental mechanisms (Zhou *et al.*, 2005, Akashi *et al.*, 2004, Navabpour *et al.*, 2003, Ledger and Gardner, 1994).

Some types of mammalian and plant MTs are clustered into two domains by the distribution of Cys motifs at their N- and C-termini, which are referred as β - and α -domains, respectively. The spacer region connecting N- and C- termini, which is devoid of Cys, has 2 to 4 amino acids in mammalian MTs whereas, in plants, it consists 30-50 amino acids (Cobbett and Goldsbrough, 2002, Rauser, 1999). Also, for fungi and yeast, single domain, MTs are observed (Peterson *et al.*, 1996).

MTs have been studied for decades after their first discovery in horse kidney (Margoshes and Vallee, 1957), and extensive structural information has been established for mammalian, yeast and fungus MTs. Despite the fact that the X-ray structure of native rat liver Cd₅-Zn₂-MT2 (Robbins *et al.*, 1991), *S. cerevisia* Cu₈-MT (Calderone *et al.*, 2005) and NMR structures of rabbit, rat and human liver Cd₇-MT2 (Arseniev *et al.*, 1988, Schultze *et al.*, 1988, Messerle *et al.*, 1990), recombinant mouse Cd₇-MT1 (Zangger *et al.*, 1999) and fungus Cu₆-NcMT (Cobine *et al.*, 2004) are available, structural information on plant MTs are limited in literature. Structural investigations on plant MTs led to two types of models: The first model was derived as a dumbbell shape for type III and type I MTs (Zhu *et al.*, 2000; Bilecen *et al.*, 2005) and the other model represents all types of plant MTs as a hairpin structure (Kille *et al.*, 1991, Domenech *et al.*, 2005, Freisinger, 2007, Peroza and Freisinger, 2007). Direct experimental data for the structure of a plant MT (NMR and/or X-ray crystallography) is still lacking in the literature. It is known that high β -sheet percentage in the secondary structure of MTs is quite rare (Vasak and Kagi, 1994). Yet in a recent study, high β -sheet percentage in the secondary structure of a plant MT was reported based on the Raman and IR spectroscopy of the Zn- and Cd- bound holo type II protein (Domenech *et al.*, 2007).

In a study by Bilecen *et al.* (2005), a novel Cd-binding MT has been identified in durum wheat (dMT). It has been cloned and over-expressed in *E.coli* as a glutathione-S-transferase and the fusion protein was purified to homogeneity (Yeşilirmak, 2008, Bilecen *et al.*, 2005). dMT is classified as a type I plant MT which comprises two Cys-rich N- and C-terminal regions (β - and α -regions, respectively) connected by a 42 amino acid long hinge region devoid of Cys residues.

The work presented in this the present thesis concerns the cloning, expression, purification and biochemical and biophysical characterization of domains of dMT constructs to gain insight into the structural and functional properties of the full-length protein.

Specific aims of this study are:

1. Cloning, expression and purification of GST fusion constructs of β -hinge (GST β hdMT), α -hinge (GST α hdMT) and hinge (GSThdMT) constructs of dMT.
2. Biochemical and biophysical characterization of the constructs using gel-filtration chromatography, electrophoresis, western blotting, spectrophotometry, inductively coupled plasma optical emission spectroscopy (ICP-OES) and dynamic light scattering (DLS) methods.
3. Modeling the structure of the constructs using solution X-ray scattering (SAXS) and *ab-initio* modeling techniques.
4. Relating the structure and Cd-binding properties of dMT constructs to those of the wild-type dMT to gain insight into the relationship between structure and function of dMT.

The thesis is organized as follows: this introductory chapter is followed by chapter 2 where an overview of the current status on structural and functional investigations on MT domains and full-length MTs is presented. Chapter 3 describes the materials and methods utilized in this study. The results of biochemical and biophysical characterizations and structural analyses are given in Chapter 4. Chapter 5 contains a brief discussion of the results in the light of current literature. The final Chapter 6 gives the conclusions of this study together with suggestions for future investigations.

Chapter 2

2. OVERVIEW

2.1 Metallothioneins (MTs)

Metallothioneins (MTs) are a family of low molecular weight proteins that have Cys -rich amino acid content and have ability to coordinate mono or divalent d^{10} metals in polymetallic thiolate clusters (Hamer, 1986, Vasak and Kägi, 1994). They are present in various organisms such as bacteria, fungi, animals and plants.

In accordance with their primary structure, MTs have been classified by different approaches. The first classification was proposed by Nordberg & Kojima in 1979 and was extended by Fowler et al. in 1987 and classified MTs in three classes. According to this classification, members of Class I show homology with horse MT whereas members of Class II do not have any homology with horse MT and are present in plants, fungi and nonvertebrates. Class III members are Cys rich polypeptides known as phytochelatins which are currently not considered as MTs (Fowler *et al.*, 1987).

In the other widely accepted classification, MTs have been classified in 15 families depending on their sequence similarities and phylogenetic relationships (Table 2.1). (Binz and Kagi, 2001). In this classification the families are divided into subfamilies, subgroups, isoforms and clans.

Table 2.1: Metallothionein families and subfamilies (Modified from Binz and Kägi, 1999).

Family	Sequence pattern	Example
Family1: vertebrate MTs	K-x(1,2)-C-C-x-C-C-P-x(2)-C	<i>M.musculus</i> MT1 MDPNCSTTGGSCACAGSCKCKECKCTSCKKCCSCCPVGCACKCAQGCVCKGSSEKCRCCA
Family2 : mollusc MTs	C-x-C-x(3)-C-T-G-x(3)-C-x-C-x(3)-C-x-C-K	<i>M.edulis</i> 10MTIV MPAPCNCIETNVICIDTGCSEGECRCGDACKCSGADCKCSGCKVVCKCSGSCACEGGCTGPSTCKCA PGCSCK
Family3: crustacean MTs	P-[GD]-P-C-C-x(3,4)-C-x-C	<i>H.americanus</i> MTH MPGPCCDKKCECAEGGCKTGCKCTSCRCAPCEKCTSGCKCPSKDECAKTCCKPCKCCP
Family4: echinodermata MTs	P-D-x-K-C-[V,F]-C-C-x(5)-C-x-C-x(4)-C-C-x(4)-C-C-x(4,6)-C-C	<i>S.purpuratus</i> SpMTA MPDVKCVCCKEGKECACFGQDCKTGECCKDGTCCGICTNAACKCANGCKCGSGCSCTEGNCAC
Family5: diptera MTs	C-G-x(2)-C-x-C-x(2)-Q-x(5)-C-x-C-x(2)D-C-x-C	<i>D.melanogaster</i> MTNB MVCKGCGTNCQCSAQKCGDNCACNKDCQCVCCKNGPKDQCCSNK
Family6: nematoda MTs	K-C-C-x(3)-C-C	<i>C.elegans</i> MT1 MACKCDCKNKQCKCGDKCECSGDKCCEKYCCEEASEKKCCPAGCKGDCKCANCHCAEQKQCGDKT HQQGTAAAH

Family7: ciliata MTs	No sequence pattern is defined since only one sequence is known	<i>T.termophila</i> MTT1 MDKVNSCCCGVNAKPCCTDPNSGCCCVSKTDNCCKSDTKECCTGTGEGCKCVNCKCCKPQANCCCG VNAKPCCFDPNSGCCCVSKTNNCCKSDTKECCTGTGEGCKCTSCQCCKPVQQGCCCGDKAKACCTD PNSGCCSNKANKCCDATSKQECQTCQCK
Family8: fungi-I MTs	C-G-C-S-x(4)-C-x-C-x(3,4)-C-x-C-S-x-C	<i>N.crassa</i> MT MGDCGCSGASSCNCGSGCSCSNCGSK
Family9: fungi-II MTs	-	<i>C.glabrata</i> MT2 MANDCKCPNGCSCPNCANGGCQCGDKCECKKQSCHGCGEQCKCGSHGSSCHGSCGCGDKCECK
Family10: fungi-III MTs	-	<i>C.glabrata</i> MT2 MPEQVNCQYDCHCSNCACENTCNCCA KPACACTNSASNECSCQTCKCQTCKC
Family11: fungi-IV MTs	C-X-K-C-x-C-x(2)-C-K-C	<i>Y.lipolitica</i> MT3 MEFTTAMLGASLISTTSTQSKHNLVNNCCSSSTSESSMPASCACTKCGCKTCKC
Family12: fungi-V MTs	-	<i>S.cerevisiae</i> CUP1 MFSELINFQNEGHECQCQCGSCKNNEQCQKSCSCPTGCNSDDKPCPGNKCEETKK

Family13: fungi- VI MTs		<i>S.cerevisiae</i> CRS5 TVKICDCEGECCKDSCHCGSTCLPSCSGGEKCKCDHSTGSPQCKSCGEKCKCETTCTCEKSKCNCEKC
Family14: prokaryota MTs	K-C-A-C-x(2)-C-L-C	<i>Synechococcus</i> spSmtA MTTVTQMKCACPHCLCIVSLNDAIMVDGKPYCSEVCANGTCKENSGCGHAGCGCGSA
Family15: planta MTs		
Type I	C-X-C-X(3)- C-X-C-X(3)- C- X-C-X(3)-spacer – C-X-C- X(3)- C-X-C-X(3)- C-X-C- X(3)	<i>Pisum</i> sativumMT MSGCGGSSCNCGDSCKCNKRSSGLSYSEMETTETVILGVGPAKIQFEGAEMSAASEDGGCKCGDNC TCDPCNCK
Type II	C-C-X(3)-C-X-C-X(3)- C-X-C- X(3)- C-X-C-X(3)-spacer- C- X-C-X(3)- C-X-C-X(3)- C-X- C-X(3)	<i>L.esculatum</i> MT MSCCGGNCGCGSSCKCGNGCGGCKMYPDMSYTESSTTTETLVLGVGPEKTSFGAMEMGESPPVAENG CKCGSDCKCNPCTCSK
Type III	-	<i>A.thaliana</i> MT3 MSSNCGSCDCADKTQCVKKGTSYTFDIVETQESYKEAMIMDVGAEENNANCKCKCGSSCSCVNCTC CPN
Type IV or Ec	C-x(4)-C-X-C-X(3)-C-X(5)-C- X-C-X(9,11)-HTTCGCGEHC- X-C-X(20)CSCGAXCNCASC- X(3,5)	<i>T.aestivum</i> MT MGCNDKCGCAVPCPGGTGCRCTSARSDAAAGEHTTCGCGEHCNCNPCACGREGTPSGRANRRANCS CGAACNCASCSTTA

Mammalian MTs which have been most thoroughly studied, have similar scaffolds: Two Cys rich domains are located in their N- and C-terminals and are referred to as β - and α - domain, respectively. These two domains are connected by a short spacer region usually 2-10 amino acids long which is devoid of Cys residues. Four major isoforms differing from each other in amino acids other than Cys exist in mammals and are expressed in different organs. MTI and MTII which are the major forms are expressed in most organs, predominantly in liver and kidney whereas MTIII expression is mostly seen in brain and recently it has found to be expressed in peripheral organs of rat. MTIV expression is seen in epithelial cells (Palmiter, 1987, Uchida *et al.*, 1991, Hozumi *et al.*, 2008, Cai *et al.*, 2005, Vasak, 2005).

Depending on the Cys arrangement in the β - and α - domains of mammalians, non-mammalian MTs can be classified as β domain like and α domain like peptides (Nemer *et al.*, 1985). According to this criteria yeast and fungal MTs have single β domains (Peterson *et al.*, 1996), crustacean MTs have two (β - β) domains (Narula *et al.*, 1995), echinodermal MTs are made of two (α - β) domains (Wang *et al.*, 1995) and vertebrate MTs have two (β - α) domains (Furey *et al.*, 1986) (Table 2.2).

Table 2.2: Amino acid sequences of different MTs. Sequences shown are those of fungus *N. crassa* MT, NcMT (NCBI accession no. CAA26793), CUP1 from *S. cerevisiae* (NCBI accession no. NP_013734), MTH from *H. americanus* (NCBI accession no. CAC80859), SpMTA from *S. purpuratus* (NCBI accession no. AAA30067). MT1 from *M. musculus* (NCBI accession no. P02802). Cys residues are shown in bold characters.

Family& sample	Sequences
Fungus NcMT	MGDCG C SGASSC N CGSG C SCS N CGSK
Yeast CUP1	MFSELINFQNEGHE C QC Q CGSCKNNE Q C Q KSCSCPTGCNSDP C GNKSEET K KSC C SGK

Crustacean MTH	MPGPCCCKDKCECAEGGCKTGCKCTSCRCAPCEKCTSGCKCP SKDECAKTCSKPCKCCP
Echino dermata SpMTA	MPDVKCVCCKEGKECACFGQDCCKTGECCCKDGTCCGICTNA ACKCANGCKCGSGCSCTEGNCAC
Vertebrate MT1	MDPNCSCSTGGSTCTSSCACKNCKCTSCCKKSCCSCPVG CSKCAQGCVCCKGAADKCTCCA

The function(s) of MTs in biological systems has not yet been determined. Their unique metal binding property suggest that they play a pivotal role in the sequestration of heavy metals such as Cd and Hg and are involved in the essential metal metabolism of e.g. Zn and Cu (Kagi and Kojima, 1987, Kagi and Schaffer, 1988, Hamer, 1986, Cherian *et al.*, 1994, Richards, 1989, Klaassen *et al.*, 1999, Haq *et al.* 2003, Mocchegiani *et al.*, 2004, Krezel and Maret, 2008). In addition, they act as protectors against oxidative stress and regulators of apoptosis. They also were shown to maintain the intracellular redox balance (Palmiter, 1998, Miles *et al.*, 2000, Hidalgo *et al.* 2001, Kang *et al.*, 2006, Krezel and Maret, 2008).

2.2 Plant MTs

The isolation of an early Cys-labeled (Ec) protein from wheat in 1987 by Lane *et al.* provided the first evidence of existence of MTs in plants (Lane *et al.*, 1987) and since then more than 100 sequences coding for MTs have been found in various species including Arabidopsis, rice, maize, pea, barley, tobacco, bean (Zhou *et al.*, 2005, Guo *et al.*, 2003, White and Rivin, 1995, Murphy *et al.*, 1997, Yu *et al.*, 1998, Tommey *et al.*, 1991, Okumura *et al.*, 1991, Choi *et al.*, 1996, Foley *et al.*, 1997). Little is known about plant MT structure and function. They generally contain two Cys- rich domains and a spacer (hinge) region (30-45 amino acids) between the two domains. Plant MTs differ in the length of the spacer sequences from their mammalian counterparts (2-10 amino acids) and variations in amino acid sequences, Cys motifs and charge are also observed (Kojima *et al.*, 1999).

2.2.1 Classification of Plant MTs

Plant MTs belonged to Class II in the earlier classification (Fowler *et al.*, 1987) but according to the most recent one they are the members of Family 15. Plant MTs are further classified in four types (Type I, II, III and IV) according to the Cys-motifs in their sequences and the length of the Cys-devoid regions named as spacer regions (Figure 2.1) (Binz and Kagi, 1999, Cobbett and Goldsbrough, 2002).

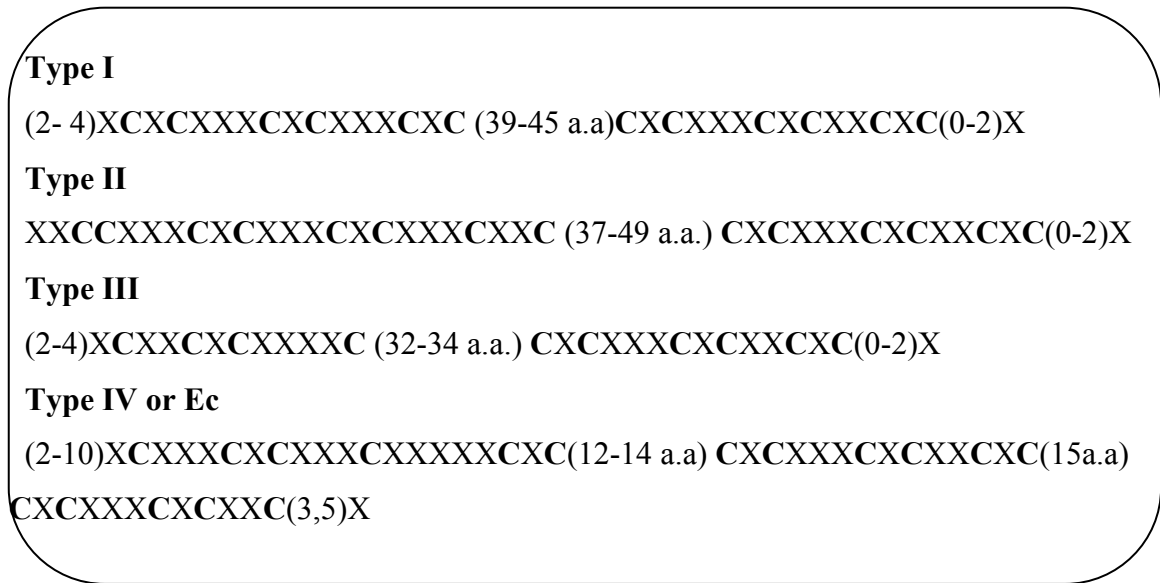


Figure 2.1: Amino acid sequences, spacer region length and Cys-motifs in different types of plant MTs (adapted from Cobbett and Goldsbrough, 2002). C stands for cysteine and X stands for any amino acid other than cysteine.

Type I MTs contain six Cys-X-Cys motifs exclusively in their N- and C-termini, where X stands for any amino acid other than Cys. The terminal domains are separated by an approximately 40 amino acids long spacer. Type I MTs from Brassicaceae have a shorter spacer and an extra Cys residue.

Type II MTs contain one Cys-Cys, two Cys-X-Cys and one Cys-X-X-Cys motifs in the N-terminal and three Cys-X-Cys motifs in their C-terminal. N-terminal sequences of Type II MTs are overall well conserved but the spacer is much more variable between the species.

Type III MTs has four Cys in their N-terminal. In the C-terminal there are six Cys arranged in Cys-X-Cys motif. The two domains are separated from each other by approximately 40 amino acids.

Type IV MTs have three Cys rich domains containing 5 or 6 Cys residues. Most of them are present as Cys-X-Cys motifs. Type IV MTs from dicots contain an extra 10 amino acids before the first Cys in their N terminal. All representatives of plant MT genes are expressed in Arabidopsis, sugarcane and rice (Rauser, 1999, Cobbett and Goldsbrough, 2002, Binz and Kägi, 1999).

Some of the representatives of different types of plant MTs and their sequences are summarized in Table 2.3.

Type I	++	++ ++					+++	+++		
AtMT1a	MADSN CGCGS	SCKCGDSCSC	EKNY.....NKEC	DNCSCGSNCS	CGSNCNC		
AtMT1c	MAGSN CGCGS	SCKCGDSCSC	EKNY.....NKEC	DNCSCGSNCS	CGSSCNC		
OsMT1a	MS... CSCGS	SCSCGSNCSC	GKKYPDLEEK	SSSTKATVVL	GVAPEKKOOF	EAAAESGETA	HGCSCGSSCR	CNP.CNC		
PsMT1	MSG.. CGCGS	SCNCGDSCCK	NKRSSGLSYS	EMETTETVIL	GVGPAKIOFE	GAEMSAASED	GGCKCGDNCT	CDP.CNCK		
Type II	++ ++	++ +	+				++	++++		
AtMT2a	MS CCGGNCGC	GSGCKCGNGC	GGCKMYPDLG	FSGETTTTTET	FVLGVAPPAMK	NOYEASGESN	NAENDACCKCG	SDCKCDPCTC	K	
BoMT2	MS CCGGNCGC	GSGCKCGNGC	GGCKMYPDLG	FSGETTTTTET	FVLGVAPPTMK	NOHEASGEGV	.AENDACCKCG	SDCKCDPCTC	E	
OsMT2	MS CCGGNCGC	GSSCQCGNGC	GGCK.YSEVE	PTTTTTFLAD	ATNKGSGAAS	GGSEMGAENG	SCGCNTCKCG	TSCGCSCNC	N	
SvMT2	MS CCNGNCGC	GSACCKGSGC	GGCKMFPDFA	E..GSSGSAS	LVLGVAP.MA	SYFDAEMEMG	VATENGCKCG	DNCQCDPCTC	K	
Type III	+++	+				+++	+++			
AtMT3	MSSN CGSCDC	ADKTQ CVKKG	TSYTFD IVET	QESYKE AMIM	DVGAEEN NAN	CKCKCGSSCS	CVNCTCCPN			
MaMT3	MS. TCGNCD	VDKSQ CVKKG	NSYGID IVET	EKSYVDE VIV	AAEAAE HDG	.KCKCGAACA	CTDCKCGN			
OsMT3	MSDK CGNCD	ADKSQ CVKKG	TSYGVV IVEA	EKSHFEE V..	.AAGEE NGG.	..CKCGTSCS	CTDCKCGK			
GhMT3	MSDR CGNCD	ADRSQ CTK.G	NSNTM. IIET	EKSYINT AVM	DAPAEND G..	.KCKCGTGCS	CTDCTCGH			
Type IV		++	+ +	+	+	+++	+	++	+++	
AtMT4a	MADTGK GSSV	AGCNDS CGCP	SP CPGGNSCR	CRM..R.EAS	AGDQGH MVCP	CGEHCGCNPC	NCPKTQTQTS	AKG...CTC	GEGCTCASCA	T
PhMT4	MADL. RGSS.	AICDER CGCP	SF CFGGVACR	CASGGAATAG	GGDMEH KKCP	CGEHCGCNPC	TCPKSEGTTA	GSGK.AHCKC	GFGCTCVQCA	S
ZmMT4	MG.....	...DDK CGCA	V PCPGGKDCR	CTS...G..S	GGQREH TTCG	CGEHCECSPC	TCGRATMPSG	RENRRANCSC	GASCNCASCA	SA
TaMT4	MG.....	..CDDK CGCA	V PCPGGTGCR	CTS...ARSG	AAAGEH TTCG	CGEHCGCNPC	ACGREGTPSG	RANRRANCSC	GAACNCASCG	SATA

Table 2.3: Four types of plant MTs. C stands for cysteine and are shown with plus sign. The protein sequences are from Arabidopsis (At), *Brassica napus* (Bn), rice (Os), pea (Ps), *Brassica oleracea* (Bo), *Silene vulgaris* (Sv), cotton (Gh), maize (Zm) and wheat (Ta) (Cobbett and Goldsbrough, 2002).

2.2.2 Function of plant MTs

The sequences of plant MTs and their functions are diverse compared to their mammalian counterparts (Cobbett and Goldsbrough, 2002). According to expression analysis, many MT genes are found to be expressed in different plant tissues including roots, stems, leaves, flowers, fruits and seeds (Rauser, 1999). Type I MTs are expressed in roots more abundantly and type II are usually expressed in leaves (Zhou *et al.*, 1994, 1995, Hsieh *et al.*, 1995, 1996). Expression of type III is observed in ripening fruits and leaves whereas type IV expression is more abundant in developing seeds (Ledger and Gardner, 1994, Kawashima *et al.*, 1992, White and Rivin 1995). It was also noticed that expression of Arabidopsis MT1a was localized to the vascular tissues of roots and leaves (Garcia-Hernandez *et al.*, 1998). Moreover type II MT expression in Arabidopsis and *Vicia faba* leaves is more plentiful in trichomes (Foley and Singh, 1994, Garcia-Hernandez *et al.*, 1998)

Despite the confirmation of existence of MTs in different tissues of different plant species, their functions are not exactly known. Most of the information about their putative function is obtained from expression studies during development and in response to various environmental factors. Plant MTs are thought to function primarily in Zn and Cu metabolism and in reactive oxygen species scavenging (Murphy and Taiz, 1995, Van Hoof *et al.*, 2001, Guo *et al.*, 2003, Navabpour *et al.*, 2003). As their expression is stimulated by drought, high light stress and low temperature they seem to be part of a general stress response rather than being involved only in heavy metal ion homeostasis and detoxification (Jin *et al.*, 2006).

Some studies reported that plant MTs respond to Cd induction and this putative Cd scavenging role were previously confirmed by yeast complementation assays by Zhou and Goldsbrough (Navabpour *et al.*, 2003, Zhou and Goldsbrough, 1994). MT overexpressing plants were shown to be able to accumulate higher levels of Cd and have an increased tolerance to Cd induced stress (Liu *et al.*, 2000). Cd resistance and tolerance has been shown in MTs expressing plant cells (Lee *et al.*, 2004 and Zimeri *et al.*, 2005). Moreover it has recently been reported that Arabidopsis MTs expressed in *Vicia* cells protect these cells from degradation after Cd exposure (Lee *et*

al., 2004). Not only Cu and Cd affect the expression of MT but also Al was shown to stimulate the expression of wheat MT (Snowden and Gardner, 1993). In contrast with the metal scavenging properties of MTs, there are also some studies reporting that MT transcript levels were not increased by metals such as Cu in *Brassica juncea* and Cu, Cd, Fe and Zn in *Vicia faba* and even repressed by Cu treatment in common monkey flower *M. guttatus* (Foley *et al.*, 1997, De Miranda *et al.*, 1990).

Increased MT RNA levels during senescence was observed in a number of studies and was first reported for a Type I MT in *Brassica napus* leaves and then confirmed in Arabidopsis, rice and bean (Cobbett and Goldsbrough, 2002, Buchanan-Wollaston, 1994, Hsieh *et al.*, 1995, Garcia-Hernandez *et al.*, 1998, Foley *et al.*, 1997).

In watermelon and rice, recombinant MTs protected plants from oxidative stress by scavenging hydroxyl radicals (Akashi *et al.*, 2004, Wong *et al.*, 2004, Gisela *et al.*, 2004). Plant MTs have also been reported to be involved in pathogen infection (Butt *et al.*, 1998), fruit ripening (Cobbett and Goldsbrough, 2002), wounding (Choi *et al.*, 1996). More recently, expression of subtypes Type IIa and IIIa MTs was reported to increase in leaves or roots during water stress (Street *et al.*, 2006, Bogeat-Triboulot *et al.*, 2007).

2.2.3 Structure and Metal Binding Properties of plant MTs

Despite the extensive knowledge about mammalian MTs, structural characteristics of plant MTs are a matter of debate and very little information is available in the literature. Plant and mammalian MTs do not show sequence homology therefore it is not possible to make structural predictions based on the available mammalian data (Leszczyszyn *et al.*, 2007).

X-ray and solution structures (NMR) for plant MTs are absent in the literature. It is hard to study MTs in plants because proteolysis occurs especially within the long spacer region and the protein is unstable in the presence of oxygen (Kille *et al.*, 1991). Careful purification techniques have helped to overcome this difficulty and several plant MTs have been successfully expressed in microbial hosts and purified (Tomme *et al.*, 1991, Domenech *et al.*, 2006, Bilecen *et al.*, 2005).

Pea Type I MT, PsMTa was expressed as a fusion to GST in *E. coli* and purified successfully. It was shown to bind Cd, Cu and Zn with the highest affinity for Cu (Tommey *et al.*, 1991). In other study, the pea MT gene was expressed in *E. coli* via heat inducible vector and it was shown to bind only Cd (Kille *et al.*, 1991).

A novel Type I plant MT was identified in cadmium (Cd) resistant durum wheat (dMT) which has three Cys-X-Cys motifs in its N- and C-termini and a 42 amino acids long hinge (spacer) region devoid of Cys. It was overexpressed in *E. coli* as a fusion protein to GST (Glutathione-S-transferase) (GSTdMT) and purified to homogeneity. The structure of GSTdMT and dMT were investigated by small angle X-ray scattering (SAXS) and computational methods. SAXS models indicated that GSTdMT existed as a dimer and dMT has an elongated structure. Homology modeling and *ab initio* models derived from SAXS indicated that dMT has a dumbbell shaped structure with two metal binding sites at opposite poles and a central long hinge region between them. The calculated Cd-content from ICP-OES was 4 ± 1 per protein molecule (Bilecen *et al.*, 2005). A dumbbell model was previously proposed for a kiwi type 3 MT (Zhu *et al.*, 2000), (Figure 2.2 A and B). The dumbbell model was also supported in *Fucus vesiculosus* MT by the observation of two-step dynamics in acid induced Cd release from the protein (Merrifield *et al.*, 2006).

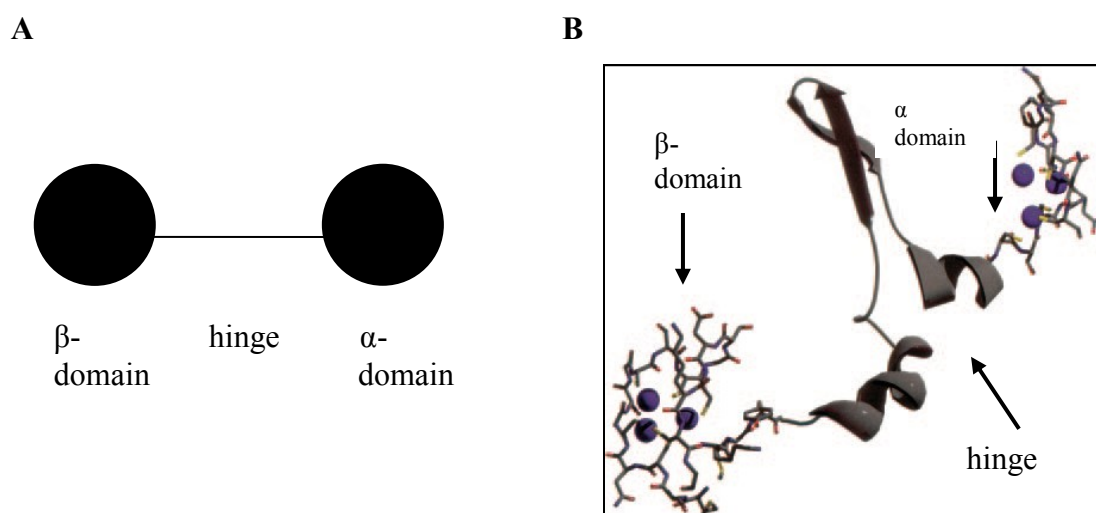


Figure 2.2: (A) Schematic representation of the dumbbell model (B) Predicted structure of dMT (Adapted from Bilecen *et al.*, 2005). Metal centers are presented in ball and stick presentation and the hinge region is depicted in ribbon presentation.

A Type II MT *Quercus suber* MT (QsMT) has one 38 amino acids long hinge region which is flanked by two Cys rich β - and α - domains. Recombinant Zn- and Cu- bound β - and α - domains and a chimera in which hinge is replaced by four glycine of QsMT was characterized by ESI-MS, ICP-OES, CD, UV-vis spectroscopy. Based on the data a hairpin model was proposed. In this model the two regions; Cys rich β - and α - domains, interact and the hinge region does not contribute to the metal binding. But in Zn-QsMT the hinge interacts with the β - and α - domains. The hairpin model was previously proposed for a pea MT PsMT_A (Kille *et al.*, 1991) (Figure 2.3 A and B). QsMT binds 4.2 Zn per protein molecule and 1.5 Zn and 4.7 Cu in Cu titrated Zn₄QsMT (Domenech *et al.*, 2007).

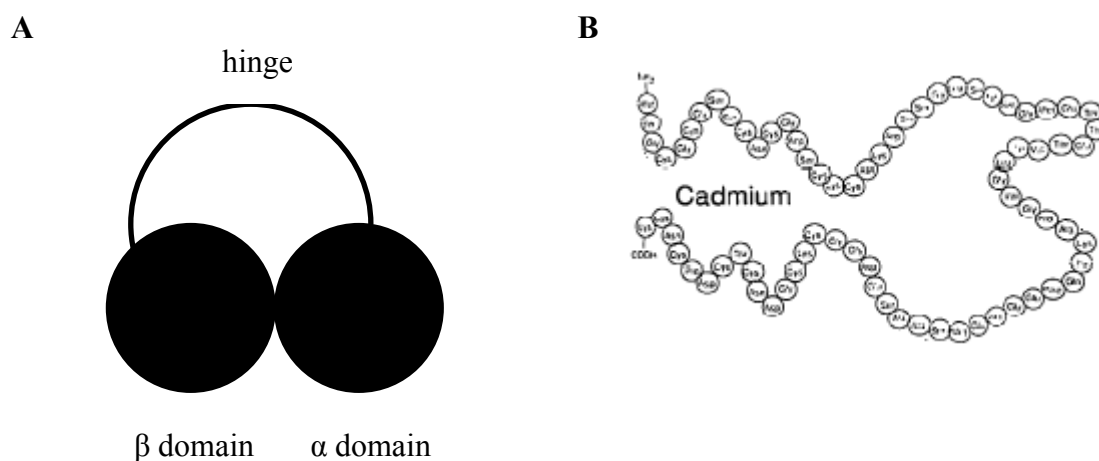


Figure 2.3: (A) Schematic representation of hairpin structure of MTs (B) Proposed hairpin structure for pea MT, PsMT_A (Adapted from Kille *et al.*, 1991).

A comparative Raman and IR spectroscopy of Zn-QsMT and Cd-QsMT, indicated that the hinge region has β -sheet elements and His residues which contribute to metal binding (Domenech *et al.*, 2007).

In a very recent study with Ec in wheat embryos, it was shown that the protein bound six zinc ions with a lower affinity compared to other MTs. Evidence for a contribution of histidines 32 and 40 to metal binding was also presented (Leszczyszyn *et al.*, 2007).

2.3 Vertebrate and Invertebrate MTs

2.3.1 Structure and Metal Binding Properties of Vertebrate and Invertebrate MTs

According to its UV-CD spectra, metal free mammalian MT (apoMT) was estimated to contain 55% disordered structure, 18% β -sheet and 26% β -turn (Vasak and Kägi, 1994). Upon binding of the metals, the folding of each of the domains is induced and as a result the metallated protein has a secondary structure which depends on metal binding (Duncan and Stillman, 2006).

MTs have been shown to coordinate essential metals Zn^{2+} and Cu^{+} *in vivo* by their cysteinyl sulphur ligands. Metal-binding studies indicate that they also bind various metals such as Cd^{2+} , Hg^{2+} , Bi^{3+} , Pt^{2+} , Ag^{+} , As^{3+} , Au^{+} , Co^{2+} and Fe^{2+} *in vitro* (Stillman, 1995).

Both NMR and X-ray crystal structures of Cd_5Zn_2 -MT2 native rat liver and Cd-reconstituted rat, rabbit and human liver Cd_7 -MT2 point to a trinuclear (M_3S_9) structure for the β -domain and a tetranuclear (M_4S_{11}) structure for α -domain where the metal ions zinc (Zn) and cadmium (Cd) are bound to 9 Cys and 11 Cys in the β - and α -domains, respectively (Figure 2.4). The architecture of various mammalian MT isoforms including recombinant mouse $113Cd_7$ -MT-1, recombinant human Zn_7 - and Cd_7 -MT-3 as well as recombinant mouse Cd_7 -MT-3 have similar M_4S_{11} and M_3S_9 clusters (Otvos and Armitage, 1980). The overall structure with two independent domains β - and α - , with the metal thiolate clusters is shown in Figure 2.5.

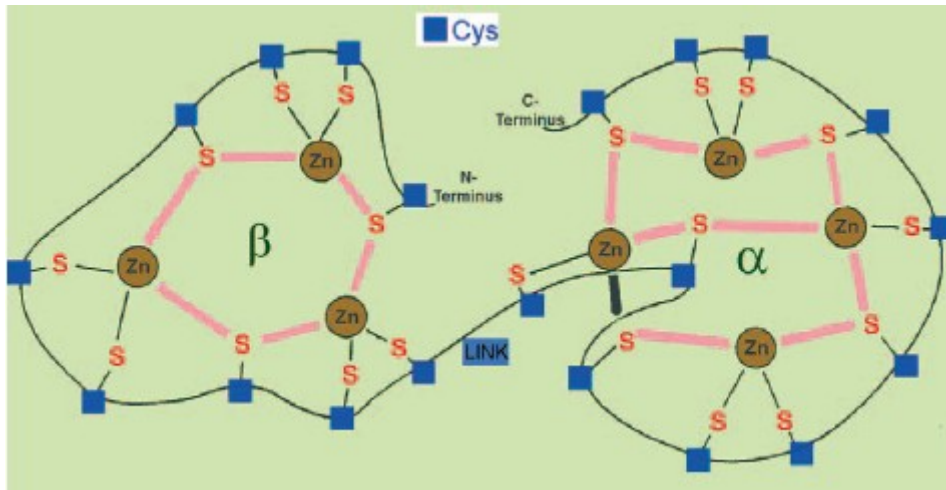


Figure 2.4: Schematic representation of mammalian MT-2 with its N- and C-terminal with 20 cysteines (blue squares) and with S- atoms. The two domains are linked by a short peptide (Penkowa, 2006).

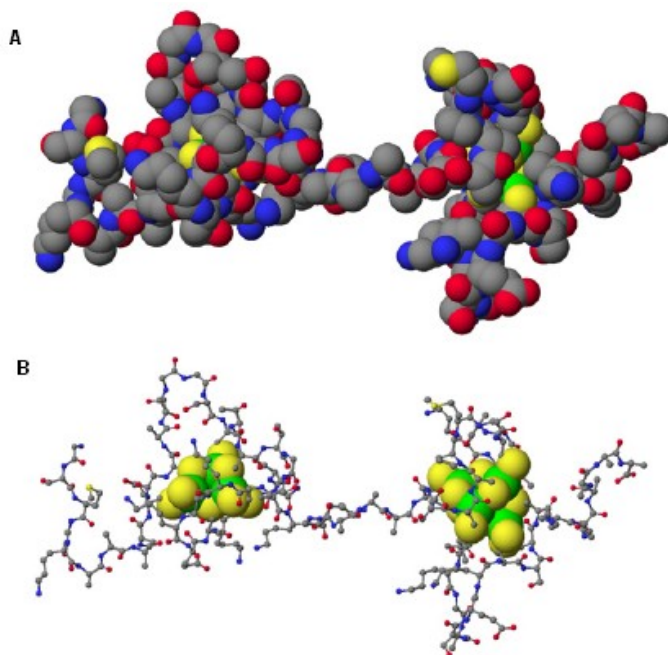


Figure 2.5: Molecular mode structure of Cd₇-mammalian MT with the N terminal β -domain on the left and the C terminal α -domain on the right (A) Space filling (B) Ball and stick representation with the domains in space filling form (Chan *et al.*, 2007).

Besides vertebrate MTs, the structure of invertebrate MTs such as crustacean blue crab Cd₆-MT-1, lobster and sea urchin Cd₇-MTA have been solved by NMR. Their

thiolate clusters are also arranged in two globular domains. Although there are similarities between vertebrate and invertebrate MTs in terms of domain arrangement, some differences are also observed. The total number of metal ions bound to each of the domains and their coordination in each domain can be different. Cd₆-MT1 crustacean blue crab (*Callinectes sapidus*) and lobster MT contain three Cd-ions in their β - and α -domains while Cd₇-MTA from sea urchin (*Strongylocentrotus purpuratus*) contains four Cd ions in its β -domain and three Cd ions in its α -domain which is the reverse ion arrangement of vertebrate M₇-MT-2. (Narula *et al*, 1995, Zhu *et al*, 1994, Riek *et al.*, 1999). Although the sequences of sea urchin and vertebrate MTs are not identical the Cys patterns are quite similar but the order is reversed (Table 2.4).

Table 2.4: Amino acid sequences of rat MT2 and sea urchin MTA. Sequences are derived from Vasak *et al.*, 2005.

MT	Sequence
Rat MT2	MDPNCSCATDGCSCAGSCKCKQCKCTSCKKSCCSCPVGCAKCSQGICKEASDKCSCCA
Sea Urchin MTA	MPDVKCVCKEKGKACFGQDCCKTGECCDKGTCCGICTNAACKCANGCKKCGSGCSCTEGNCAC

Fungus *Neurospora crassa* and yeast *Saccharomyces cerevisiae* MTs are the only MTs consisting of single domains that have been characterized at the structural level so far. *Neurospora crassa* has a single 25 amino acid long domain MT (NcMT) containing 7 Cys. Although human MT has two additional cysteines in its β -domain, the Cys arrangement in the NcMT is identical to the first seven N-terminal Cys of the β -domain of human MT. In vivo NcMT only binds Cu but in vitro it can bind other metals such as Cd, Ni, Zn and Co (Cobine *et al.*, 2004). According to the NMR studies on this protein, unlike other MTs it lacks a secondary structure. NcMT has an unusual structure: one half of the protein is left handed, the other half is right handed and it is oriented around the Cu (I)- Cys cluster (Figure 2.6).

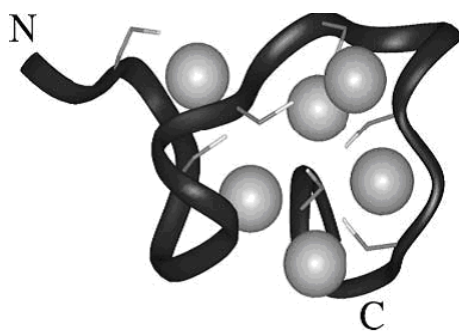


Figure 2.6: Ribbon presentation of NMR solution structure of NcMT. Cu (I) atoms bound are modeled into possible positions within the structure. The cysteine side chains turned to point towards the protein's center (Cobine *et al.*, 2004).

The solution NMR structure of Cu and Ag containing yeast MT indicated the presence of Cu_7S_{10} cluster but the distribution of the Cu atoms can not be identified within the structure. Several cluster structures were obtained, when the Cu ions were fitted into the well resolved sulphur frame. Moreover, the NMR models for Cu and Ag bound MTs have different backbones with the AgMT backbone having a more rectangular shape and CuMT a dog-bone shape because of the smaller ionic radius of Cu ions (Peterson *et al.*, 1996, Bertini *et al.*, 2000).

The crystal structure of yeast Cu thionein has been determined recently (Calderone *et al.*, 2005). It shows the Cu-thionein complex in which six of the Cu ions are coordinated trigonally and two of them are coordinated digonally to 10 Cys. Although this synthetic truncated MT binds eight Cu ions, the comparison of structure of Cu_8 -MT with the available NMR structure of Cu_7 -MT showed that the seven Cu ions are arranged similarly but not identically to the native Cu_7 -MT. The structure was also found to be different from the NMR structure of Ag₇-MT (Calderone *et al.*, 2005), (Figure 2.7).

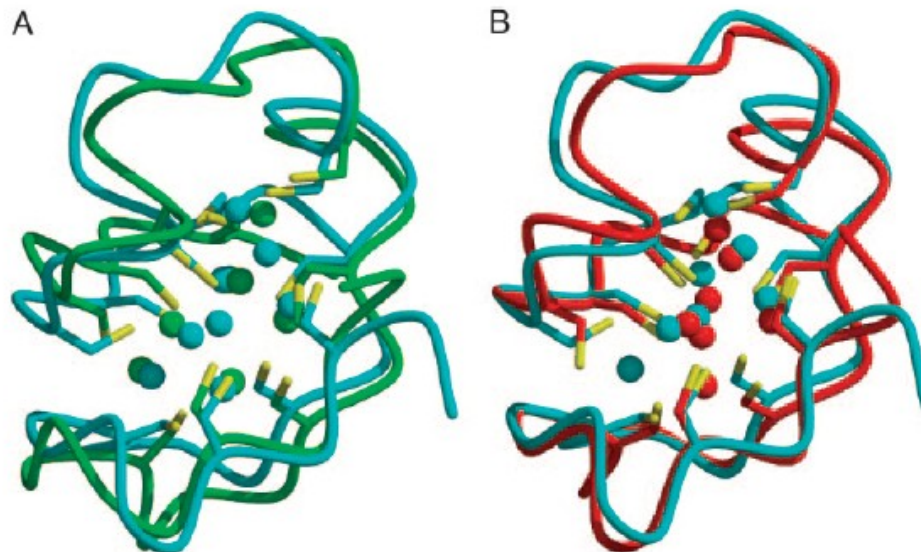


Figure 2.7: Comparison of the X-ray crystal structure of Cu₈-MT (cyan) with Ag₇-MT NMR model (green) (Peterson *et al.*, 1996) (A) and Cu₇-MT NMR model (red) (Bertini *et al.*, 2000) (B). The Cu₈-MT copper atoms are represented as cyan spheres, the silver and copper atoms of the Ag₇-MT and Cu₇-MT NMR models are represented as green and red spheres, respectively. The Cys side chains are also represented in the figure (Calderone *et al.*, 2005).

2.3.2 Structure and Metal Binding Properties of Vertebrate β - and α -domains

The number of Cys and the Cys motifs in each of the domains are diverse in vertebrate MTs and this may be required for the characteristic metal binding properties of these proteins. Single, double and triple replacements of Cys and other conserved amino acids such as lysines in mutants of Chinese hamster MTs, revealed that unique structure and metal binding abilities of MTs are highly dependent on their sequences. (Cody *et al.*, 1993, Cismowski *et al.*, 1991, Cherniak *et al.*, 1991, Cody *et al.*, 1994). Despite the extensive information of metallated MTs in vertebrates especially in mammals, the order of metal binding to the domains, and the rate of binding of each metal ion is still not totally understood.

There are two mechanism proposed for metal binding to the domains: cooperative and non-cooperative. Cooperative binding is most frequently proposed whereby binding of one metal ion facilitates the binding of the next metal ion (Gehrig *et*

al., 2000, Good *et al.*, 1988). In non-cooperative mechanism, metal ions bind independently of each other (Vasak *et al.*, 1981, Willner *et al.*, 1987, Duncan *et al.*, 2007). In a recent study by Sutherland *et al.*, under limiting Cd amount, noncooperative binding of Cd to the two domain (β rhMT) and single domain (β rhMT) mammalian MT was shown with electrospray mass spectrometry experiments (Sutherland and Stillman, 2008).

The coordination properties of the metal ions affect the maximum number of metal ions bound to the β - and α -domains. As tetrahedral coordination of Zn^{2+} and Cd^{2+} limits the maximum number of bound ions, four Zn^{2+} and Cd^{2+} ions are coordinated in the α -domain and three Zn^{2+} and Cd^{2+} are coordinated in the β -domain of vertebrate MTs. On the other hand Cu^+ , Ag^+ and Hg^+ are capable of accommodating tetrahedral, trigonal and diagonal coordination geometries and as a result β - and α - domains can both bind four, six or nine metal ions depending on the amount of metal loaded to the protein (Stillman *et al.*, 2000, Salgado *et al.*, 2004).

The binding affinity and stability of a given type of ion in the thiolate cluster is different in separate domains. Cd bound to the β domain was found to be more labile and EDTA was preferentially removed the Cd ion from this domain (Winge and Miklossy, 1982, Armitage and Boulanger, 1983). The Cd_4 - α MT mammalian cluster was shown to be highly stable (Capdevila *et al.*, 1997). It is also shown by saturation NMR that Cd moves among the sites in the β -domain and between the β -domains on a time scale of seconds and metal exchange within and between α - domains and between β and α -domains are much slower (Nettesheim *et al.*, 1985).

Chapter 3

3. MATERIALS and METHODS

3.1 MATERIALS

3.1.1 Chemicals

All chemicals were supplied by Aldrich (Germany), GE Healthcare (USA), Amresco (USA), Biorad (USA), Fermentas (Germany), Fluka (Switzerland), Invitrogen (Germany), Merck (Germany), Promega (USA), Roche (Germany), Qiagen (Germany) and SIGMA (USA). All chemicals are listed in Appendix A.

3.1.2 Primers

Primers were designed according to the sequence of dMT (Bilecen *et al.*, 2005) and synthesized by Iontek (Turkey) and Seqlab (Germany). Primer sequences are shown in Table 3.1. *EcoRI* and *XhoI* restriction sites were included in the sequences to facilitate insertion into the pGEX4T-2 vector.

Table 3.1: Primers used in the PCR amplification of GSTdMT constructs.

Primer name	Sequence of the primer
HEF	5'CTATAGAATTCCCAAGATGTACCCT 3'
HXSR	5'TATACTCGAGTTACTCGCCGGACTG 3'
P3Rstop	5' CTATGCTCGAGTTAACAGTTGCAGG 3'
P#6_F	5' CTATGGAATTCCCATGTCTTGCAAC 3'

3.1.3 Enzymes

Restriction enzymes *Eco*RI and *Xho*I were purchased from Fermentas and Promega. T4 DNA ligase, Taq Polymerase and Taq Pfu Polymerase were supplied by Fermentas. Thermo Sequenase II DNA polymerase used in DNA sequencing was provided by DYEnamic ET dye terminator kit (MegaBACE) (GE Healthcare).

3.1.4 Vectors

pGEM®-T Easy (Promega) and pGEX-4T-2 (GE Healthcare) vectors were used. Map of vectors are shown in Appendix B.

3.1.5 Cells

E.coli strains BL21(DE3), DH5 α and TOP10 were used.

3.1.6 Buffers and Solutions

All buffers and solutions, except those provided by commercial kits were prepared according to Sambrook *et al.*, 1989. Buffers and their compositions are given in Appendix C.

3.1.7 Commercial Kits

pGEM®-T Easy Vector Systems (Promega), Qiaquick PCR purification kit (250) (Qiagen), Qiaquick Gel Extraction kit (250) (Qiagen), Qiaquick Spin Miniprep Kit (250) (Qiagen) and Qiaquick Plasmid Midi Kit (100) (Qiagen) were used in recombinant DNA manipulations.

3.1.8 Culture Media

3.1.8.1 Liquid medium

LB (Luria-Bertani) Broth from SIGMA was used to prepare liquid culture media for bacterial growth. The components of LB broth are 10 g/L Tryptone (pancreatic digest of casein), 5 g/L Yeast extract and 5 g/L NaCl. In order to prepare 1 L of LB broth 20 g powder is suspended in 1 L of distilled water.

3.1.8.2 Solid medium

LB (Luria-Bertani) Agar from SIGMA was used to prepare solid culture media for bacterial growth. The components of LB agar are 10 g/L Tryptone (pancreatic digest of casein), 5 g/L Yeast extract and 5 g/L NaCl and 15 g/L agar. In order to prepare 1 L of LB agar 40 g powder is suspended in 1 L of distilled water.

3.1.9 Equipments

List of equipments used in this study are listed in Appendix D.

3.2 METHODS

3.2.1 Nucleic acid methods

Basic procedures were carried out according to Sambrook *et al.*, 1989.

3.2.1.1 PCR

Triticum durum MT hinge (hdMT), β -hinge (β hdMT) and α -hinge (α hdMT) cDNAs were amplified by PCR with the 5' and 3' primers containing *EcoRI* and *XhoI* (upstream and downstream, respectively) using the full length dMT cDNA as a template. Amplification was performed with 5 units of Taq Pfu DNA polymerase, 1 μ M of each primers and 0.2 mM dNTPs (final concentration) (Promega). The mixture was buffered with 10X PCR buffer (Promega). Reaction was carried out in a Thermocycler following below conditions (Table 3.2).

Table 3.2: PCR conditions used for amplification of hdMT, β hdMT and α hdMT cDNAs

Initial denaturation	95 °C for 2 minutes
Denaturation	95 °C for 1 min
Annealing	57 °C for 1 min A total of 30 cycles
Extension	
	72 °C for 1 min
Final extension	72 °C for 7 min

PCR products were analyzed by 2% or 1% agarose gel electrophoresis with TAE buffer. Samples were mixed with 6X loading buffer and gels were run at 100mV constant voltage for 30 minutes. Size of DNA fragments were estimated by using MassRuler DNA ladder mix (Fermentas), Mass ruler DNA low range (Fermentas) and Gene ruler 100bp plus DNA ladder (Fermentas) and visualized by ethidium bromide staining.

3.2.1.2 Subcloning of hdMT

hdMT cDNA was amplified and gel purified using a Qiaquick gel-extraction kit (Qiagen) and subcloned into pGEM®-T Easy vector (Promega) according to the given protocols by the manufacturers.

3.2.1.3 Ligation

Absorbance of gel extracted PCR product of hdMT at 260 nm was measured by using Nanodrop Spectrophotometer (Thermoscientific). Concentration of the PCR product was determined by using the formula: $C(\mu\text{g}/\mu\text{l})=A_{260} \times 50 \times \text{dilution factor}$ where C represents concentration and A stands for absorbance at 260 nm. PCR products of hdMT were ligated into pGEM®-T Easy vector (Promega) by using 3:1 and 5:1 insert: vector ratio. 10µl of reaction mixture contained 5µl of 2X ligation buffer, 1 µl (50ng) pGEM®-T Easy vector, calculated amount of PCR product, 1 µl 3 units of T4 DNA ligase and distilled water. The reaction mixture was either incubated at room temperature for 2 hours or for overnight at 4 °C if maximum number of transformants were required.

3.2.1.4 Transformation

E.coli DH5α and Top10F' chemically competent cells were used for transformation reactions. 2 µl of ligation mixture was gently added to the 50 µl of competent cells and the tube was incubated on ice for 20 minutes followed by incubation at 42 °C for 45 seconds to induce heat shock. Finally the tube was put back on ice for 2 minutes. 950 µl of LB was added to the mixture and incubated at 37 °C water bath for 1 hour. 100-200 µl transformed cells and controls were plated on ampicillin selective LB plates that contained IPTG and X-gal. The plates were incubated at 37 °C for 16 hours for bacterial cells to grow.

3.2.1.5 Colony selection

Utilizing the blue/white screening property of the pGEM®-T Easy Vector System I positive colonies with white color were selected and grown in liquid LB-ampicillin culture for plasmid isolation.

3.2.1.6 Plasmid isolation

White colonies were grown in 5 ml of LB-ampicillin medium overnight at 37 °C with shaking at 280 rpm. Cells were centrifuged at 4 °C at 5000 g for 3 minutes

and plasmid isolation was carried out from the pellets either using Qiaquick Spin Miniprep Kit (Qiagen) or following the alkaline lysis protocol from Sambrook *et al.*, 1989. The final concentration of plasmid DNA was calculated by measuring the absorbance at 260 nm in Nanodrop spectrophotometer. DNA samples were stored at -20 °C for further use in restriction enzyme digestion and sequencing reactions.

3.2.1.7 Restriction enzyme analysis

Isolated plasmids containing hdMT cDNA were digested with *EcoRI* and *XhoI* restriction enzymes according to suppliers' instructions to verify the presence of corresponding gene. hdMT cDNA was further extracted from 2% agarose gel to be cloned into expression vector.

3.2.1.8 Sequence verification

Isolated plasmids were sequenced by the dideoxynucleotide method using the DYEnamic™ ET Dye Terminator Kit (MegaBACE™). Plasmids were also monitored by colony PCR before sequencing.

3.2.1.9 Cloning into expression vector

hdMT was obtained from restriction digestion of the isolated subcloning construct with *EcoRI* and *XhoI* restriction enzymes according to supplier instructions. PCR amplified β hdMT and α hdMT cDNAs were also digested with the same restriction enzymes. Fragments containing necessary sites for bidirectional cloning were then ligated into the corresponding sites of the expression vector pGEX-4T-2 using the 3:1 and 5:1 vector: insert ratio. Transformation and plasmid isolation was carried out basically as described above.

Isolated plasmids containing pGEXhdMT, pGEX β hdMT and pGEX α hdMT were digested with *EcoRI* and *XhoI* restriction enzymes to verify the presence of corresponding hdMT, β hdMT and α hdMT cDNAs. Samples were analyzed on 2% agarose gels and visualized by ethidium bromide.

Verified plasmids were sequenced by the dideoxynucleotide method using the DYEnamic™ ET Dye Terminator Kit (MegaBACE™) and also were sent for sequencing to Mclab sequencing company (USA).

3.2.2 Protein expression

3.2.2.1 Monitoring expression of the recombinant fusion proteins

In order to monitor the expression of the construct fusion proteins, for each one 5mL of LB broth with a final concentration of 100µg/ml ampicillin was inoculated with BL21(DE3) cells containing pGEXhdMT or pGEXβhdMT or pGEXαhdMT plasmid. Cultures were induced with 0.75 mM isopropyl β-D-thiogalactoside (IPTG) when the OD₆₀₀ was around 1. Cells were continued to be grown at 37⁰C by shaking at 280 rpm. Inductions were monitored by taking aliquots from the cultures before induction (t=0) and after induction at regular intervals for a maximum of about 6 hours (t=1,2...) and pelleting the cells. Pellets were lysed in the lysis buffer (150 mM NaCl, 20 mM HEPES, 2.5mM MgCl₂, 10 mg/mL lysozyme, pH 8) and were analyzed by 12% SDS polyacrylamide gels. Gels were first run at 80V and after the bands entered the separating gel at the voltage was increased to 100V constant voltage for 1 hour 30 minutes. Protein bands were visualized by coomassie blue staining. Protein molecular weight markers and protein ladders (Fermentas) were used to identify the molecular weights of expressed proteins.

3.2.2.2 Culture growth for purification

Bacterial cells containing recombinant plasmids pGEXhdMT, pGEXβhdMT and pGEXαhdMT were grown in 50 ml of LB broth containing 100µg/ml ampicillin at 37⁰C overnight shaking at 280 rpm. The overnight cultures were diluted 100-fold using 1 liter of fresh LB broth plus ampicillin and 0.1 mM CdCl₂ for pGEXβhdMT and 0.1 mM for pGEXαhdMT. Incubation was continued at 37⁰C, 280 rpm. When the OD₆₀₀ reached 0.8, IPTG was added to a final concentration of 0.75 mM. Cells were incubated at 37⁰C for a further 5.5 hours for pGEXhdMT and for 4.5 hours for pGEXβhdMT and pGEXαhdMT containing bacteria. Cellular were pellets were obtained by centrifugation

at 7000 rpm for 30 minutes using a Sorvall centrifuge with SLA-3000 rotor and washed once with Buffer I (150 mM NaCl, 20 mM HEPES, 2.5mM MgCl₂, pH 8). Pellets of pGEXβhdMT and pGEXαhdMT expressing cells were washed in a glove box to provide the anaerobic environment. Pellets were kept at -80 °C until further use.

3.2.3 Purification and analysis

Similar procedures were applied for purification of all constructs. The major difference was use of anaerobic environment with argon for purification of GSTβhdMT and GSTαhdMT and all buffers used for their purification were degassed and purged with argon.

Purification of GSTdMT constructs involved the expression of the proteins, lysis of the cells by sonication, affinity fractionation of the cell lysate using GSTrap® FF column (GE Healthcare) by using reduced glutathione, dialysis of the proteins against size exclusion column buffer and size exclusion chromatography of the dialysed protein using Hiload™ 16/60 Superdex™ 75 column (GE Healthcare).

3.2.3.1 Affinity Chromatography

Cell pellets were resuspended in 8% of the original volume of culture with Buffer II (20mM HEPES, 2.5 mM MgCl₂, 100mM NaCl, 1 mM DTT, 0.5 mM PMSF, 2 EDTA-free protease inhibitors tablet Roche, pH8). 0.1 mM CdCl₂ was added to this buffer for the purification of GSTβhdMT and GSTαhdMT. All cells were lysed by 10 minutes of sonication at 4 °C with 8 seconds of pulse followed by 9 seconds of waiting period. Triton X-100 was added to a final concentration of 1% and the suspension was mixed gently at 4 °C for 45 minutes to facilitate solubilization of proteins. Lysate was centrifuged at 13000 rpm, 4 °C for 1 hour. GSThdMT, GSTβhdMT and GSTαhdMT were purified by affinity chromatography using a 5 ml High GSTrap® FF column (GE Healthcare) equilibrated with 25 ml of HEPES buffer (20 mM HEPES, 100mM NaCl, 2.5 mM MgCl₂, 1mM DTT, 0.5 mM PMSF, pH8). The supernatant was applied to the GSTrap® FF prepacked affinity column (GE Healthcare). The column was previously washed with 30 ml of HEPES buffer. GSThdMT, GSTβhdMT and GSTαhdMT were

eluted at a speed of 1 ml/min in 1 ml of fractions using Tris-HCl buffer (50mM Tris HCl, 100mM NaCl, 1 mM DTT, 0.5 mM PMSF, 10 mM reduced glutathione, 1 protease inhibitors cocktail tablet, pH8). Fractions were pooled according to A₂₈₀ measurements. Pooled GSThdMT, GSTβhdMT and GSTαhdMT were dialyzed against HEPES buffer overnight with three changes of buffer.

3.2.3.2 Size exclusion chromatography

Dialyzed protein was loaded on a column of HiloadTM 16/60 SuperdexTM 75 (GE Healthcare) equilibrated with 3 column volumes of HEPES buffer. Column eluate was collected at a speed of 1 ml/min in 1 ml fractions and monitored by A₂₈₀ measurements using an AKTA FPLC system (GE Healthcare). Fractions were either kept separately or pooled as described in results section and kept at 4 °C for analysis.

3.2.4 SDS polyacrylamide gel electrophoresis (PAGE)

Protein samples were mixed with 2X SDS-PAGE sample buffer (0.125 mM Tris-HCl pH (6.8), 4% SDS, 20% glycerol, 10% 2-mercaptoethanol, 0.04% bromphenol blue) heated at 100 °C and loaded onto 12% SDS polyacrylamide gels having 5% of stacking gel. Gels were run at 80 V constant voltages in 1X SDS running buffer (25 mM Tris, 192 mM glycine, 0.1% (w/v) SDS). When the samples passed from stacking gel to resolving gel voltage was increased to 120 V and electrophoresis was completed at this constant voltage.

3.2.5 Native polyacrylamide gel electrophoresis (PAGE)

Protein samples were mixed with 2X Native-PAGE sample buffer (0.125 mM Tris-HCl pH6.8, 20% glycerol, 10% 2-mercaptoethanol, 0.04% bromphenol blue), and loaded onto 10% native polyacrylamide gels. In order to avoid denaturing samples were not boiled. Gels were run at 80 V constant voltage in 1X Native-PAGE running buffer (25 mM Tris, 192 mM glycine) until the bands passed to the resolving gel and the electrophoresis was completed at 120 V.

3.2.6 Coomassie blue staining

For visualization, SDS- and Native-PAGE gels were stained with coomassie blue solution and destained in distilled water.

3.2.7 Western blotting

Protein samples were mixed with 2X SDS-PAGE sample buffers (0.125 mM Tris-HCl pH (6.8), 4% SDS, 20% glycerol, 10% 2-mercaptoethanol, 0.04% bromphenol blue) heated at 100 °C and loaded onto 12% SDS polyacrylamide gels with 5% of stacking gel. After electrophoresis was performed for approximately two hours at 25 amp, proteins were transferred to PVDF membrane using western transfer apparatus (Novex/USA) at 25V overnight at 4 °C using transfer buffer (96mM glycine, 12 mM Tris-base and 20% methanol). The transfer sandwich consisted of three pre-soaked blotting pads, a piece of 3MM Whatman paper, the gel, the PVDF membrane, another piece of 3MM Whatman paper and the other set of pre-soaked blotting pads. After overnight transfer, PVDF membrane was incubated in blocking solution (5% non-fat dry milk, in PBS-T (80 mM Na₂HPO₄, 20 mM NaH₂PO₄, 100 mM NaCl, 0.2% Tween-20, pH 7.4) for 1 hour at room temperature with shaking. Membrane was then washed with PBS-T for 15 minutes at room temperature with shaking and incubated with anti-GST HRP conjugate (GE Healthcare) at a dilution of 1/20000 in 10 ml fresh blocking solution for 1 hour at room temperature on an orbital shaker. After the incubation membrane was washed three times with PBS-T for 15 minutes at room temperature. Proteins were visualized by using ECL advance western detection kit (GE Healthcare).

3.2.8 Thrombin cleavage

3.2.8.1 Small scale cleavage

400 µl of purified GSThdMT with a concentration of 1.15 mg/ml was incubated with 7U of thrombin o/n in the cold room. During the incubation samples were collected after 45 minutes, 3 hours 30 minutes and finally after o/n incubation. The

remaining cleaved protein was incubated with glutathione sepharose 4B beads (GE Healthcare) for 3 hours in the cold room. Samples were collected after 1 hour and 3 hours of incubation with beads. The sample cleaved for 3 hours was concentrated using a speedvac (Savant/USA). Cleaved protein and the samples collected during incubation were analysed by 16% Tris-tricine gel.

3.2.8.2 Large scale cleavage and purification of the cleaved protein

pGEX4T2hdMT transformed E.coli BL21DE3 cells were grown in LB broth containing 100µg/ml ampicillin at 37 °C overnight for purification. The overnight culture was diluted 100-fold using fresh 3 liters of LB broth plus ampicillin and incubation was continued at 37 °C. When the OD₆₀₀ reached to 0.8, IPTG was added to a final concentration of 0.75 mM. After incubation for a further 5.5 hours at 37 °C cells were pelleted by centrifugation at 7000 rpm for 30 minutes and washed once in Buffer I.

Pelleted cells were resuspended in Buffer II and lysed by mild sonication at 4 °C. Triton X-100 was added to a final concentration of 1% and the suspension was mixed gently at 4 °C for 45 minutes to facilitate solubilization of proteins. Lysate was centrifuged at 13000 rpm for 1 hour using Sorvall centrifuge with SS-34 rotor. The supernatant was incubated with glutathione sepharose 4B beads for 4 hours at 4 °C with gentle agitation on a rotating plate. The beads were then centrifuged and washed with HEPES buffer several times in order to discard the unbound protein. Thrombin was added to the beads and incubated for 23 hours at 4°C on a rotating plate.

The next day hdMT was separated from GST-bound beads by centrifugation at 5000 g for 5 minutes with Sorvall centrifuge. Eluted hdMT was concentrated using centriprep with a swinging rotor at 2000 g with Sorvall centrifuge at 4°C until 2 ml of sample solution was obtained. Thrombin and contaminated proteins were separated by size exclusion chromatography using Hiload™ 16/60 Superdex™ 75 (GE Healthcare) equilibrated with 3 column volumes of HEPES buffer. Column eluate was collected at a speed of 1 ml/min in 1 ml fractions and monitored by A₂₈₀ measurements using an AKTA FPLC system (GE Healthcare). Collected fractions during the purification were then analysed by 12% SDS and 16% Tris-tricine gel electrophoresis.

3.2.9 Protein concentration determination

Absorption at 280 nm was measured by using Nanodrop spectrophotometer (Thermo Scientific/USA) and protein concentration was determined according to the formula $A_{280}=1$ is obtained from a 0.5 mg/ml of GST solution. Since the proteins were fused to GST, the formula mentioned were used for concentration calculations.

For Small Angle X-ray Scattering (SAXS) measurements calculated extinction coefficient values were used. These are 1.36 for GSThdMT, 1.289 for GSTβhdMT and 1.279 for GSTαhdMT.

3.2.10 Dynamic light scattering

Dynamic light scattering also known as Photon Correlation Spectroscopy or Quasi-Elastic Light Scattering) is a technique where the size of particles are measured typically at the sub micron level. It measures the brownian motion which is the random movement of particles due to bombardment of solvent molecules around and relates it with the size. Usually DLS concerned with the particles in liquids.

When the measured particle get bigger in size, the brownian motion will be slower. The velocity of brownian motion is determined by translational diffusion coefficient and this coefficient also used for determination of the size (diameter) of particle. Since the diameter is measured in DLS is related with the diffusion of the particle in the liquid environment, the diameter measured is the hydrodynamic diameter and it is the size of a sphere that has the same translational diffusion coefficient.

Size distribution of particles are generated first by intensity distribution and converted to volume and number distributions. So size distribution by intensity is the most reliable analysis for the measurement of polydispersity and the size of particles.

Fractions of recombinant GSThdMT, GSTβhdMT and GSTαhdMT were analyzed for the presence of different oligomeric forms by DLS using Zeta-sizer Nano ZS (Malvern Instruments).

3.2.11 Limited proteolytic cleavage with trypsin

Trypsin is a serine protease which predominantly cleaves peptide chains at the carboxyl side of the amino acids lysine and arginine, except when either is followed by a proline. 100 µg of purified GSTdMT constructs were incubated with 24 µl of 0.0025 mg/ml trypsin in trypsin buffer (20 mM HEPES, pH 8, 2.5 mM MgCl₂, 10 mM KCl, 2 mM DTT). Before treatment with trypsin, protein samples were incubated at 30 °C for 30 minutes with an rpm of 300. In order to follow the cleavage pattern, samples were collected before and after trypsin incubation at different time points and flash frozen in liquid nitrogen. They were analyzed by 14- 16 % Tris-tricine gel analysis.

3.2.12 Small angle X-ray scattering (SAXS)

SAXS is a technique where the elastic scattering of X rays (wavelength 0.1 nm) by a sample in the nm-range is recorded at very low angles (typically 0.1 - 10°) (Svergun and Koch, 2003). In this angular range information about gross structural features such as shape, quaternary and tertiary structure of molecules are obtained, however results lack information about the atomic structure. It provides structural information on inhomogeneities of electron density with dimensions between about ten to a few thousand angstrom (Svergun and Koch, 2002). The scattered intensity $I(s)$ is recorded as a function of momentum transfer s ($s = 4\pi\sin\lambda/\theta$, where 2θ is the angle between the incident and scattered radiation and λ is the X-ray wavelength) in the range $X_1 < s < X_2$ (Koch *et al.*, 2003).

The synchrotron radiation X-ray scattering data were collected on the X33 camera at the European Molecular Biology Laboratory (EMBL) on the storage ring DORIS III of the Deutsches Elektronen Synchrotron (DESY) in Hamburg, using a mar345 Image Plate detector. Scattering data was recorded in the range of momentum transfer $0.15 < s < 3.5 \text{ nm}^{-1}$.

Solutions of GSThdMT, GSTβhdMT and GSTαhdMT in HEPES buffer were measured at several concentrations between 0.68 and 16.8 mg/ml. Because at higher concentrations large portion of the protein formed higher order oligomers, the

scattering curves measured below 2 mg/ml concentrations were used for structural analysis. Bovine serum albumin (BSA) was also measured as a molecular mass standard at 5mg/ml in 50 mM HEPES, pH8 and 150 mM NaCl.

The program used for data reduction and initial processing was PRIMUS. It is a Windows- PC-based program (Konarev *et al.*, 2003) with which raw data analysis and manipulations such as background subtraction, correction for beam intensity and detector response and concentration effects are performed on the experimental data.

Data regularization was done with GNOM which is an indirect transform program that computes distribution functions for monodisperse and polydisperse systems. Preprocessing by GNOM usually gives the opportunity to reduce unwanted interference effects in the scattering data and to define the D_{\max} (maximum particle) value which is the maximum fitting range for the $p(r)$ (pair distribution function of profile) (Koch *et al.*, 2003).

For *ab initio* structure analysis a program named DAMMIN and the faster version DAMMIF were used. These do not fit the experimental data directly, they read the output files as well as the value of D_{\max} and regularized scattering curve $I_{\text{GNOM}}(s)$ produced by the indirect transform program GNOM. This use of pre-processed data also allows to desmear the scattering patterns and in some cases to correct for concentration effects or aggregation (Konarev *et al.*, 2006).

Not only a single model existed for the GSTdMT constructs from their SAXS data. In order to make sure that the models obtained from different runs of DAMMIN or DAMMIF converge to each other, several runs should be performed. It was time consuming and was difficult to compare the models with each other. Instead a model averaging program known as DAMAVER was used. It is a set of programs to align *ab initio* models. It selects the most typical one and build an averaged model. It contains 5 programs: DAMAVER, DAMFILT, DAMSEL, DAMSUP AND DAMSTART. DAMAVER provides the average model of aligned models and DAMFILT gives the filtered model in which the averaged model was filtered at a given cut-off volume. DAMSEL compare all models and find the most probable one where DAMSUP align all models with the most probable one. If you want to refine the

averaged, DAMSTART generates an input file for DAMMIN from the averaged model (http://www.emblhamburg.de/ExternalInfo/Research/Sax/manual_damaver.html).

In order to determine the three dimensional structure of GSTdMT constructs, based on the available three dimensional structure of GST dimer, a rigid body modelling program BUNCH was used. It is an simulated annealing protocol where the optimal positions and orientations of available high resolution models of domains are found and the probable conformations of the dummy residues chains are attached to the appropriate terminal residues of domains. It fits the experimental scattering data from all constructs simultaneously.

(http://www.emblhamburg.de/ExternalInfo/Research/Sax/manual_bunch.html).

3.2.13 Inductively coupled plasma optical emission spectroscopy (ICP-OES)

ICP-OES is an analytical technique in which the trace elements in solid and liquid samples can be detected. It uses inductively coupled plasma to produce excited atoms and ions. The atoms and ions emit radiation and every element has a characteristic emission at certain wavelengths. The intensity of this emission is indicative of the concentration of the element within the sample.

In order to determine Cd^{2+} content of purified GST β hdMT and GST α hdMT, inductively coupled plasma optical emission spectrometry (ICP-OES, Varian, Australia) measurements were carried on solutions of protein with known concentrations. Molarity of purified protein and bound Cd^{2+} were calculated and the protein:metal ion ratio was found accordingly.

Chapter 4

4. RESULTS

4.1 Cloning of constructs for domains of dMT

4.1.1 Amplification of hinge dMT, β -hinge dMT and α -hinge dMT cDNAs

The dMT domains; hinge (hdMT), β -domain including hinge (β hdMT) and α - domain including hinge (α hdMT) were amplified using the primers given in Table 3.1 and cloned separately for studies. hdMT, β hdMT and α hdMT cDNAs corresponding to 126 bp, 206 bp and 200 bp respectively were observed after PCR reactions (Figure 4.1 A. B and C). The cDNA sequences of dMT constructs and their amino acid sequences are shown in Figure 4.2.

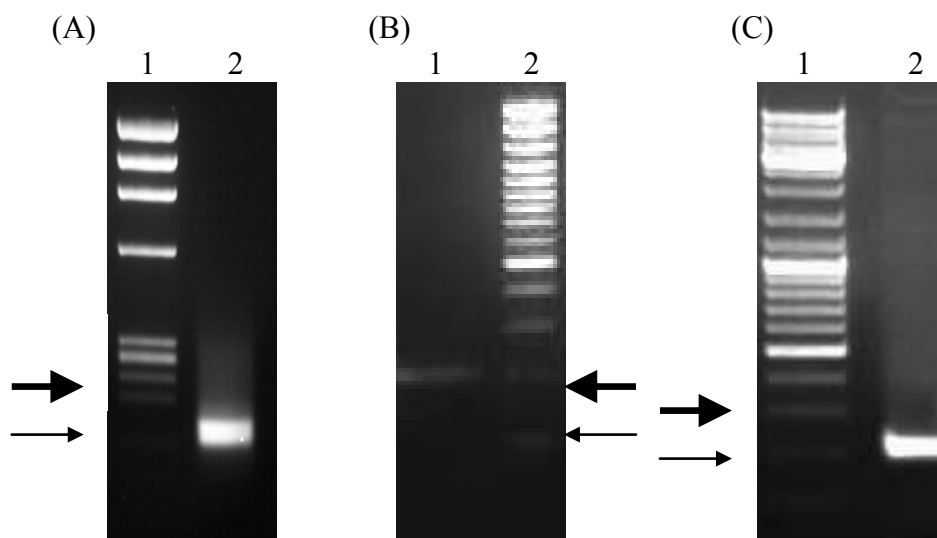


Figure 4.1: 2 % Agarose gel analysis of PCR amplified domains of dMT. Lanes 1: (A) 174M DNA ladder (B) β hdMT fragment (206 bp) and (C) Mass ruler DNA ladder mix. Lanes 2: (A) hdMT fragment (126 bp) (B) Gene ruler 100bp plus DNA ladder and (C) α hdMT fragment (200bp). Thick and thin arrows specify the molecular weights 200 bp and 100 bp respectively.

(A) hdMT

cDNA sequence

5'AAGATGTACCCTGATCTGACAGAGCAGGGCAGCGCCGCCGCCAGGTC
GCCGCCGTGGTCGTGCTCGGCGTGGCTCCTGAGAACAAGGCGGGGCAGTTC
GAGGTGGCCGCCGGCCAGTCCGGCGAG 3'

amino acid sequence

KMYPDLTEQGSAAAQVAAVVVLGVAPENKAGQFEVAAGQSGE

(B) β hdMT

cDNA sequence

5'ATGTCTTGCAACTGTGGATCCGGTTGCAGCTGCGGCTCAGACTGCAAGTG
CGGGAAGATGTACCCTGATCTGACGGAGCAGGGCAGTGCCGCGGCCAGGT
CGCCGCCGTGGTCGTCTCGGCGTGGCGCCTGAGAACAAGGCGGGGCAGTT
CGAGGTGGCCGCCGGCCAGTCCGGCGAG 3'

amino acid sequence

MSCNCGSGCSCGSDCKCGKMYPDLTEQGSAAAQVAAVVVLGVAPENKAGQF
EVAAGQSGE

(C) α hdMT

cDNA sequence

5'AAGATGTACCCTGATCTGACAGAGCAGGGCAGCGCCGCCGCCAGGTCGC
CGCCGTGGTCGTGCTCGGCGTGGCTCCTGAGAACAAGGCGGGGCAGTTCGA
GGTGGCCGCCGGCCAGTCCGGCGAGGGCTGCAGCTGCGGCGACAACCTGCAA
GTGCAACCCCTGCAACTGT

amino acid sequence

KMYPDLTEQGSAAAQVAAVVVLGVAPENKAGQFEVAAGQSGEGCSCGDNC
KCNPCNC

Figure 4.2: cDNA and amino acid sequences of GSTdMT constructs. (A) hdMT (B) β hdMT and (C) α hdMT.

4.1.2 Subcloning and cloning of hdMT

hdMT cDNA obtained in PCR reaction was subcloned into pGEM®-T Easy vector (Promega) and transformed into DH5α competent cells. The presence of hdMT fragment in the colonies was screened either by colony PCR or double digestion of the pGEM®-T Easy vector by *EcoRI* and *XhoI* (Figure 4.3).

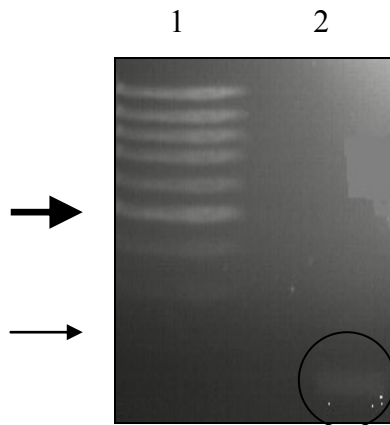


Figure 4.3: 2% Agarose gel analysis of double digested pGEM®-T Easy hdMT construct. Lane 1: Mass ruler DNA low range. Thick and thin arrows specify 500 bp and 200 bp respectively. Lane 2: hdMT fragment (circled).

The pGEM®-T Easy vector, containing the hdMT cDNA was digested with *EcoRI* and *XhoI* restriction enzymes (Figure 4.3). The resulting fragment was extracted from gel and ligated into the corresponding sites of pGEX-4T-2 the GST fusion vector and transformed to the BL21(DE3) cells. The presence of hdMT sequence in pGEX-4T-2 vector was controlled by colony PCR (Figure 4.4). The presence of a band around 126 bp was an indication of the presence of hdMT in the vector. Insertion was further verified by sequencing of the plasmids isolated from positive colonies.

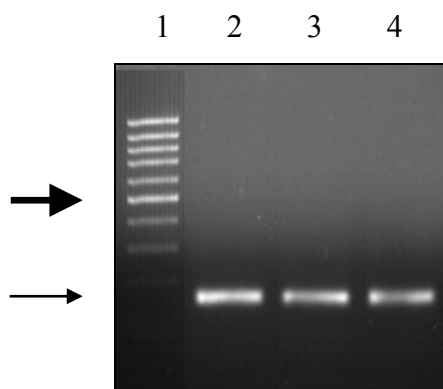


Figure 4.4: 1.5% Agarose gel analysis of PCR from pGEXhdMT construct positive colony. Lane 1: Mass ruler DNA ladder low range. 500 bp and 200 bp fragments are indicated by thick and thin arrows respectively. Lane 2-4: hdMT fragment (126 bp). Numbers from 2 to 4 indicate different colonies.

4.1.3 Cloning of β hdMT and α hdMT

EcoRI and *XhoI* digested PCR amplified β hdMT and α hdMT cDNAs were directly ligated with the *EcoRI* and *XhoI* digested pGEX-4T-2 expression vector as described in Materials and Methods. The resulting constructs were named pGEX β hdMT and pGEX α hdMT.

E. coli BL21(DE3) host cells were transformed with pGEX β hdMT and pGEX α hdMT constructs and screened for the presence of insert by double digestion and colony PCR (Figure 4.5 A and B. 4.6 A and B). The existence of a band around 206 bp for β hdMT and 200 bp for α hdMT was an indication of the insert in the constructs and the positive colonies were sequenced to validate the sequences.

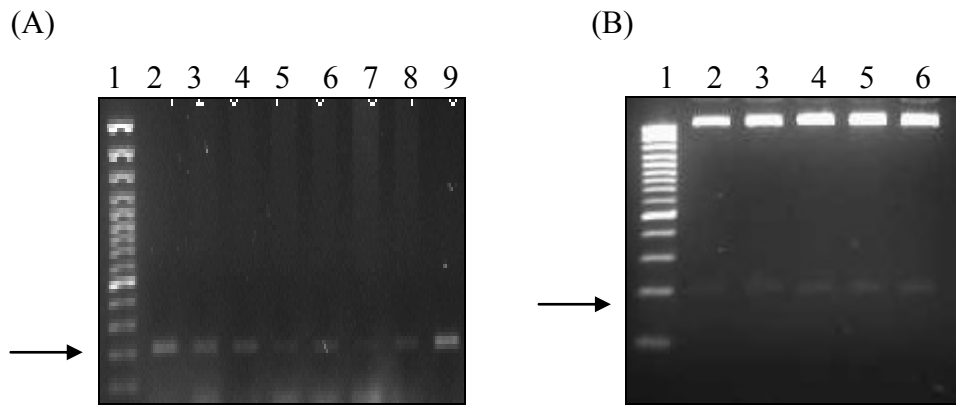


Figure 4.5: 2% Agarose gel analysis of (A) colony PCR (B) double digestion of pGEX β hdMT constructs. Numbers from (A) 2 to 9 (B) 2 to 6 specify different colonies. β hdMT migrate close to 206 bp. Lanes 1: (A) and (B) DNA ladder mix. Arrows specify 200 bp fragments.

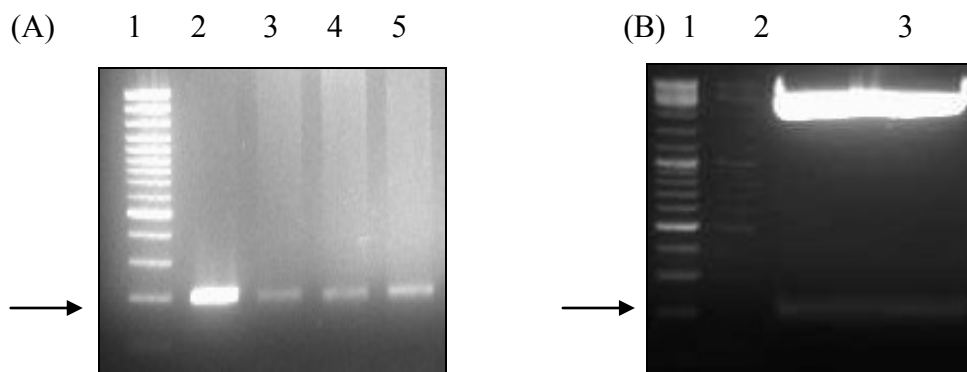


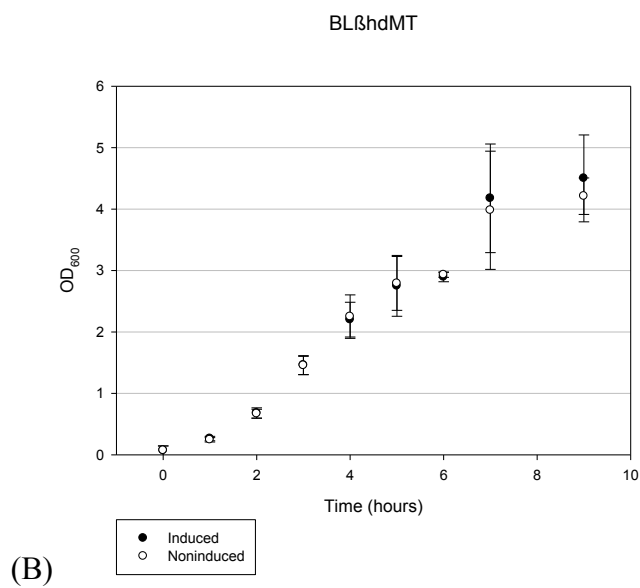
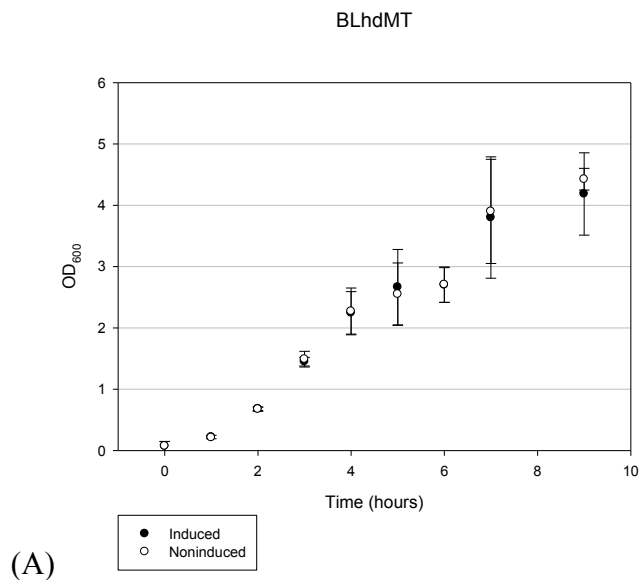
Figure 4.6: 2% Agarose gel analysis of (A) colony PCR (B) double digestion of pGEX α hdMT constructs. Numbers from (A) 2 to 5, (B) 3, points out different colonies. α hdMT migrate close to 200 bp. Lanes 1: (A) and (B) and Lane 2: (B) Mass ruler DNA ladder mix. Arrows specify 200 bp fragments.

4.2 Expression of the recombinant GSThdMT, GST β hdMT and GST α hdMT in *E. coli*

4.2.1 Monitoring growth of transformed *E. coli* cells

The growth of *E. coli* BL21(DE3) host cells transformed with pGEXhdMT (BLhdMT), pGEX β hdMT (BL β hdMT) and pGEX α hdMT (BL α hdMT) were monitored by measuring OD₆₀₀ values before and after induction with 0.75 mM IPTG. During the

growth of BL β hdMT and BL α hdMT transformed cells 0.1 mM Cd was added to the LB medium and protein expression was induced 3 hours after starting culture growth at an OD₆₀₀ of about 1 (Figure 4.7 A. B and C). According to their growth curves after 4 hours of induction the growth of BLhdMT, GST β hdMT and GST α hdMT expressing cells were not affected.



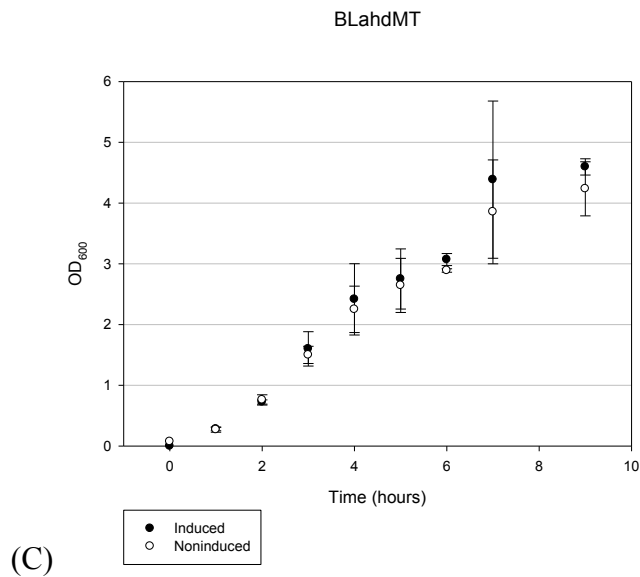


Figure 4.7: Growth curves of 0.75 mM IPTG induced BL21(DE3) bacterial cells containing (A) pGEXhdMT (B) pGEXβhdMT and (C) pGEXαhdMT. The data shown in the figures represent the means of two independent experiments. Standard deviations are indicated in the figures (error bars).

pGEX-4T-2 transformed (BLpGEX-4T-2) and untransformed BL21(DE3) grown in the presence of 0.1 mM Cd were also monitored for their growth as controls (Figure 4.8). Comparison of the growth curves showed that transformed bacterial cells grew at about the same rate as controls in the medium with Cd.

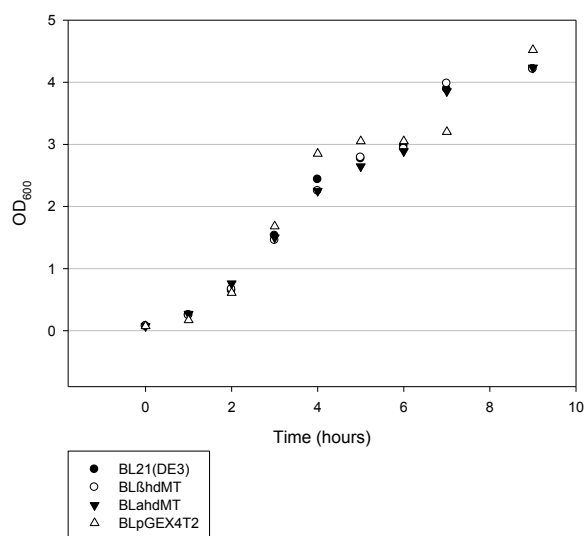


Figure 4.8: Growth curves of noninduced BL21(DE3), BLβhdMT, BLαhdMT and BLpGEX-4T-2 grown in the presence of 0.1 mM CdCl₂.

Comparison of the growth curves of BL β hdMT and BL α hdMT indicated that until induction and after induction both constructs grew at the same rate (Figure 4.9).

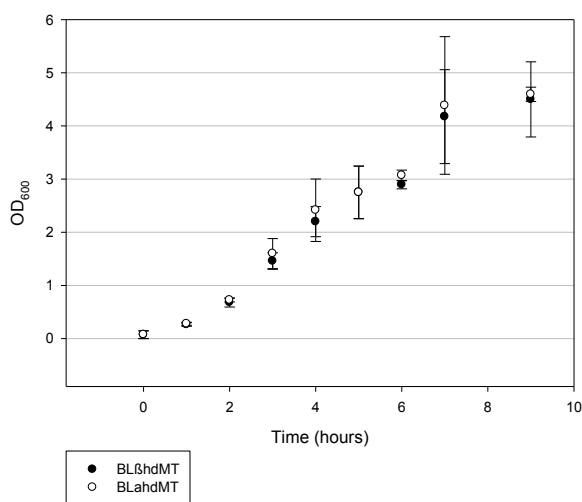


Figure 4.9: Growth curves of induced BL β hdMT and BL α hdMT grown in the presence of 0.1 mM CdCl₂.

4.2.2 Monitoring expression of the recombinant fusion proteins

Expression of GSThdMT (~30.8 kDa), GST β hdMT (~32.5 kDa) and GST α hdMT (~32.35 kDa) were monitored by SDS page. GSThdMT was expressed without adding Cd (Figure 4.10A). In a control experiment empty pGEX-4T-2 was introduced into BL21DE3 competent cells and expression of GST (27 kDa) was also monitored (Figure 4.10B). GST β hdMT and GST α hdMT were expressed both in the presence and in the absence of 0.1 mM Cd (Figures 4.11A and B). According to the gel results, the highest level of expression was achieved 5 hours after induction. Here also high levels of aggregation of the recombinant proteins were observed.

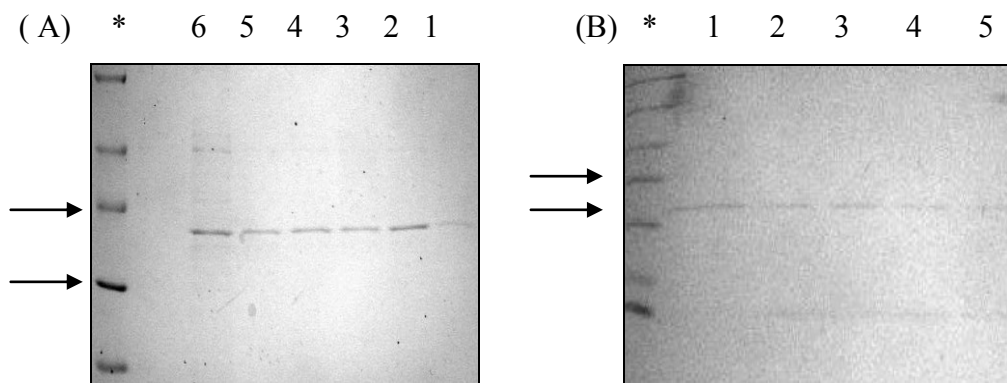


Figure 4.10: Time course of expression of (A) GSThdmt (B) GST monitored by 12 % SDS PAGE analysis. Lanes 1: (A) and (B) before induction. Lanes 2: (A) and (B) 1 hour after induction. Lanes 3: (A) and (B) 2 hours after induction. Lanes 4: (A) and (B) 3 hours after induction. Lanes 5: (A) and (B) 4 hours after induction. Lane 6: 5 hours after induction. Protein molecular weight markers are labeled with *. Arrows specify 35 kDa and 25 kDa respectively.

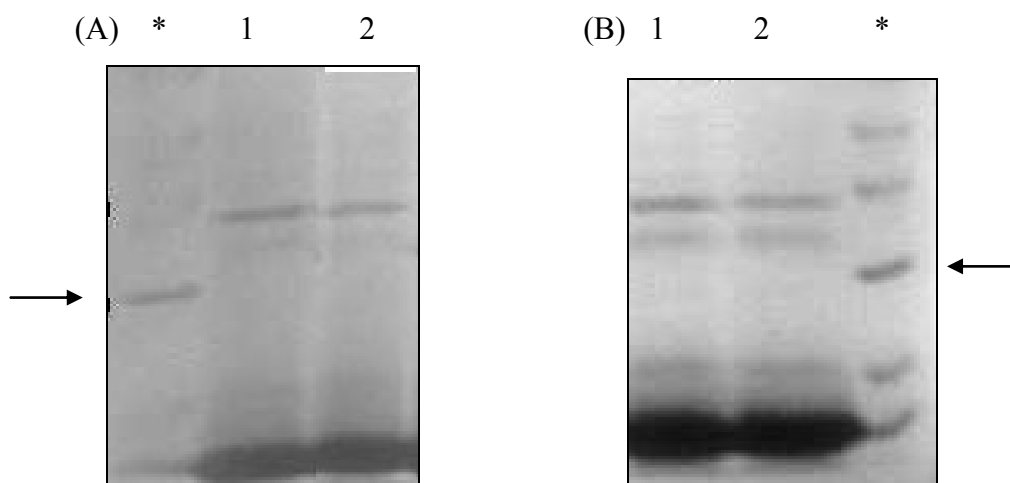


Figure 4.11: Expression of (A) GSTβhdMT (B) GSTαhdMT analyzed by 12 % SDS PAGE. Lanes 1: (A) GSTβhdMT expressed without Cd²⁺ after 4 hours of induction (B) GSTαhdMT expressed with Cd²⁺ after 5 hours of induction. Lanes 2: (A) GSTβhdMT expressed with Cd²⁺ after 4 hours of induction (B) GSTαhdMT expressed without Cd²⁺ after 5 hours of induction. Protein molecular weight markers are labeled with *. Arrows specify the 25kDa fragments.

4.3 Purification of recombinant GSThdMT, GSTβhdMT and GSTαhdMT

The basic procedure used for purification of recombinant proteins is summarized in Figure 4.12. Cell lysates from 1 L of bacterial cultures were loaded on the GStrap® FF column (GE Healthcare) and recombinant GST tagged proteins were eluted from the column with 10 mM reduced glutathione in Tris buffer (pH. 8). Eluted fractions were then pooled and dialysed overnight against HEPES buffer. The protein was further purified by using Hiload™ 16/60 Superdex™ 75 size exclusion column (GE Healthcare).

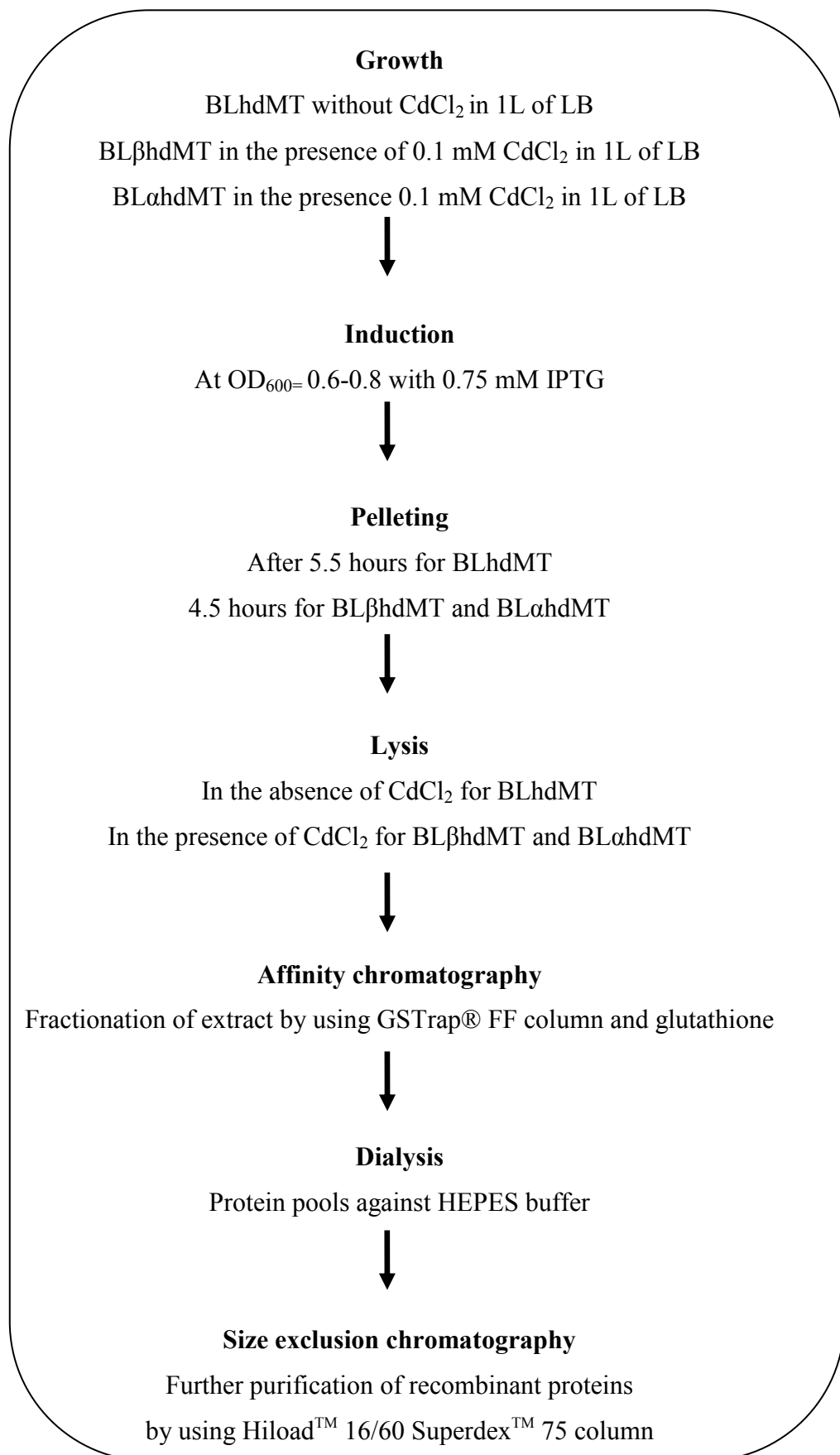


Figure 4.12: Schematic representation of the purification procedure of recombinant proteins.

4.3.1 Affinity Chromatography

GSThdMT, GSTβhdMT and GSTαhdMT are eluted with 10 mM reduced glutathione in Tris-HCl buffer (50mM Tris HCl, 100mM NaCl, 1 mM DTT, 0.5 mM PMSF, 1 protease inhibitors cocktail tablet, pH8). GSThdMT started to be eluted from the GST affinity column at 3ml and GSTβhdMT and GSTαhdMT at 4 ml (Figures 4.13A, B and C). Peak fractions were pooled according to the A_{280} measurements. The total protein eluted from the affinity column ranged from 5 mg to 21 mg in 4 to 5 ml for GSThdMT from 1 to 3 liters of culture. 14 mg to 22 mg in 6 to 7 ml for GSTβhdMT and 9.9 mg in 6 ml for GSTαhdMT from 1 liter of culture.

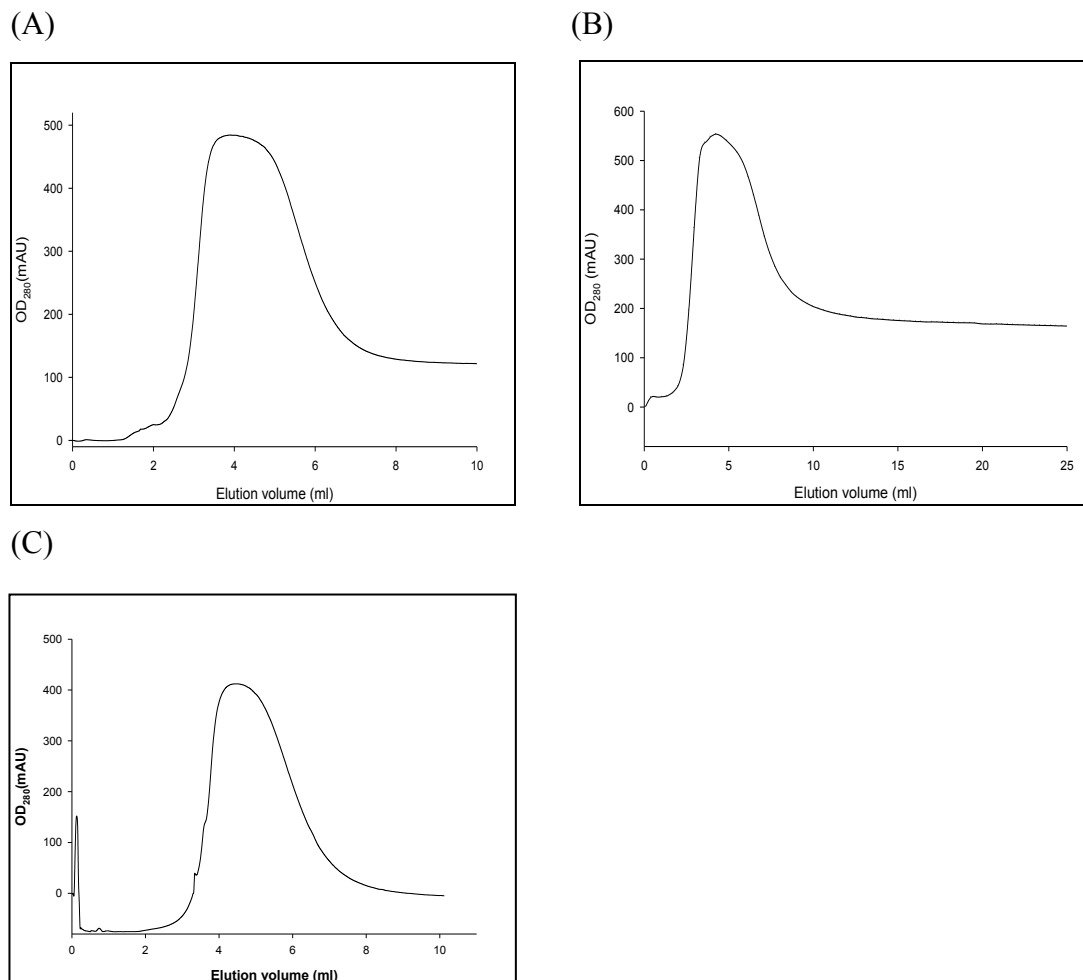


Figure 4.13: Elution profiles of (A) GSThdMT, (B) GSTβhdMT and (C) GSTαhdMT from GSTrap® FF affinity column.

Analyses of pools from affinity purification by 12% SDS-PAGE showed the expected major band around 30.8 kDa corresponding to GSThdMT, 32.5 kDa corresponding to GST β hdMT and 32.3 kDa corresponding to GST α hdMT (Figure 4.14). High molecular weight (hmw) and low molecular weight (lmw) bands were also visible on the gels of the three proteins. Lmw bands corresponded to degradation products whereas hmw bands indicated oligomeric species of the purified proteins. When GSThdMT was analyzed by 8% Native-PAGE a major band corresponding to the protein and a faint band corresponding to aggregated species were present. In the pools of GST β hdMT and GST α hdMT more than one band was observed indicating the presence of heavy aggregation (Figure 4.15).

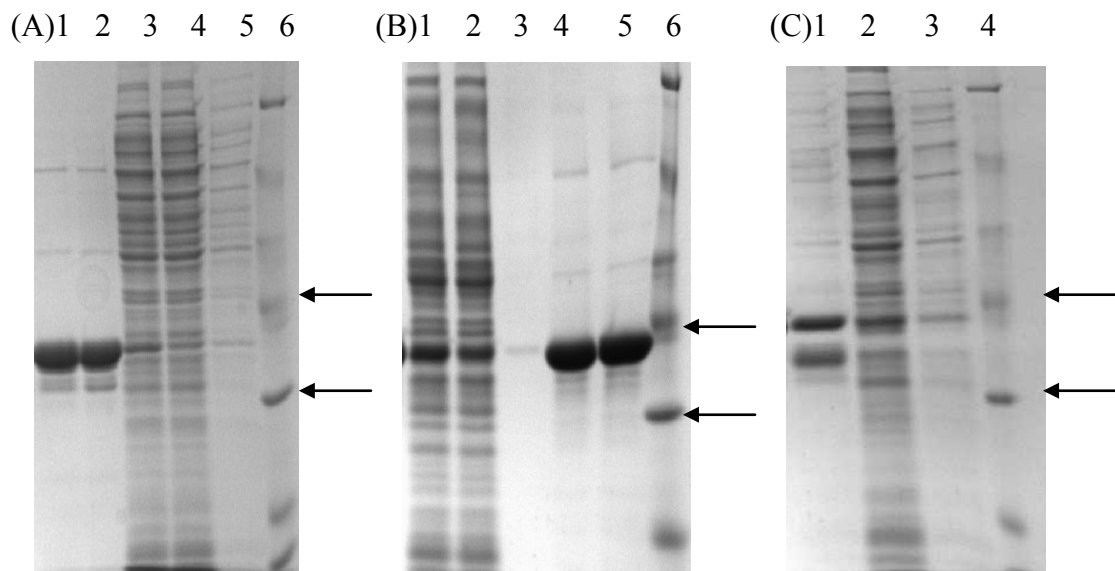


Figure 4.14: 12% SDS PAGE analysis of purified samples of (A) GSThdMT (B) GST β hdMT (C) GST α hdMT. Samples from different steps are indicated in Figure 4.12. (A) Lane 1: Before dialysis. Lane 2: After dialysis. Lane 3: Cell lysate. Lane 4: Flow through. Lane 5: Wash. Lane 6: Protein molecular weight marker. (B) Lane 1: Cell lysate. Lane 2: Flow through. Lane 3: Wash. Lane 4: Before dialysis. Lane 5: After dialysis. Lane 6: Protein molecular weight marker. (C) Lane 1: After dialysis. Lane 2: Cell lysate. Lane 3: Wash. Lane 4: Protein molecular weight marker. Arrows specify 35 kDa and 25 kDa respectively.

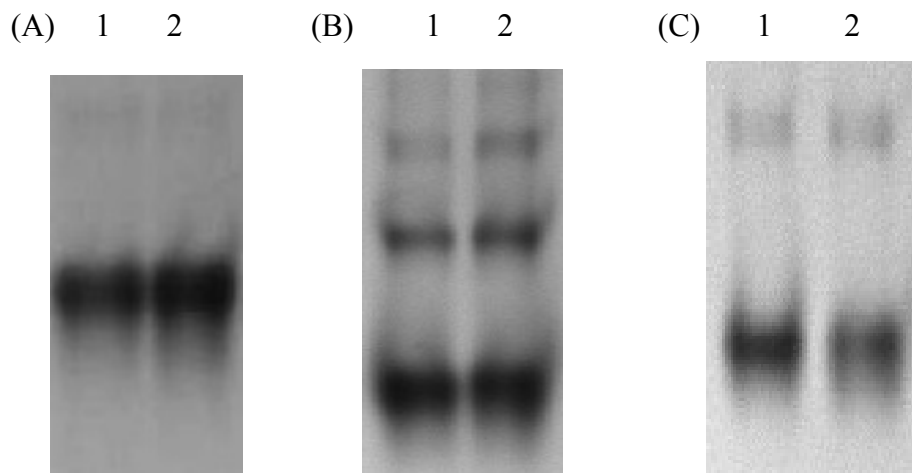


Figure 4.15: Native-PAGE analysis of (A) GSThdMT (B) GSTβhdMT (C) GSTαhdMT purified from GST affinity column. Lanes 1: Before dialysis. Lanes 2: After dialysis.

4.3.2 Size Exclusion Chromatography

4.3.2.1 Purification of GSThdMT by size exclusion chromatography

In the size exclusion chromatography elution profile of GSThdMT two well resolved peaks were observed. Peak II corresponds to the dimer of GSThdMT. Peak II 51-63 ml (Figure 4.16). Fractions were stored at +4 °C separately until further use. According to the calibration of the column peak I of GSThdMT correspond to 125 kDa and peak II corresponds to 60 kDa.

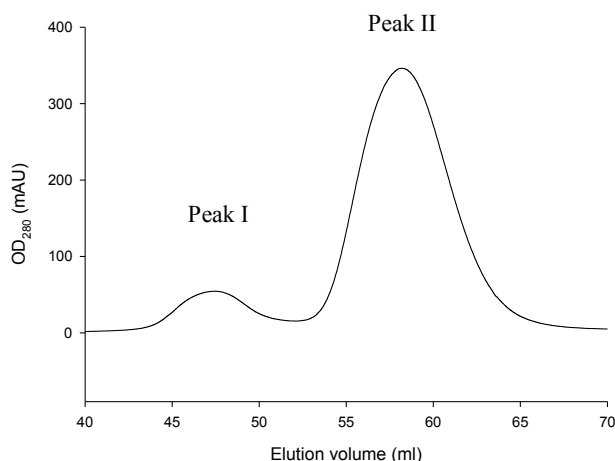


Figure 4.16: Elution profile of GSThdMT from Hiload™ 16/60 Superdex™ 75 gel filtration column.

The fractions collected during size exclusion chromatography were analyzed by 12% SDS-PAGE and 8% Native-PAGE (Figure 4.17 and 4.18). A major band at 30.8 kDa was observed together with hmw bands. Fractions on the front part of peak II from the size exclusion column showed more aggregates than the fractions on the back part of this peak where some degradation products were also observed.

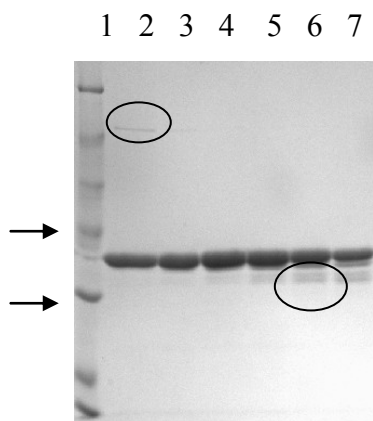


Figure 4.17: SDS-PAGE analysis of fractions from purification of GSThdMT. Lanes 1: Protein molecular weight marker. Lanes from 2 to 7: Fractions from peak II of size exclusion column. Lane 5: Top fraction. Arrows specify the 35 kDa and 25 kDa respectively.

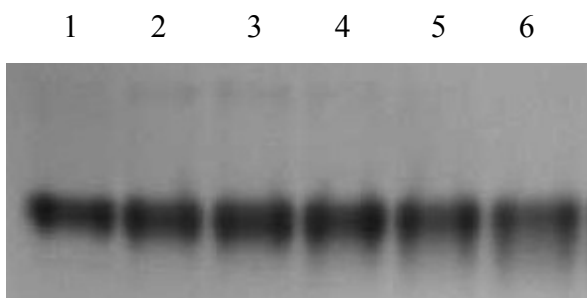


Figure 4.18: Native-PAGE analysis of fractions after purification of GSThdMT. Lanes from 1 to 6: Fractions from peak II of gel filtration column. Lane 4: Top fraction.

The top fraction in peak II was analyzed by DLS in order to monitor monodispersity which is necessary for small angle X-ray solution scattering measurements (SAXS). According to the size distribution by intensity only a small amount of aggregates existed in the GSThdMT fraction (Figure 4.19).

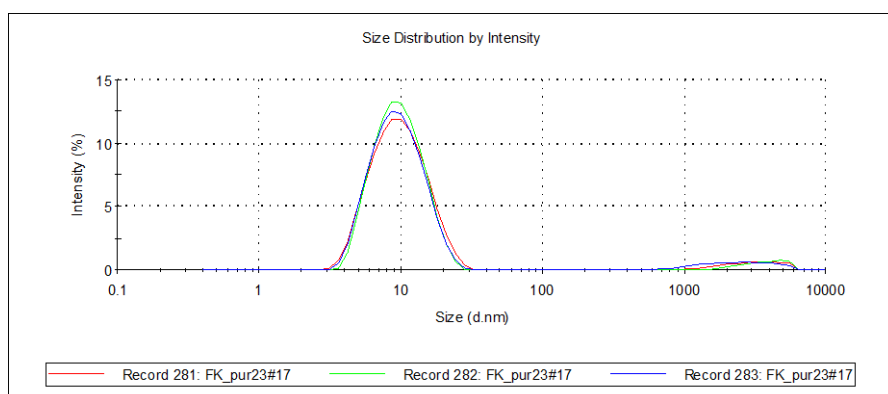


Figure 4.19: Size distribution by intensity DLS measurements of GSThdMT eluted from size exclusion chromatography.

4.3.2.1.1 Optimization of the expression conditions for GSThdMT

During the monitoring of expression of GSThdMT, aggregates as well as degradation products of the recombinant protein were observed by SDS-PAGE analysis. This may be due to the chaperoning not being able to function properly under the conditions of overproduction of the recombinant protein in the cell and protein misfolding. To overcome this problem, lowering the expression temperature, decreasing the amount of inducer and increasing the concentration of osmolytes can be

tried (Diament *et al.*, 2003). In order to prevent aggregation and misfolding leading to degradation, expression was done at 37⁰C in the presence of the osmolyte betaine (5mM) and NaCl (0.5M final) which induces osmolyte accumulation. This did not help. However, to overcome the aggregation problem, in a different trial, 10 mM an organic compound benzyl alcohol (BA) which induces chaperone overexpression was used during expression and cells were grown at 20⁰C for 20 hours. This method was also not effective in preventing protein degradation.

Consequently it was decided to grow the bacteria at 37⁰ C without any additives.

4.3.2.1.2 Determination of storage conditions for GSThdMT

In order to find the optimum condition for storage, GSThdMT fractions were incubated at 4⁰ C, -20⁰ C and -80⁰ C in the presence and absence of 50% glycerol and 0.5 mM PMSF. Fractions were analyzed by SDS- and Native-PAGE analysis and DLS in the second and fifth day after purification. The SDS- and Native-PAGE patterns of the two sets of samples were almost identical (Figure 4.20A, B and Figure 4.21A, B). The samples of the second day contained fewer aggregates than those of the fifth day.

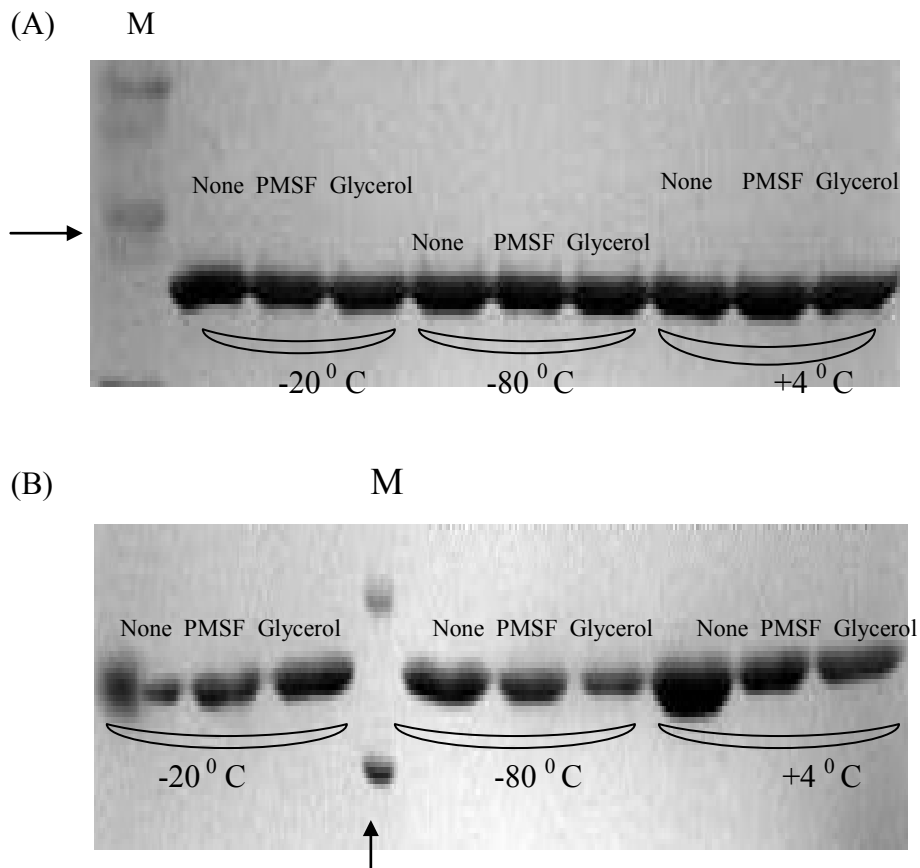


Figure 4.20: 12% SDS PAGE analysis of GSThdMT fractions stored for (A) two days (B) five days at different temperatures and with/without additives. Storage temperatures and additives are indicated. M corresponds to protein molecular weight markers. Arrows specify 25kDa.

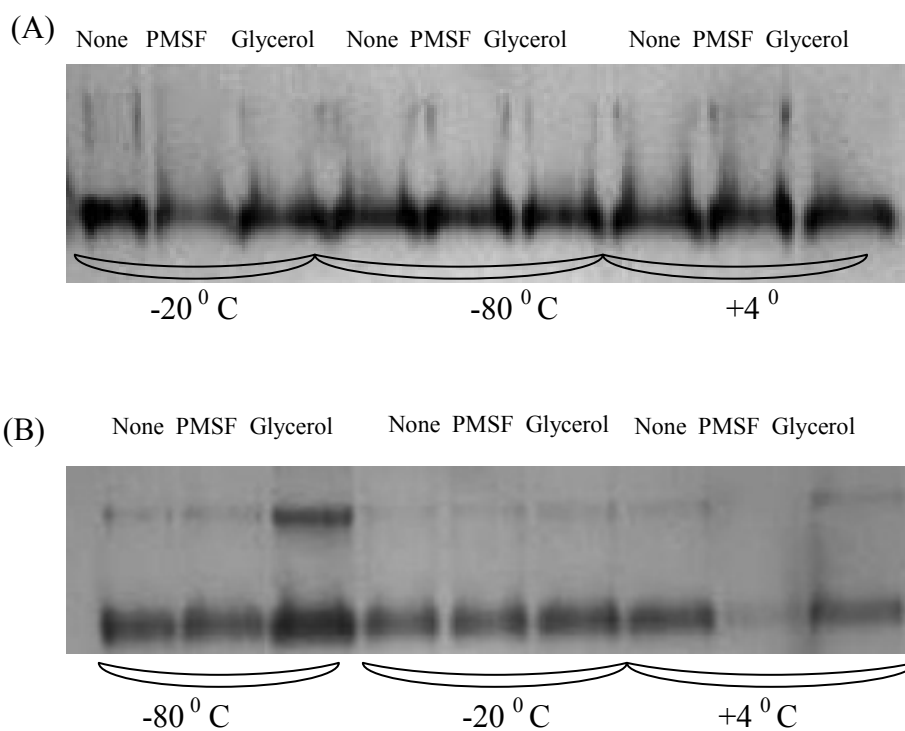
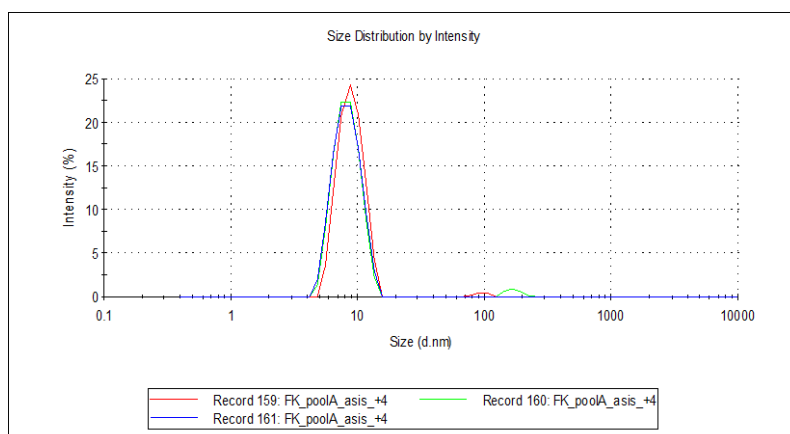


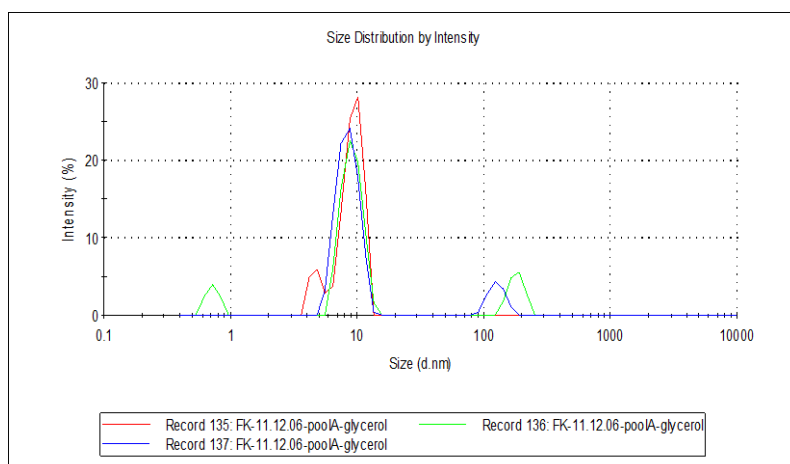
Figure 4.21: 8% Native PAGE analysis of GSThdMT fractions stored for (A) two days (B) five days at different temperatures and with/without additives. Storage temperatures and additives are indicated.

According to the DLS measurements, however, in the second day the intensity distribution of scattered light from fractions stored at different conditions gave different results. Although some aggregates were present, a single peak centered around 10 nm indicated that the fractions stored at 4⁰C with and without 50% glycerol and 0.5 mM PMSF contained mainly dimers but the fractions without additives had a larger fraction of dimers and less aggregation (Figure 4.22A, B and C).

(A)



(B)



(C)

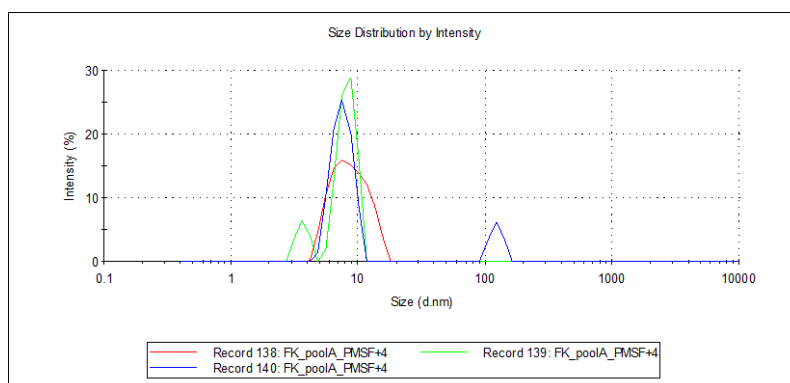
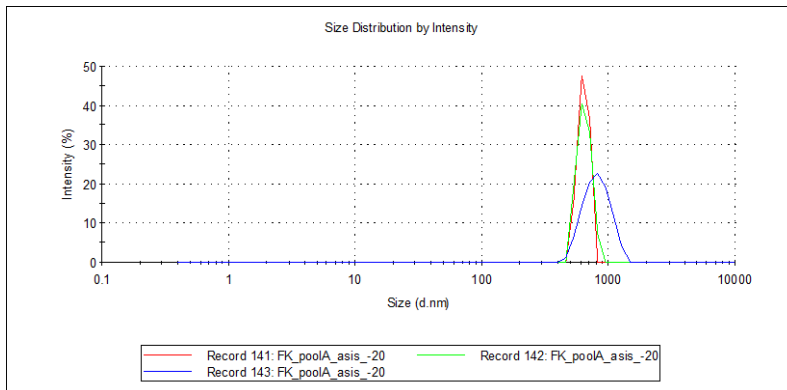


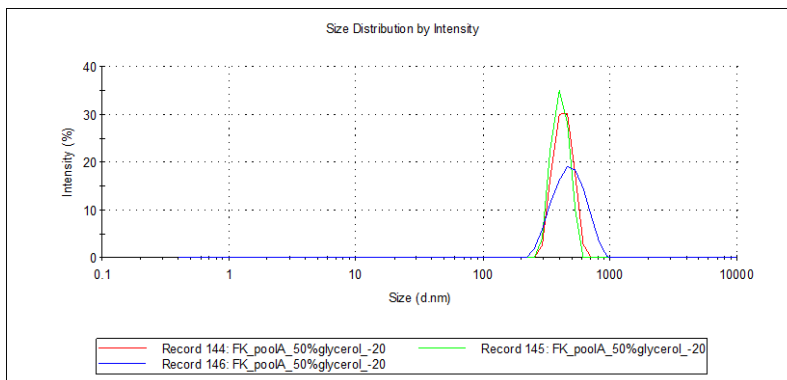
Figure 4.22: Size distribution by intensity profile of GSThdMT (A) without additive (B) with 50% glycerol (C) with 0.5 mM PMSF stored at 4 °C for two days.

In other fractions stored at -20°C and -80°C with and without additives a single peak centered around 1000 nm indicated that the protein heavily aggregated but the aggregates were smaller in fractions stored at -20°C –the peak was between 100 nm and 1000 nm- compared to the aggregates at -80°C (Figure 4.23A, B and C and Figure 4.24A, B and C).

(A)



(B)



(C)

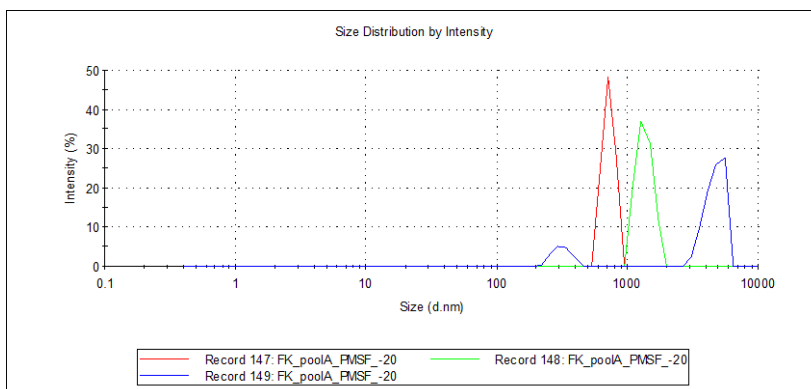
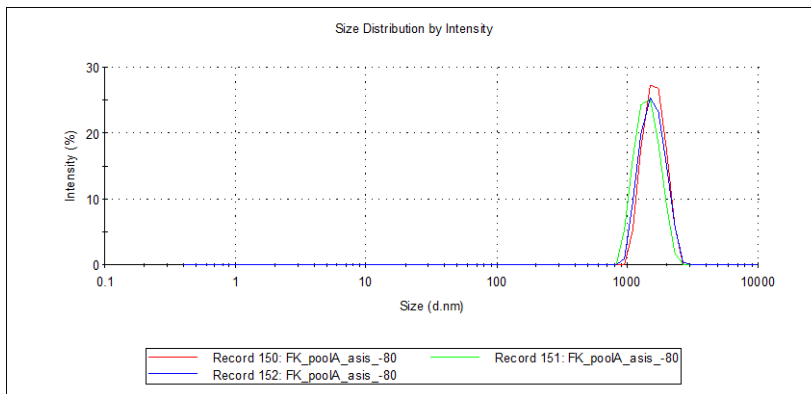


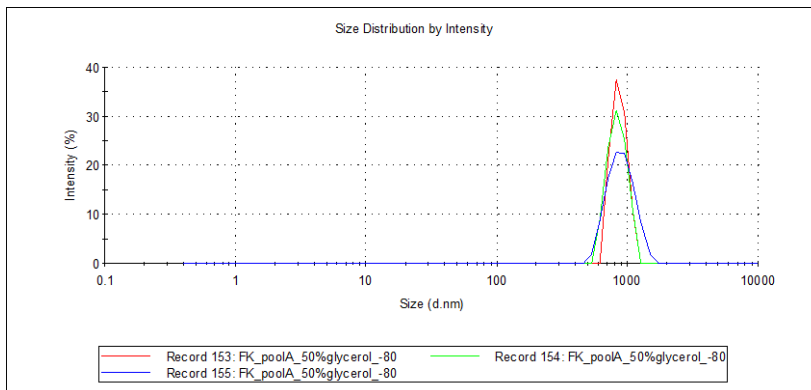
Figure 4.23: Size distribution by intensity profile of GSThdMT (A) without additive (B) with 50% glycerol (C) with 0.5 mM PMSF stored at -20°C for two days.

The peak observed between 1000 and 10000 nm in the size distribution by intensity of the fractions stored at -80 °C indicated that they were heavily aggregated. But the fractions with 50% glycerol and 0.5 mM PMSF had a peak around 1000 nm indicating that the aggregation is less severe compared to the fraction without any additives (Figure 4.24A, B and C).

A



B



C

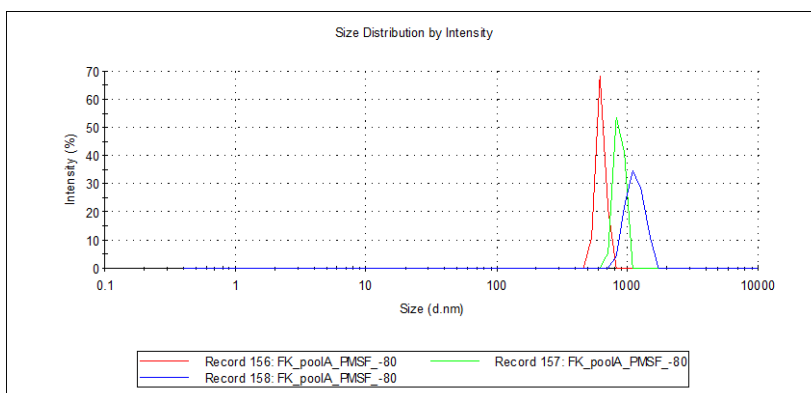


Figure 4.24: Size distribution by intensity profile of GSThdMT (A) without additive (B) with 50% glycerol (C) with 0.5 mM PMSF stored at -80°C for two days.

+ 4°C without using additives was chosen for storage condition.

4.3.2.1.3 Western blot analysis of GSThdMT

GSThdMT was further analysed by western blot in order to further confirm that the isolated protein was GSThdMT. GST-HRP conjugate was used to show the presence of GST. A 0.2 mg/ml GSThdMT sample was first run on a 12% SDS gel and then incubated with 1:20000 diluted anti-GST HRP conjugate. When the protein is overloaded it is possible to detect an lmw band, close to the main GSThdMT band corresponding to a degradation product of the recombinant protein. This degradation is likely to take place within the hinge region since the GST antibody is still able to bind to GST (Figure 4.25).

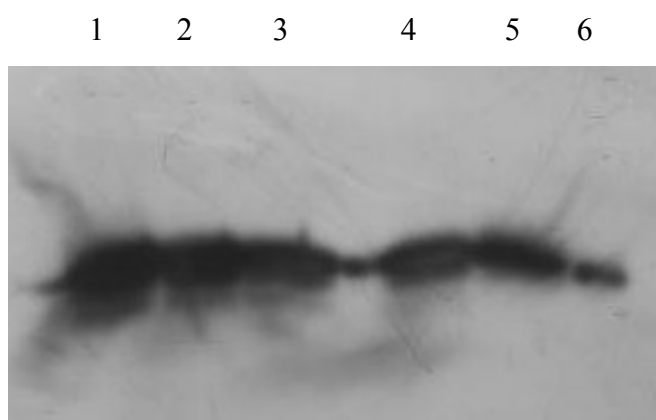


Figure 4.25: Western blot analysis of GSThdMT fractions eluted from HiloadTM 16/60 SephadexTM G75 column. Lane 1: 1.1 μg . Lane 2: 0.55 μg . Lane 3: 0.275 μg . Lane 4: 0.162 μg . Lane 5: 0.32 μg . Lane 6: The sample passed from lane 5 during loading to the gel.

4.3.2.1.4 Thrombin cleavage of GSThdMT

In order to determine whether hdMT can be cleaved from the GST partner by thrombin, first a small scale cleavage was performed with 1.15 mg/ml of purified GSThdMT. Samples were taken before and during the incubation with thrombin and run on 16% Tris-tricine gels. Two bands, one at about 25 kDa corresponding to GST and another small molecular band could be detected on the gels. hdMT whose expected size is 4.1 kDa runs very close to the dye front (Figure 4.26).

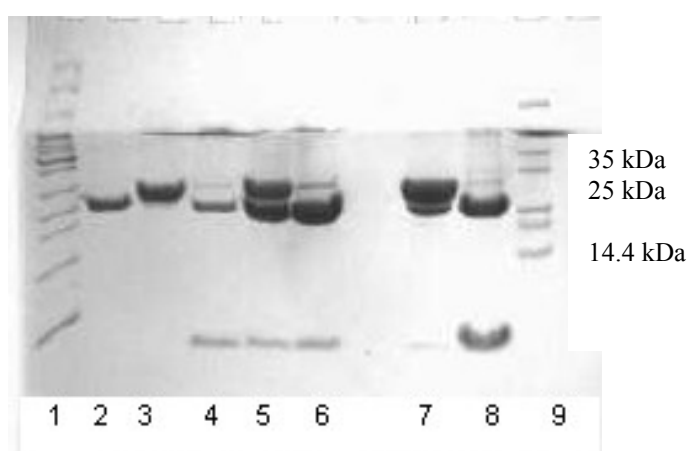


Figure 4.26: 16% Tris-tricine PAGE analysis of thrombin cleavage of GSThdMT. Lane 1: Protein ladder (Fermentas). Lane 2: GST. Lane 3: Undigested GSThdMT. Lane 4: 1 hour of incubation with thrombin. Lane 5: 4 hours of incubation with thrombin. Lane 6: o/n incubation with thrombin. Lane 7: 45 min of thrombin cleavage. Lane 8: Concentrated cleaved GSThdMT (after 3 hours of cleavage). Lane 9: Protein molecular weight marker.

In order to characterize hdMT by itself, the protein should be purified after cleavage. For this purpose 3 liters of GSThdMT liquid culture were prepared and the protein was purified from the pellet. After 23 hours of cleavage by thrombin the protein was loaded to the HiloadTM 16/60 SephadexTM G-75 column. According to the elution profile of cleaved GSThdMT cleaved components were separated (Figure 4.27). Lanes 5, 6 and 7 are samples from the first, second and third peaks and bands correspond to uncleaved and partially cleaved GSThdMT. But it was not possible to detect the cleaved

hdMT on the gel no bands were observed in lanes 8 and 9 (Figure 4.28). It is possible that some portion of hdMT was cleaved from GST and since the cleaved product was dilute-as can be seen from the y-axis of Figure 4.27-at the expected band size on SDS-PAGE in Figure 4.28 was not observed.

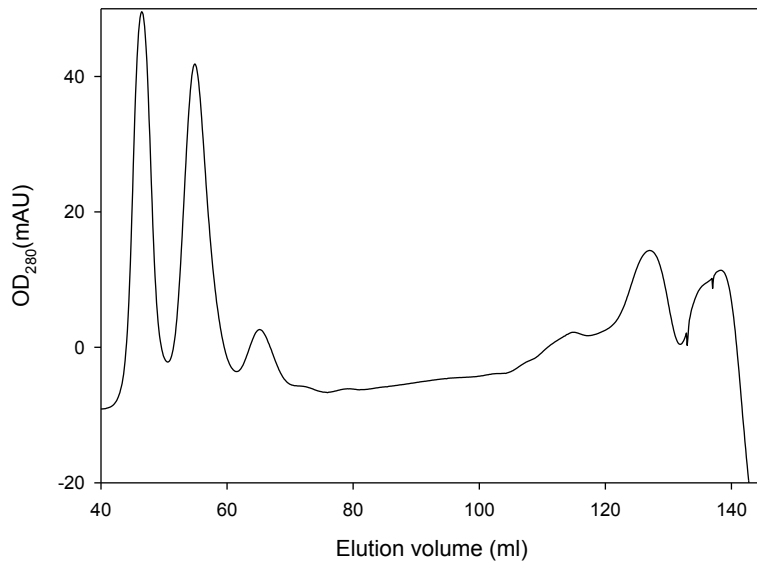


Figure 4.27: Elution profile of cleaved GSThdMT on Hiload™ 16/60 Superdex™ 75 gel filtration column.

1 2 3 4 5 6 7 8 9



Figure 4.28: 16% Tris-tricine PAGE analysis of GSThdMT thrombin cleavage products. Lane 1: Protein molecular weight marker. Lane 3: Sample before concentration. Lane 4: Concentrated sample loaded onto Hiload™ 16/60 Sephadex™ G-75. Lane 5: Fraction from the first peak. Lane 6: Fraction from the second peak.

Lane 7: Fraction from the third peak. Lane 9: Fraction from the fourth peak. Lane 10: Fraction from the fifth peak. Arrow specifies 25 kDa.

4.3.2.2 Purification of GST β hdMT and GST α hdMT by size exclusion chromatography

In the size exclusion chromatography elution profiles of GST β hdMT and GST α hdMT two or three peaks were observed depending on the amount of protein loaded to the column. When the amount of GST β hdMT loaded was between 9.5 mg and 11 mg two poorly resolved peaks were observed. The fractions in the second peak were eluted between 54-64 ml. According to the calibration of the column peak I of GST β hdMT corresponds to 129 kDa and peak II corresponds to 69 kDa. When the load amount was about 8 mg of protein, three poorly resolved peaks could be observed. In this case the fractions in the third peak was eluted between 58-68 ml. Similar to the previous elution profile peak I corresponds to 129 kDa, peak II corresponds to 79 kDa and peak III corresponds to 50.1 kDa. Peak II (Figure 4.29A) and Peak III (Figure 4.29B) in the elution profile corresponds to the dimer of the recombinant fusion protein. Fractions were stored at +4 °C separately until further use.

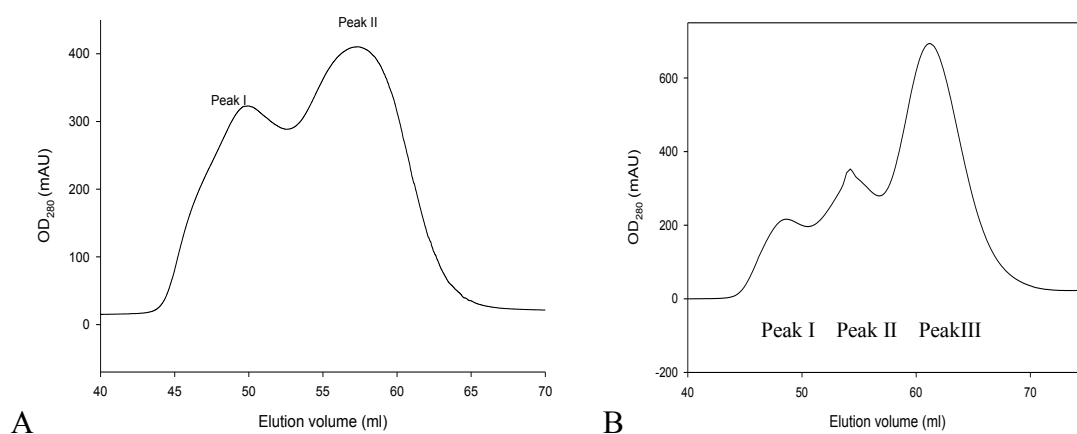


Figure 4.29: Elution profiles of GST β hdMT (A) 11 mg and (B) 8.25 mg loaded to HiloadTM 16/60 SuperdexTM 75 gel filtration column.

Size exclusion of GST α hdMT yielded an elution profile similar to that of GST β hdMT. When the amount loaded exceeded 8 mg two poorly resolved peaks were observed. The recombinant protein eluted between 54-64 ml and according to the calibration peak I corresponds to 129 kDa and peak II corresponds to 69 kDa (Figure 4.

29 (A)). The position of Peak II corresponds to the dimer of the recombinant protein. When protein amounts below 8.25 mg were loaded on the size exclusion column, three peaks were seen and the protein eluted between 55-65 ml. According to the calibration of the column peak I of GST α hdMT correspond to 120 kDa, peak II to 79 kDa and peak III to 50 kDa. Fractions were stored at +4 °C separately until further use.

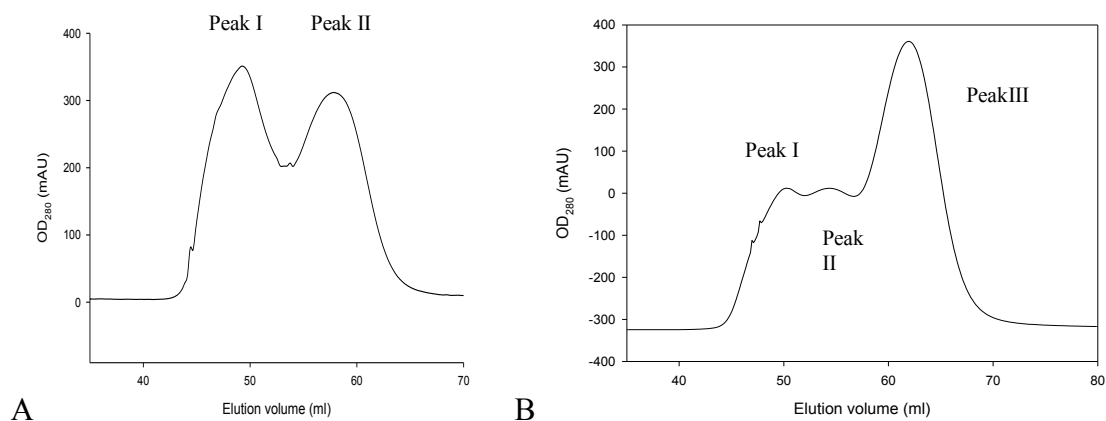


Figure 4.30: Elution profiles of GST α hdmt (A) 11 mg and (B) 8 mg loaded to Hiload™ 16/60 Superdex™ 75 gel filtration column.

Samples eluted from size exclusion chromatography were analyzed by SDS-PAGE to monitor aggregation and degradation. As can be seen from the analyses shown in Figures 4.31 A and B hmw bands are present in the fractions from the size exclusion column. Fractions on the front part of peak II (when loaded amount was more than 8.25 mg) and peak III (when loaded amount was 8.25 mg and less) from the size exclusion column contained more aggregates than the fractions on the back part of this peak, where different levels of degradation products are also observed for the two proteins. GST α hdmt seems more susceptible to proteolysis. Although GST β hdmt seemed to be less degraded, it is possible that it degraded as much as GST α hdmt but that this cannot be detected by SDS PAGE analysis. In peaks II (when loaded amount was more than 8.25 mg) and peak III (when loaded amount was 8.25 mg and less) for the two proteins, fractions on the back part of the peak are degraded than those of the front part.

In both cases peak II top fraction in lane number 4 for GST β hdmt and GST α hdMT appeared to be suitable for SAXS and further analyses.

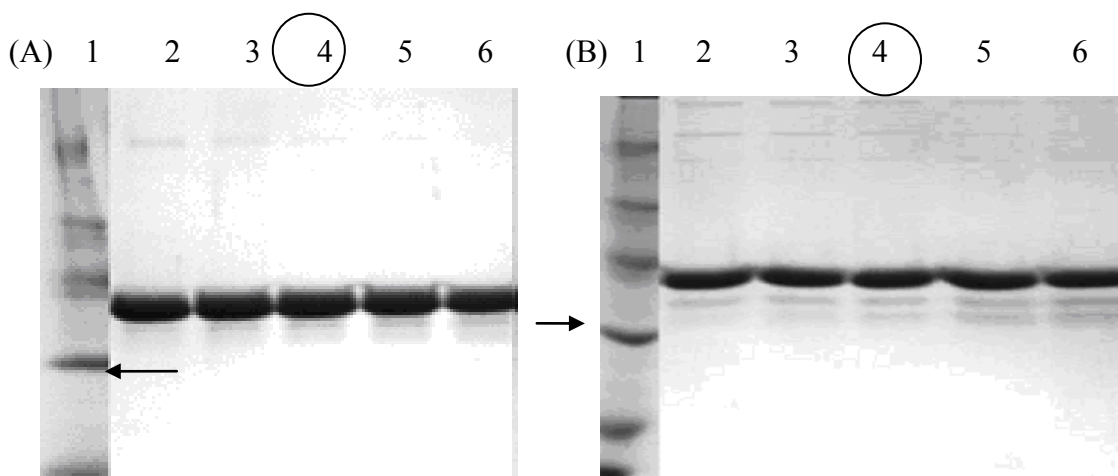


Figure 4.31: SDS-PAGE analysis of purified fractions of GSTdMT constructs. (A) GST β hdMT and (B) GST α hdMT. Lanes 1: Protein molecular weight marker. Lanes from 2 to 6 fractions from peak II of the gel filtration column. Lanes 4: Circled (A) and (B) Top fraction of GST β hdMT and GST α hdMT. Arrows specify 25 kDa.

Samples eluted from size exclusion chromatography were also analyzed by Native PAGE to monitor hmw and lmw bands. As can be seen from the Native PAGE analyses in Figures 4.32 A and B proteins were already aggregated after elution from affinity column and higher oligomeric forms could not be totally removed by size exclusion chromatography.

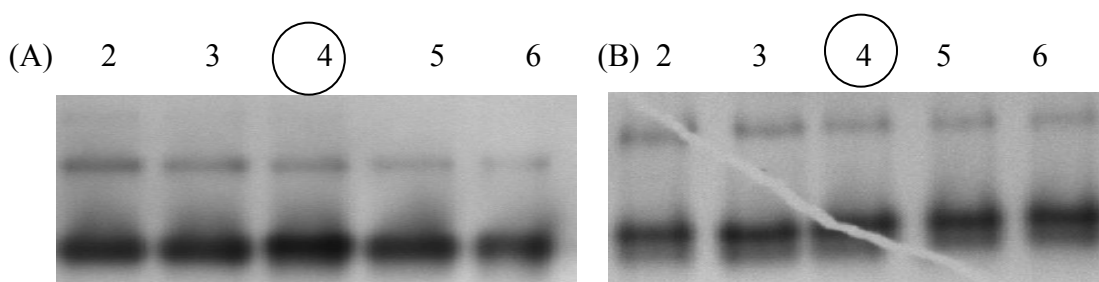
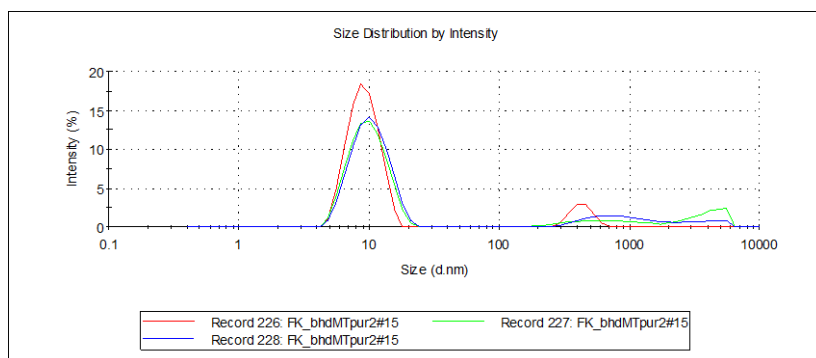


Figure 4.32: Native-PAGE analysis of fractions of purified GSTdMT constructs. (A) GST β hdMT and (B) GST α hdMT. The top fraction is indicated with a circle. Lanes are labeled as in Figure 4.30A and B.

Top fractions were analyzed also by DLS in order to monitor the degree of oligomerization. According to the size distribution by intensity there were very small amount of aggregates in fractions of GST β hdMT and GST α hdMT (Figure 4.33A and B).

(A)



(B)

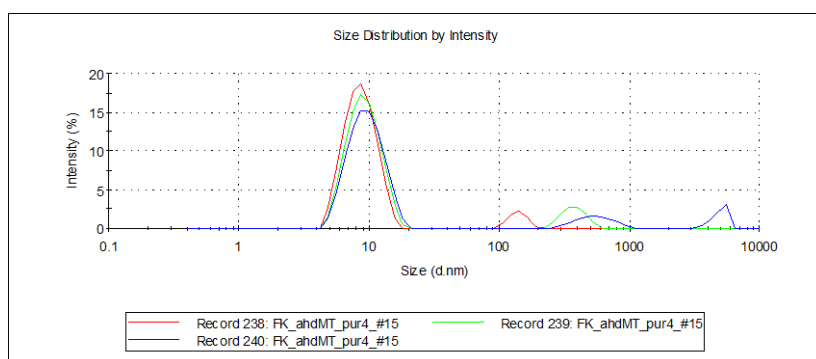


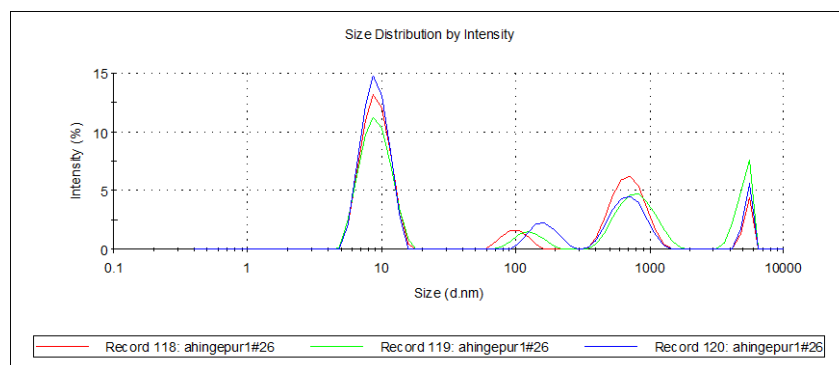
Figure 4.33: Size distribution by intensity DLS measurements of GSTdMT constructs. (A) GST β hdMT and (B) GST α hdMT fractions eluted from size exclusion chromatography.

4.3.2.2.1 Optimization of expression condition for GST α hdMT

Comparison of expression of GSTdMT constructs by SDS-PAGE analysis revealed that GST α hdMT degraded and aggregated more than GST β hdMT. In an attempt to minimize degradation and aggregation the amount of Cd²⁺ used during expression of GST α hdMT was increased from 0.1 mM to 0.3 mM although higher amounts of Cd²⁺ were avoided because of its toxic effect on the bacteria. The impact of

higher amount of Cd^{2+} on the aggregation and degradation was monitored by DLS measurements of the purified fractions and a reduced aggregation was detected when 0.3 mM Cd^{2+} was used regularly during the expression of GST α hdMT (Figure 4.34 A and B).

(A)



(B)

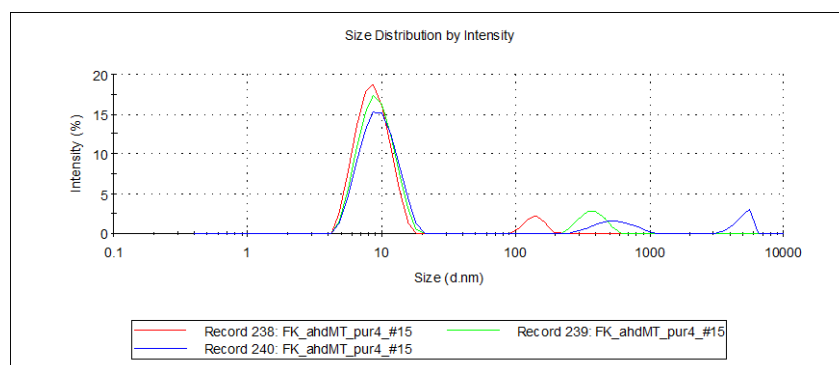


Figure 4.34: Dynamic light scattering (DLS) measurements of purified GST α hdMT. Expression was done in the presence of (A) 0.1 mM Cd^{2+} and (B) 0.3 mM Cd^{2+} .

4.4 Determination of Cd^{2+} /Protein ratio for GST β hdMT and GST α hdMT

In order to determine the binding ratio of Cd^{2+} to GST β hdMT and GST α hdMT, concentration of GST β hdMT and GST α hdMT were calculated from A_{280} absorbance and bound Cd^{2+} was measured by ICP-OES.

According to the Z test, although there were some differences in the calculated Cd^{2+} concentration of the same samples (3A, B, C and D), they were within

the upper and lower limits (Table 4.1). This indicated that ICP-OES measurements of the samples were precise.

Table 4.1: ICP-OES results of samples with known concentrations, calculated Cd²⁺ concentration (μM), average values and standard deviations. Numbers indicate different samples with the same concentration, 1, 2, 3 are different samples. 3A, B, C and D are the aliquots of the same sample.

Molarity (μM)	Samples	Cd214.4 ICP measurement(ppm)	Calculated Cd amount (μM)	Average	Standard deviation	Z –test	Z –test
						Upper value	Lower value
0.003 (μM)	(1)	0.000334	0.0029				
	(2)	0.000309	0.0027				
	(3A)	0.000337	0.0033	0.003125	0.000435	0.003977	0.002273
	(3B)	0.000401	0.0035				
	(3C)	0.000364	0.0032				
	(3D)	0.000278	0.0032				
0.008 (μM)	(1)	0.000673	0.006				
	(2)	0.000759	0.0067				
	(3A)	0.000825	0.0073	0.007625	0.001056	0.009695	0.005555
	(3B)	0.000982	0.0087				
	(3C)	0.000707	0.0063				
	(3D)	0.000919	0.0082				
0.03 (μM)	(1)	0.002892	0.026				
	(2)	0.003052	0.027				
	(3A)	0.01272	0.113	0.11525	0.003862	0.12282	0.10768
	(3B)	0.013643	0.121				

	(3C)	0.012702	0.113				
	(3D)	0.002892	0.026				
0.05 (μM)	(1)	0.005154	0.046				
	(2)	0.005141	0.046				
	(3A)	0.008743	0.077	0.77	0	0.77	0.77
	(3B)	0.008663	0.077				
	(3C)	0.008969	0.077				
	(3D)	0.008689	0.077				
0.1 (μM)	(1)	0.010185	0.09				
	(2)	0.010578	0.094				
	(3A)	0.01131	0.1	0.36975	0.540167	1.428477	-0.68
	(3B)	0.011163	0.099				
	(3C)	0.011248	0.1				
	(3D)	0.132612	1.18				

According to different purifications the average Cd²⁺ /Protein ratio was found to be 1.53 ± 0.6 for GSTβhdMT when expressed and purified in the presence of 0.1 mM CdCl₂ and 1.5 ± 0.8 and 2.1±0.68 for GSTαhdMT when expressed and purified in the presence of 0.1 and 0.3 mM CdCl₂ respectively (Table 4.2).

Table 4.2: Cd/Protein binding ratio for (A) GSTβhdMT and (B) GSTαhdMT * proteins purified in the presence of 0.3 mM CdCl₂.

(A)

	Cd²⁺ (μM)	GSTβhdMT (μM)	Cd²⁺ /protein
Sample 1	91	65	1.4
Sample 2	94	45	2.08
Sample 3	50	85	0.6
Sample 4	9	10	0.9
Sample 5	50	20	2.5
Sample 6	46	33	1.39
Sample 7	47	33	1.42
Sample 8	41	21	1.95
Sample 9	53	14	3.78 *
Average±Stdev			1.53 ± 0.6

(B)

	Cd²⁺ (μM)	GSTαhdMT (μM)	Cd²⁺ /protein
Sample 1	8.3	8.95	0.93
Sample 2	8.2	17	0.48
Sample 3	71.4	29.05	2.45
Sample 4	83.75	53.25	1.57
Average±Stdev			1.5 ± 0.8

	Cd²⁺ (μM)	GSTαhdMT (μM)	Cd²⁺ /protein
Sample 5	9.375	4.04	2.3 *
Sample 6	77.6	29.05	2.67 *
Sample 7	101.25	75.03	1.35 *
Average±Stdev			2.1±0.68

The Cd^{2+} /Protein ratio of GST α hdMT was higher than expected when the protein was expressed and purified in the presence of 0.3 mM CdCl_2 . To investigate whether this was a property of the protein or it was due to the higher amount of Cd^{2+} used during expression and cell lysis (0.3 mM CdCl_2), GST α hdMT was expressed and cells were lysed in the presence of 0.1 mM CdCl_2 . Under this condition the Cd^{2+} /Protein ratio was found to be similar to that observed with GST β hdMT.

4.5 UV-Vis Spectrophotometric Characterization of GST β hdMT and GST α hdMT

Due to characteristic absorption bands originating from the metal ions, MTs have unique UV-vis spectra features. The position and intensity of the charge transfer bands are indicative of bound metals.

In the UV-vis spectra of 1.2 mg/ml of GST β hdMT, 1.5 mg/ml GST α hdMT and 2.2 mg/ml GSThdMT between 220 and 300 nm a peak at 280 nm which is due to the aromatic residues in GST was observed. A metal charge transfer band between 240 and 260 nm is seen in GST β hdMT and GST α hdMT which originates from the Cd-thiol interactions (Figure 4.35).

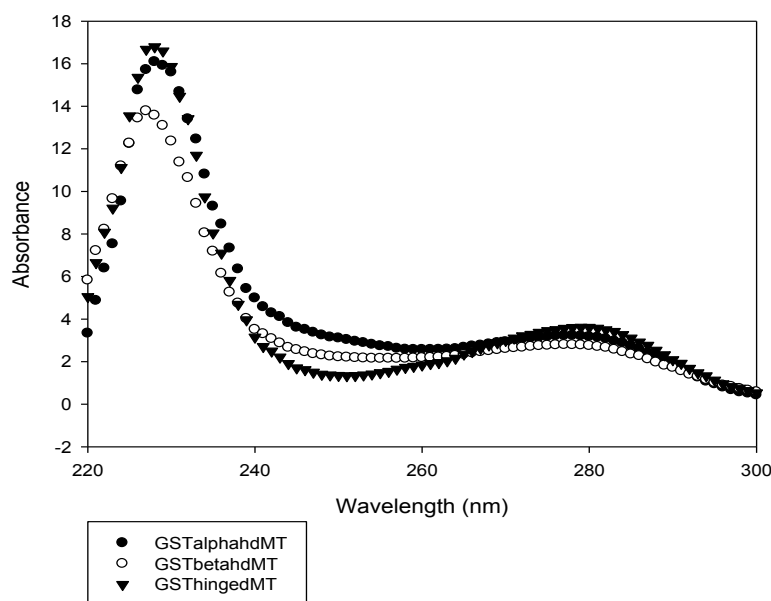


Figure 4.35: Absorbance spectrum of GtabST β hdMT (○) GST α hdMT (●) and GSThdMT (▼).

4.6 Structural Analysis of GST and GSTdMT constructs

4.6.1 Native Gel Analysis of GST and GSTdMT constructs

In order to compare folding and charge distribution of GSTdMT constructs purified recombinant proteins were analyzed by Native-PAGE together with GSTdMT and GST. As can be seen from Figure 4.36, both GST β hdMT and GST α hdMT migrate faster than GSTdMT but GST β hdMT migrates almost as fast as the GST control. Implications of this for the structural properties of dMT will be discussed in Chapter 5.

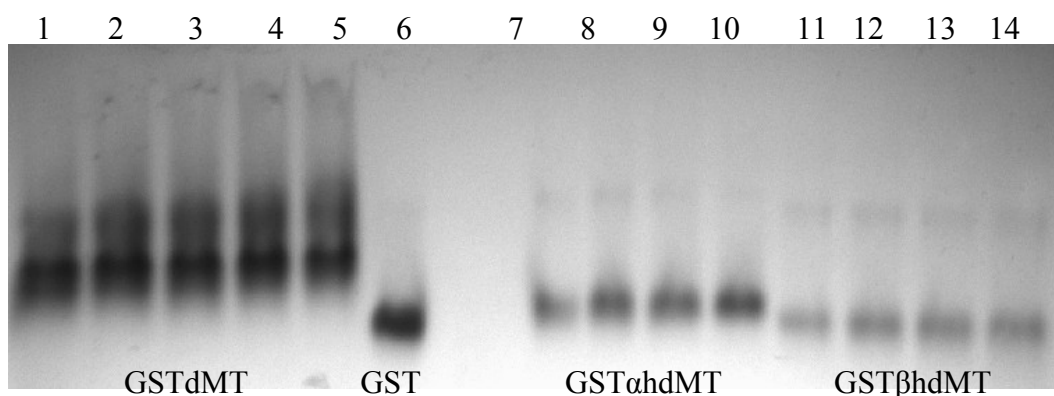


Figure 4.36: 8% Native-PAGE gel analysis of GSTdMT constructs. Lanes 1-5: GSTdMT. Lane 6: GST. Lane 7-10: GST α hdMT. Lane 11-14: GST β hdMT.

4.6.2 Structural Characterization of GSTdMT constructs by limited proteolytic cleavage

Proteolytic cleavage of the GSTdMT constructs was performed with trypsin. It is a serine protease which predominantly cleaves peptide chains at the carboxyl side of the amino acids lysine and arginine, except when either is followed by a proline. The possible cleavage sites in the dMT molecule are K16, K19, K47 and K69 as shown in Figure 4.37. There is also an R residue at position 224 very close to the C terminal of GST (not shown) which appears to be accessible to trypsin. In the analysis of digestion results for GST, GSThdMT, GST β hdMT and GST α hdMT 14% or 16% Tris-tricine PAGE was used.

Limited tryptic cleavage of GSThdMT started within 30 seconds and after 2 hours hinge region was completely digested off GST. During the cleavage first a faint band under the main GSThdMT band was observed then a second band appeared within 1 minute (Figure 4.38). Molecular weight estimation using the regression analysis showed that the faint band below the main band had an apparent MW of 30.4 kDa which after corrections with respect to the reference proteins gives 32 kDa. This shows that the recombinant construct is cleaved first from K47 in the center of the hinge domain as shown in Figure 4.37.

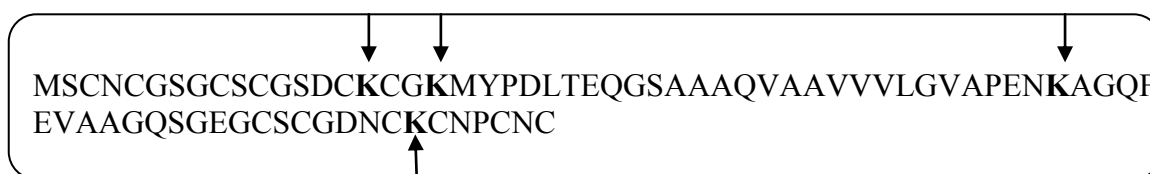


Figure 4.37: dMT amino acid sequence. Cleavage sites K16, K19, K47 and K69 (numbered from the N terminal of dMT) of trypsin are shown with arrows.

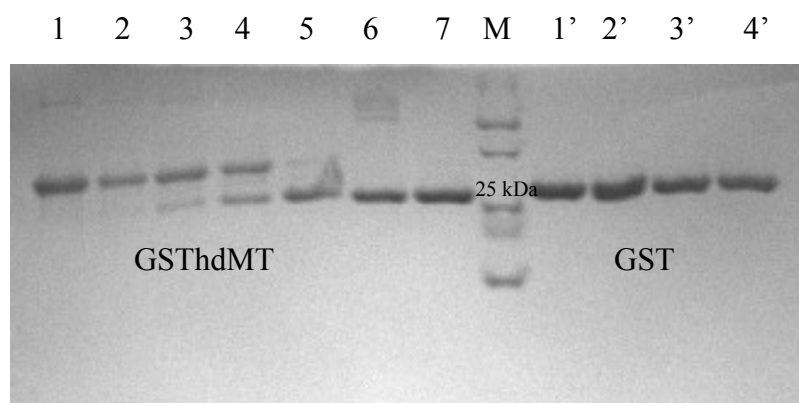


Figure 4.38: 14 % Tris-tricine PAGE analysis of cleavage products of GSThdMT and GST. Samples taken before $t=0$ (Lane 1) and after $t=30$ sec (Lane 2), $t=1$ min 30 sec (Lane 3), $t=5$ minutes (Lane 4), $t=40$ minutes (Lane 5), $t=1$ hour (Lane 6), $t=2$ hours, $t=0$ (Lane 1'), $t=40$ minutes (Lane 2'), $t=1$ hour (Lane 3'), $t=2$ hours (Lane 4') of tryptic cleavage.

The cleavage pattern of GST β hdMT is shown in Figure 4.39. The cleavage product appeared within 30 seconds. According to the regression analysis, the band under the main band had a calculated MW of 27.5 kDa which is very close to the MW of GST. It appears that the cleavage sites within the hinge region are not readily accessible for trypsin. This observation is also confirmed by the fact that large

quantities of GST β hdMT remain uncleaved in the time period where GSThdMT is completely digested. Complete cleavage is achieved only when the enzyme concentration is increased 10 fold.

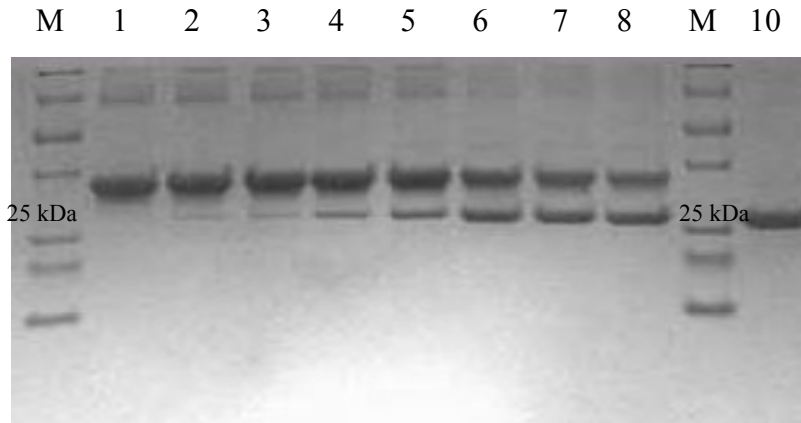


Figure 4.39: 16 % Tris tricine PAGE analysis of cleavage products of GST β hdMT Samples taken before $t=0$ (Lane 1) and after $t= 30$ sec (Lane 2), $t=1$ min (Lane 3), $t= 5$ minutes (Lane 4), $t= 10$ minutes (Lane 5), $t= 40$ minutes (Lane 6), $t=1$ hour (Lane 7), $t= 2$ hours (Lane 8) of tryptic cleavage with 0.0025 mg/ml trypsin. $t= 2$ hours (Lane 10) of tryptic cleavage with 0.025 mg/ml trypsin.

In the cleavage pattern of GST α hdMT two faint bands appear immediately (Figure 4.40). These correspond to cleavage from K47 and from R224 in the GST sequence. According to the regression analysis the GST α hdMT band has a molecular weight of 33 kDa and the faint band below had a MW of 30 kDa. The completely cleaved protein had a MW of 25.22 kDa.

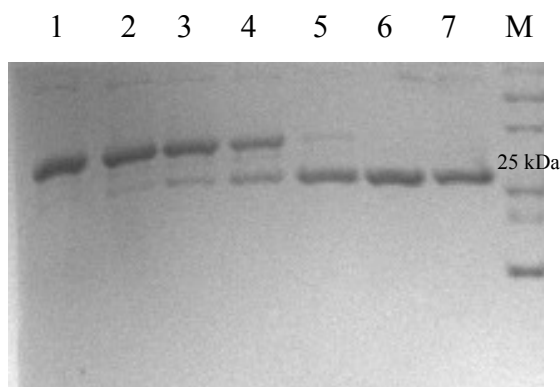
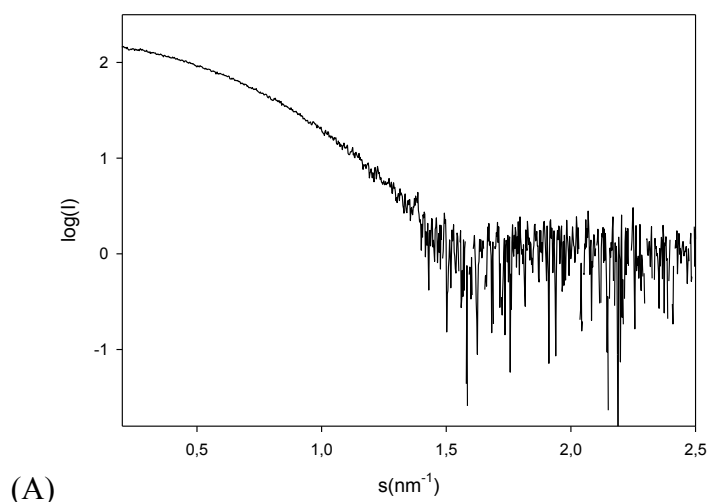


Figure 4.40: 14 % Tris tricine PAGE analysis of cleavage products of GST α hdMT. Samples taken before $t=0$ (Lane 1) and after $t= 30$ sec (Lane 2), $t=1.5$ min (Lane 3), $t= 5$ minutes (Lane 4), $t= 40$ minutes (Lane 5), $t= 1$ hour (Lane 6), $t=2$ hours (Lane 7) of tryptic cleavage.

4.6.3 Structural Characterization of GSTdMT constructs using SAXS

Solutions of GST, GSThdMT, GST β hdMT and GST α hdMT in HEPES buffer were measured by SAXS at several concentrations between 0.68 and 16.8 mg/ml. Because at higher concentrations, large portion of the protein formed higher order oligomers, where necessary low angle regions of scattering curves from low concentration samples were merged with high angle regions from high concentration curves as indicated in the text. Bovine serum albumin (BSA) was also measured as a molecular mass standard at 5mg/ml in 50 mM HEPES, pH8.

SAXS curves for GST solutions and those for constructs are given in Figure 4.41 A-D. Figure 4.41 A shows the scattering from a 1.8 mg/ml GST solution. Figure 4.41 B is generated by merging (0.69.dat) 0.89 mg/ml GSThdMT (points 1-400) with (.299.dat) 18.9 mg/ml GSThdMT (points 200-2164). Figure 4.41C is generated by merging (.85.dat) 0.5 mg/ml GST β hdMT (points 55-325) with (118.dat) 3.8.mg/ml GST β hdMT (points 150-1460) and Figure 4.41D shows the scattering pattern from a 0.7 mg/ml GST α hdMT solution.



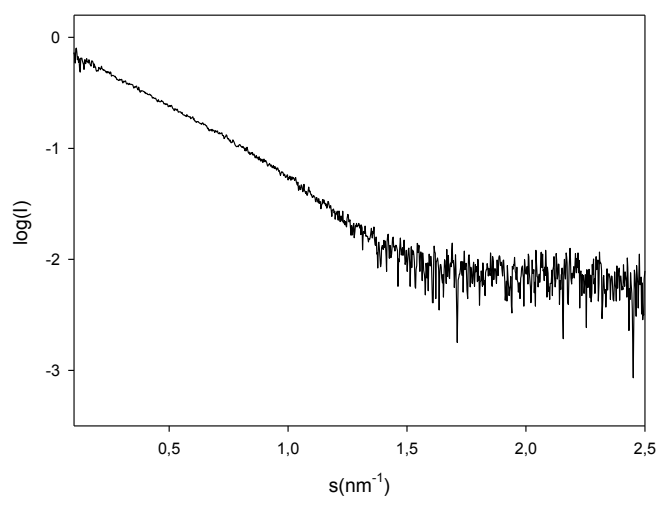
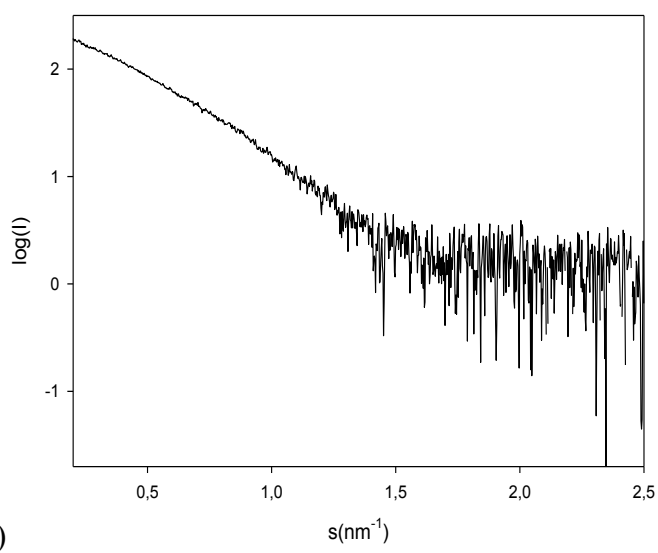
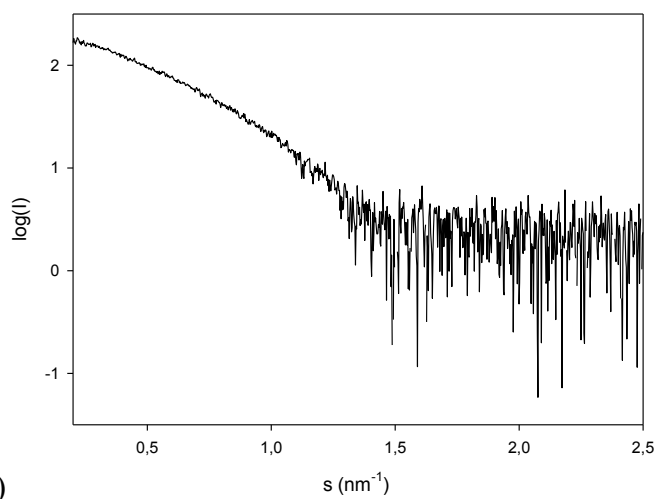


Figure 4.41: SAXS curves of GST and GSTdMT constructs. (A) 1.8 mg/ml GST (B) GSThdMT (C) GST β hdMT and (D) GST α hdMT measured in HEPES buffer. Scattering data is given in the range $0 < s < 2.5 \text{ nm}^{-1}$.

Scattering pattern of GSThdMT resembles that of GST (Figure 4.42) indicating the similarity in the shape of the two proteins and that the shape can be approximated by a sphere.

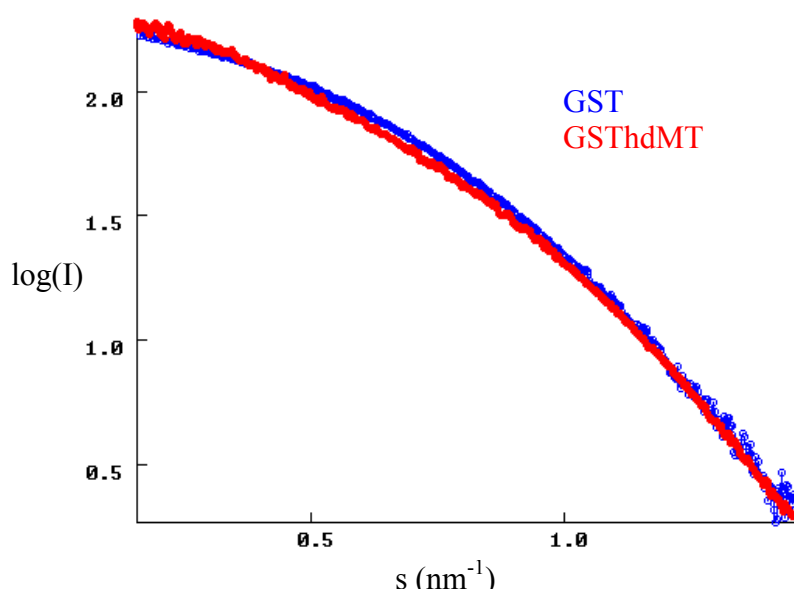


Figure 4.42: Superposition of scattering curves of GST and GSThdMT in the range $0 < s < 1.5 \text{ (nm}^{-1}\text{)}$.

SAXS curves obtained from GST β hdMT and GST α hdMT reflect the deviation of the structures of these proteins from that of GST (Figure 4.43).

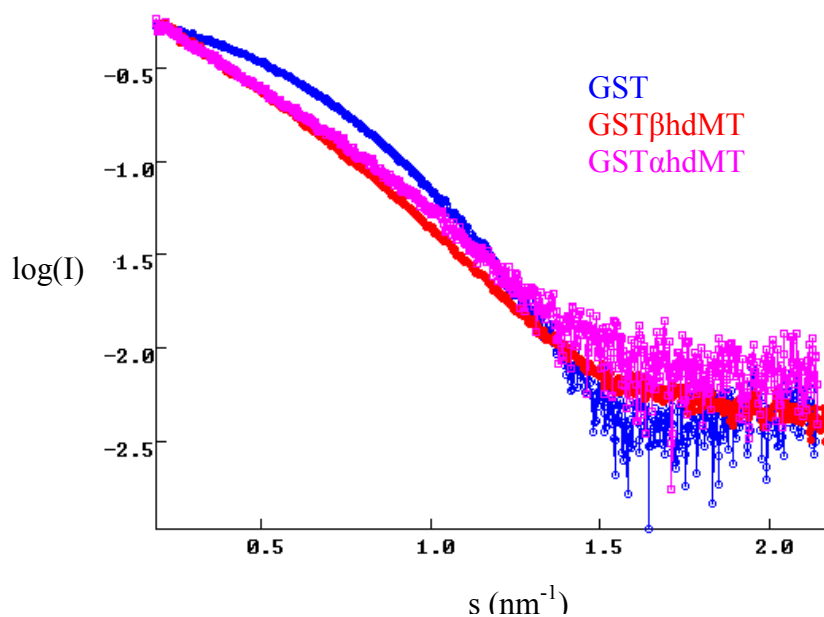
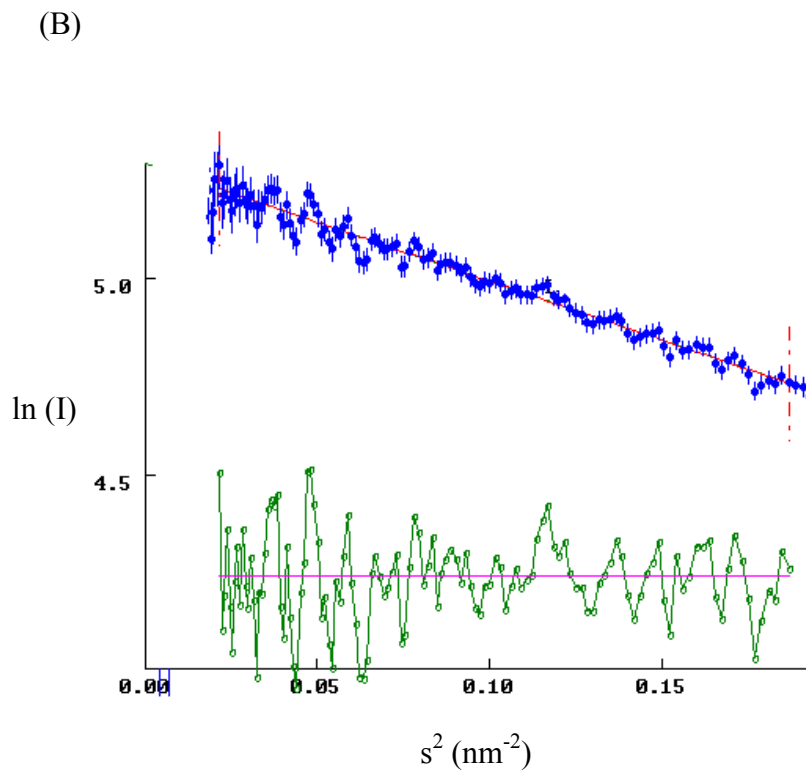
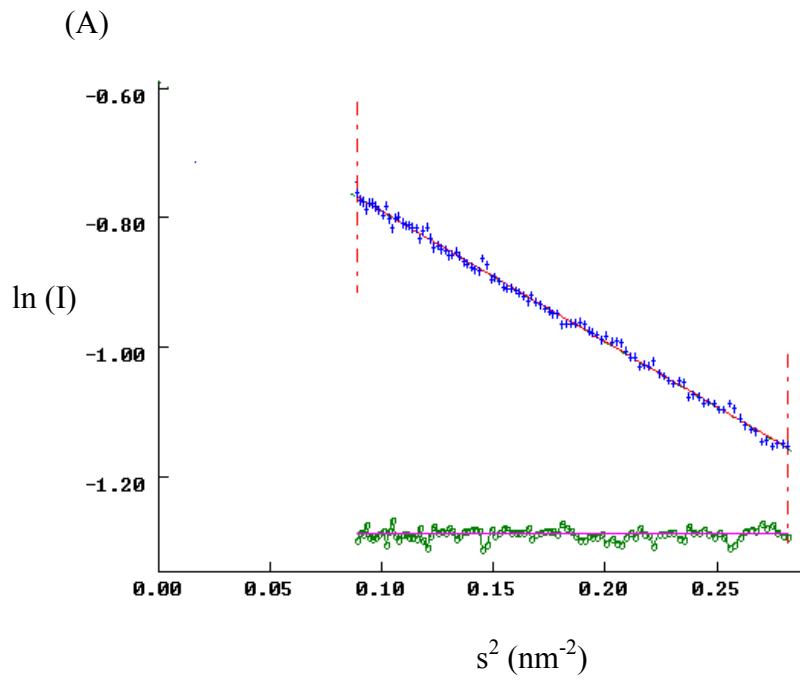


Figure 4.43: Superposition of the scattering curves of GST and GSTdMT constructs in the range $0 < s < 2.5$ (nm^{-1}). Concentrations of the proteins measured in HEPES buffer are the same as those in Figure 4.41.

For ideal monodisperse and homogenous systems, Guinier plots can be used to determine the radius of gyration and the molecular mass of particles at very small angles ($s < 1.3/R_g$). The scattering intensity is represented as $I(s) = I(0) \exp(-(sR_g)^2/3)$ and the Guinier plot ($\ln(I(s))$ versus s^2) is a linear function. The intercept, $I(0)$, is proportional to the molecular mass and the slope yields the radius of gyration R_g . The molecular mass can be estimated from $I(0)$ relative to a protein with known molecular mass or some other standard.

Guinier plots for GST, GSThdMT, GSTβhdMT and for GSTαhdMT in HEPES buffer, in different momentum transfer ranges ($0.6 < sR_g < 1.3$) are shown in Figure 4.44 A, B, C and D.



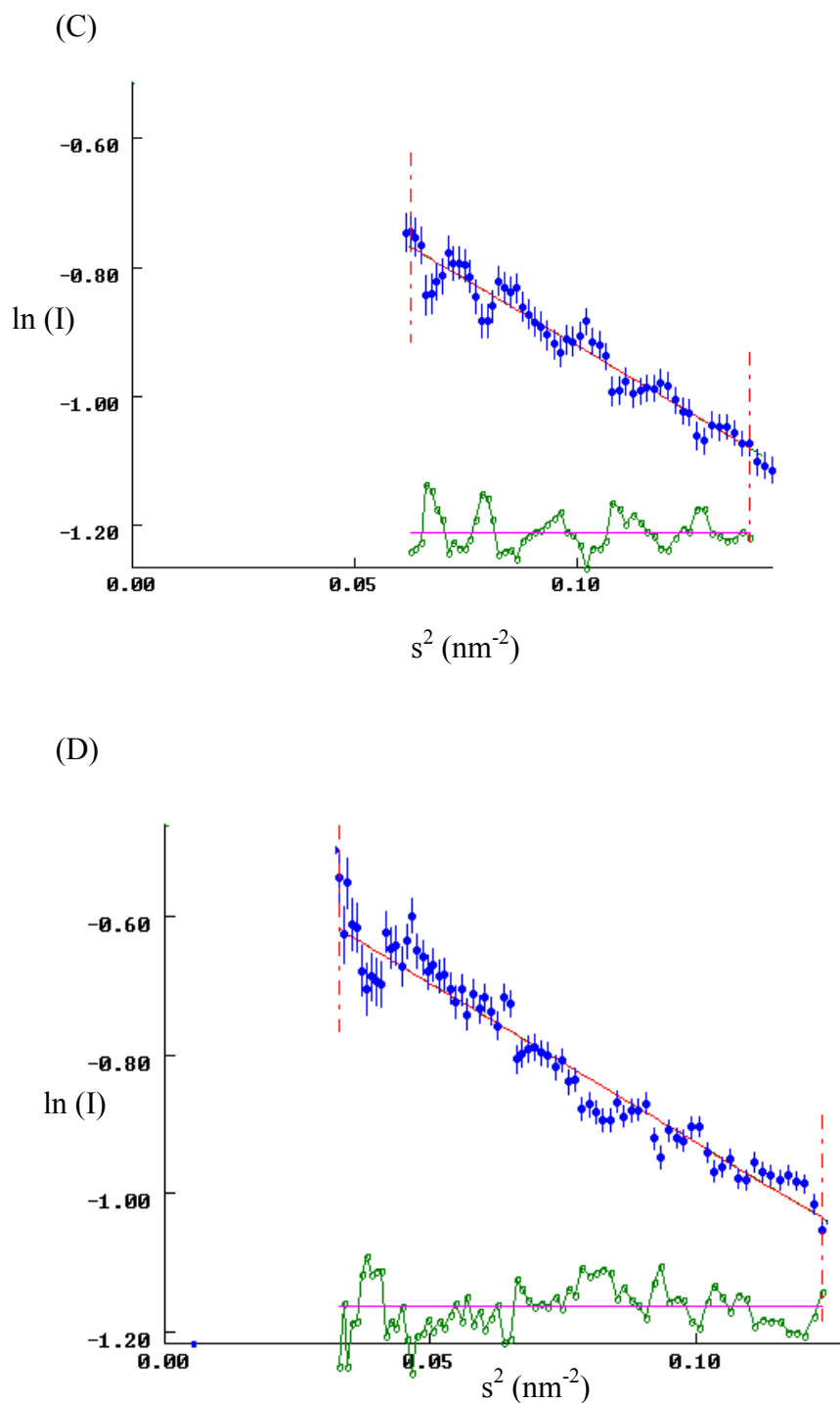


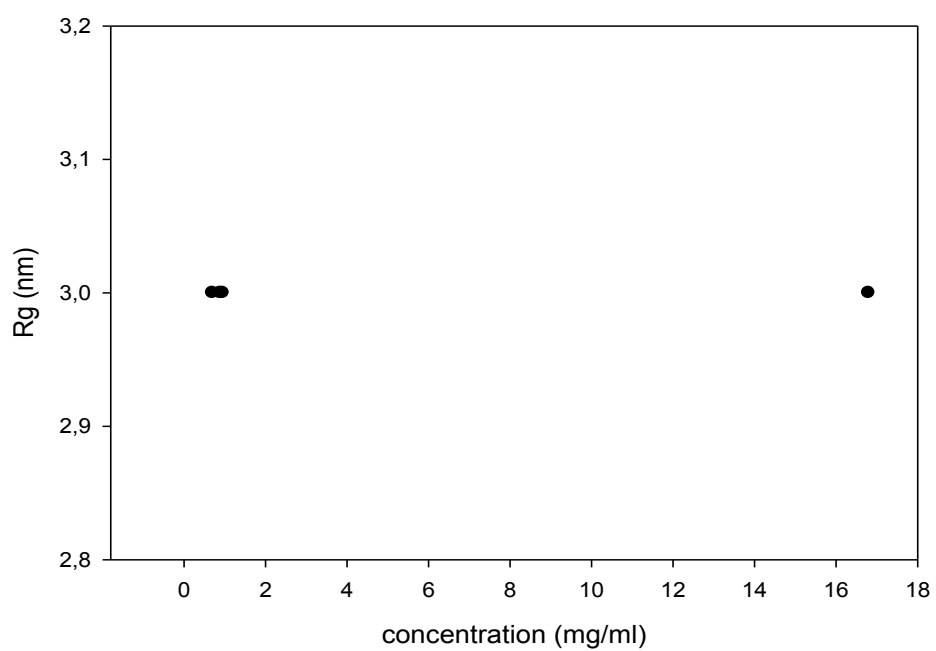
Figure 4.44: Guinier plots for GST and GSTdMT constructs. (A) GST, (B) GSThdMT, (C) GST β hdMT and (D) fGST α hdMT measured in HEPES buffer.

Structural parameters were calculated from the scattering curves shown in Figure 4.41 and are shown in Table 4.3. Molecular masses of GST, GSThdMT, GST β hdMT and GST α hdMT were estimated from the excluded molecular volume calculated during modelling as described below.

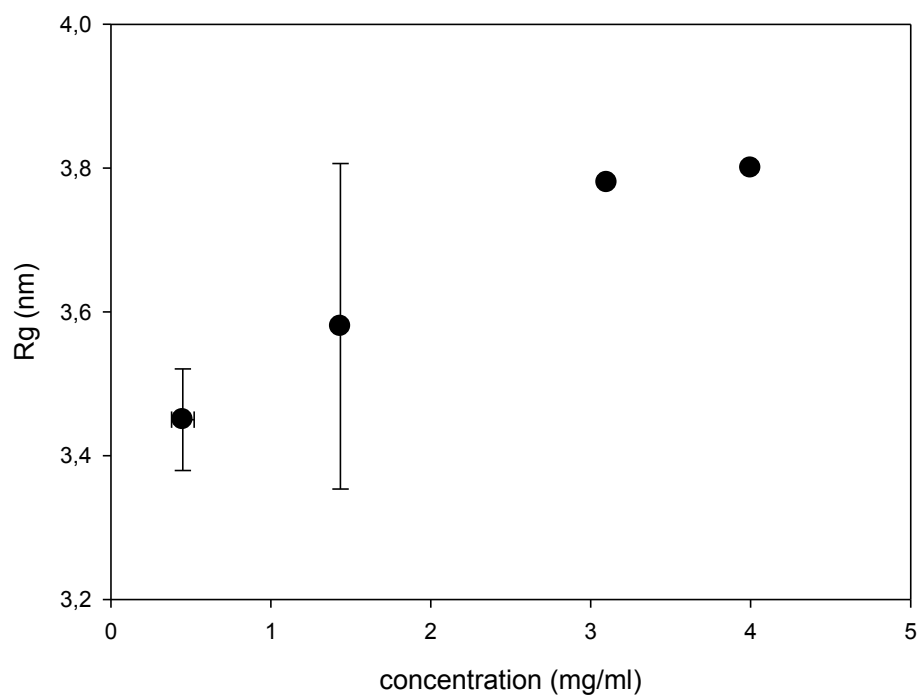
Table 4.3: Structural parameters of GSTdMT and mutants calculated from SAXS measurements. Rg, radius of gyration; Dmax, maximum particle diameter; MMexp, molecular mass of the dimer determined from SAXS by using Porod volume; MMth theoretical value for molecular mass of the monomer calculated from amino acid sequence of the proteins.

	Rg (nm)	Dmax	Volume	MMexp(kDa)	MMth(kDa)
GSThdMT	2.91	10.5	120.45	60.22	30.8
GSTβhdMT	3.46	14	127	63.5	32.5
GSTαhdMT	3.66	12.5	130	65	32.3
GST	2.45	8	96	48	26.67

The effect of aggregation on the scattering curves for GSTdMT constructs was controlled by checking the correlation between Rg and protein concentration as shown in Figure 4.45. Rg was found to be 2.45 for GST, 2.91 for GSThdMT, 3.46 for GSTβhdMT and 3.66 for GSTαhdMT. Effect of aggregation on the scattering curves for three constructs was analyzed by checking the correlation between Rg values and protein concentration from two data sets obtained at different SAXS measurements (Figure 4.45A, B and C). Rg values of GSTdMT constructs were independent of concentration.



(A)



(B)

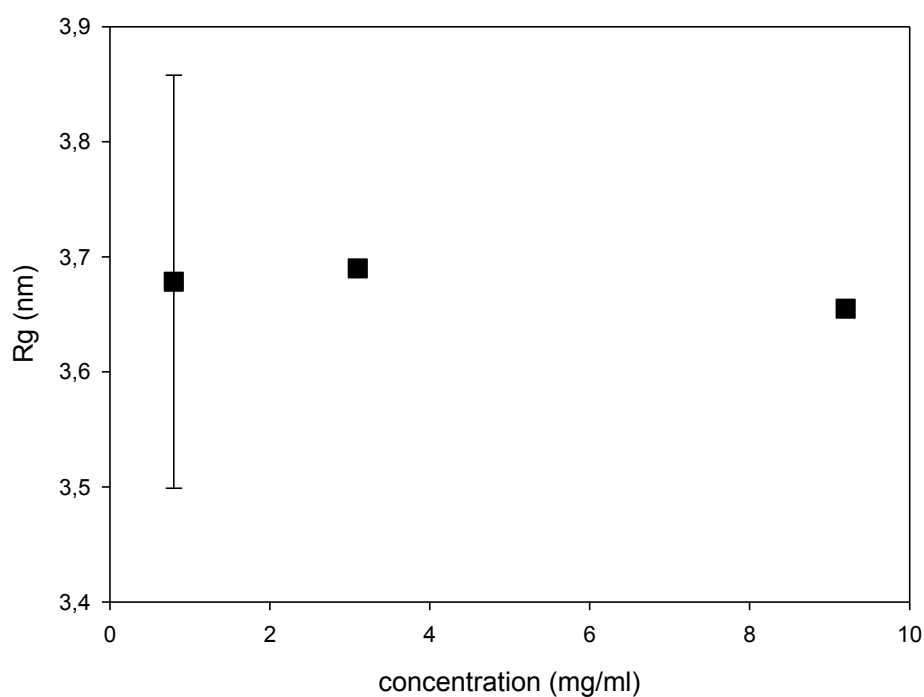
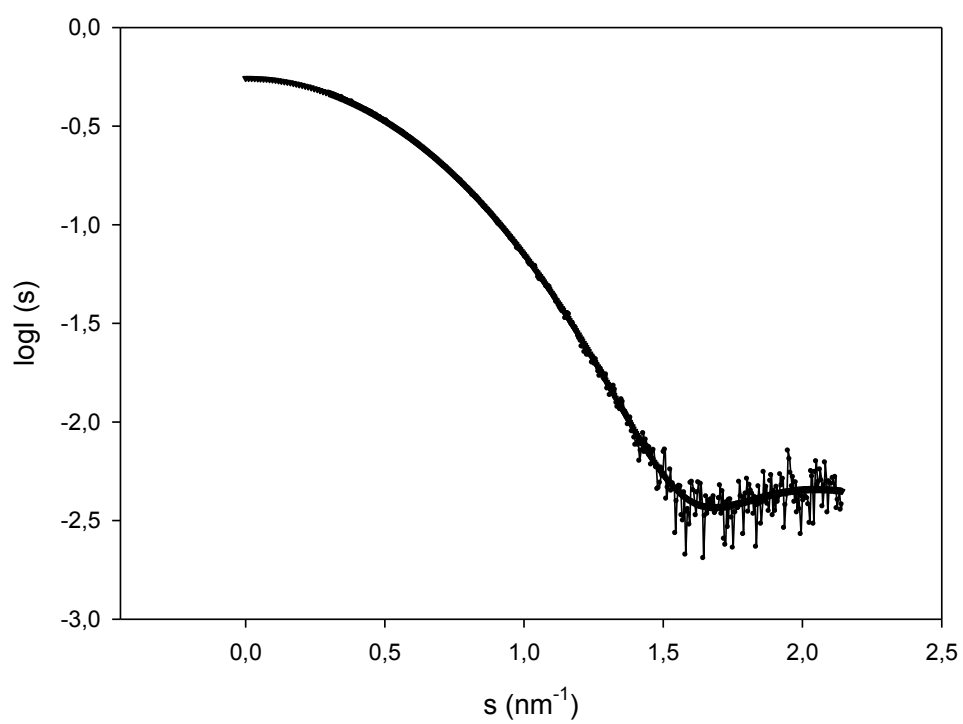


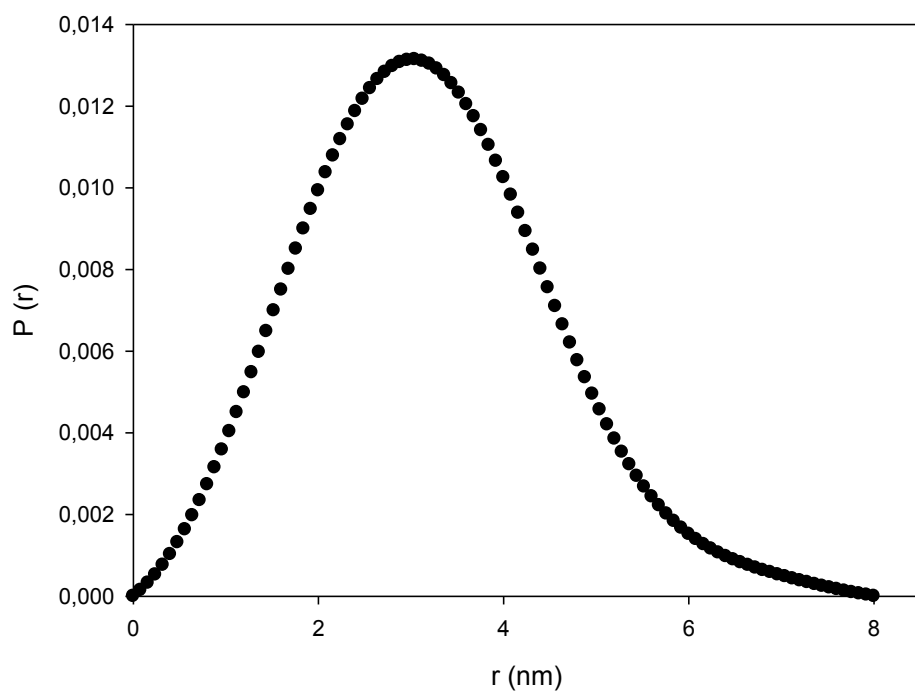
Figure 4.45: Correlation between Rg and concentration for GSTdMT constructs. (A) GSThdMT (B) GSTβhdMT and (C) GSTαhdMT were obtained from two different sets of measurements. Rg was determined using AutoRg software in the range of $0.6 < sRg < 1.2$.

The indirect transform algorithm GNOM was used for obtaining preliminary shape information from the SAXS scattering curves.

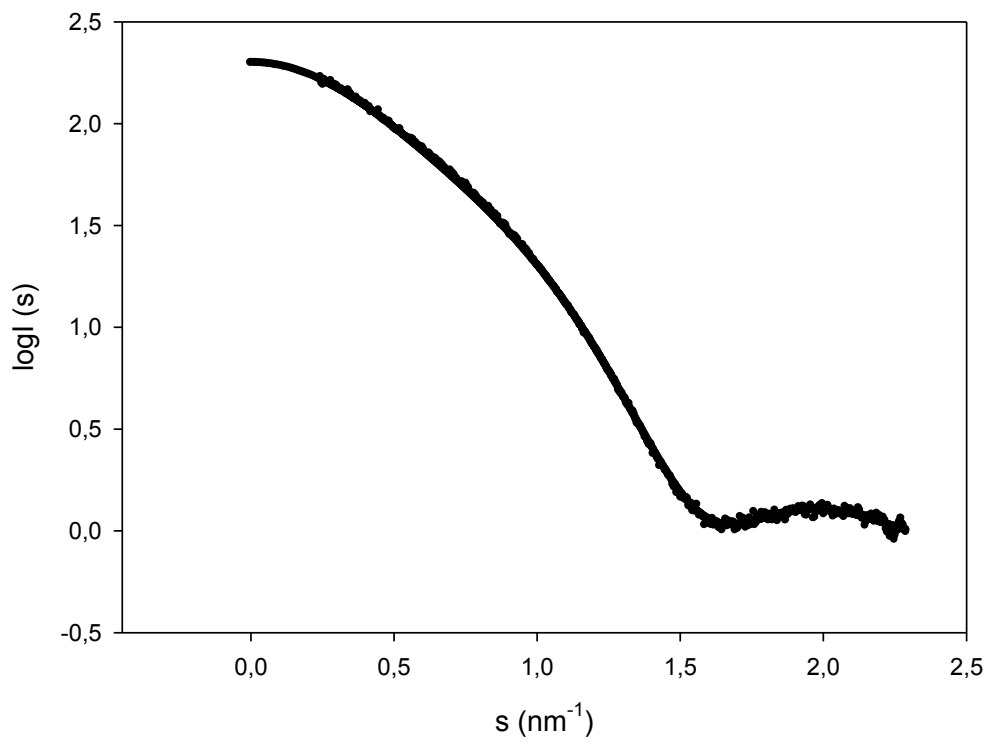
Results of GNOM analysis using the scattering patterns from GST, GSThdMT, GSTβhdMT and GSTαhdMT (Figure 4.41) and the maximum particle dimensions given in Table 4.3, are shown in Figure 4.46 A, B, C and D.



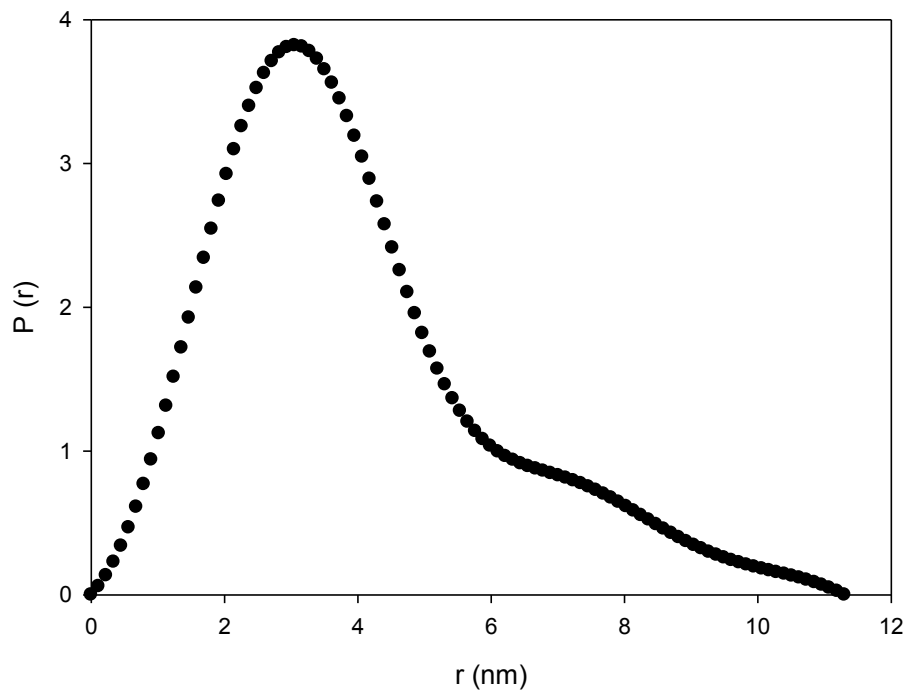
(A1)



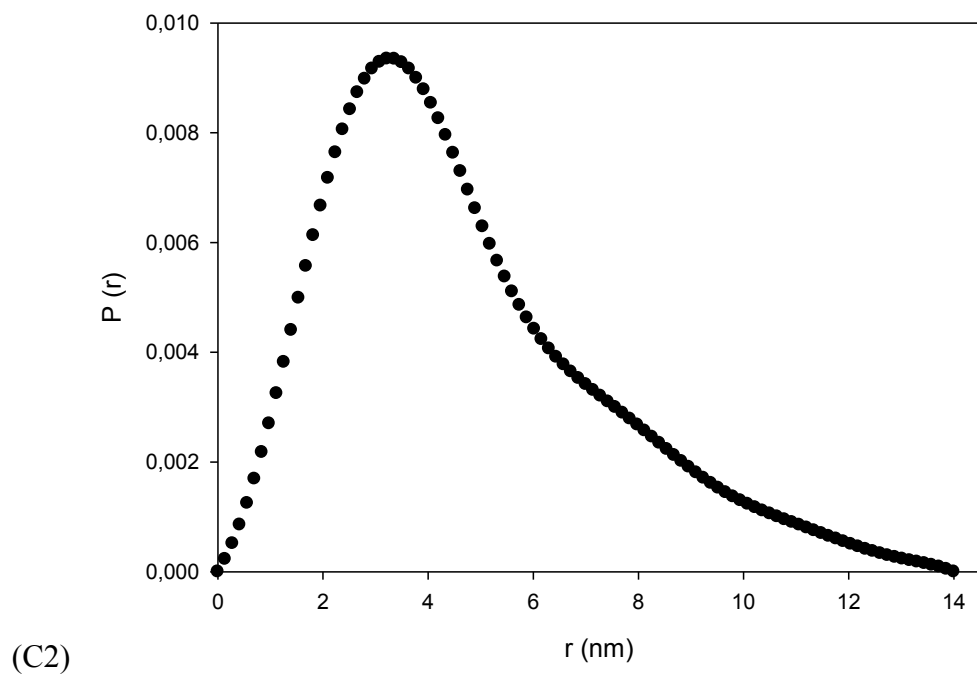
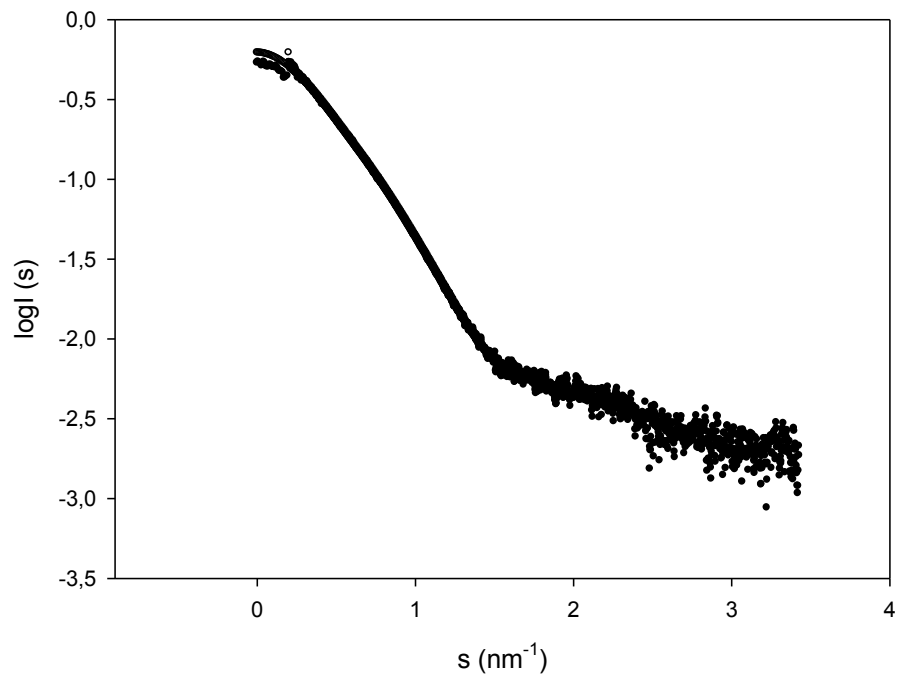
(A2)



(B1)



(B2)



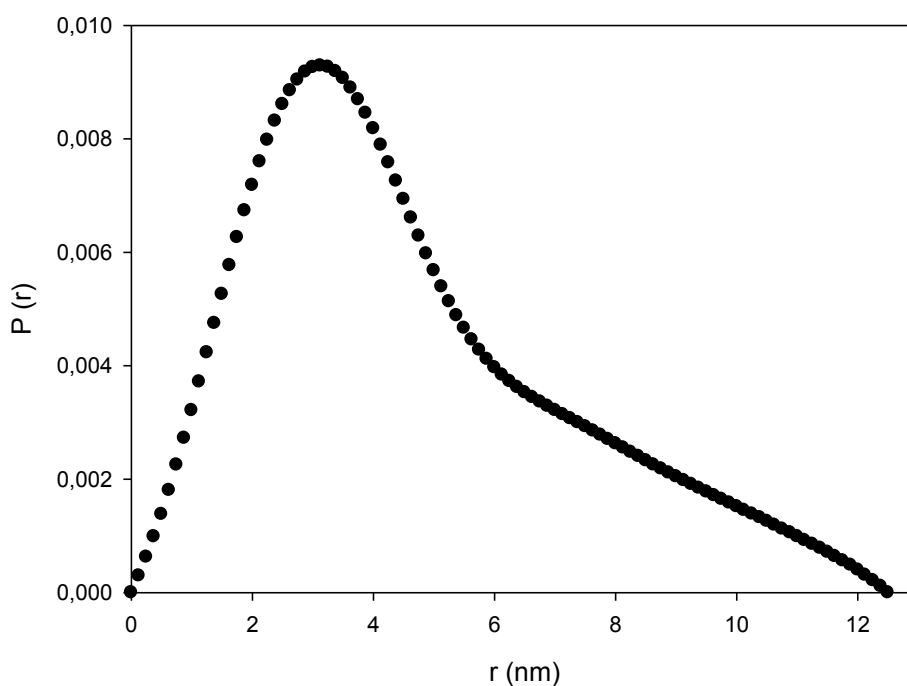
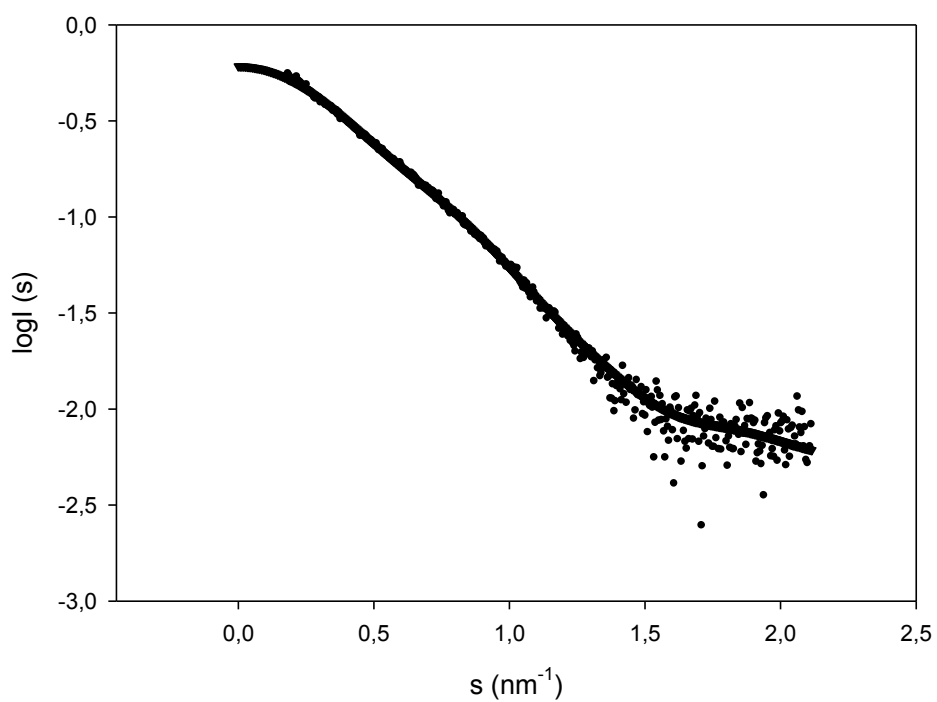
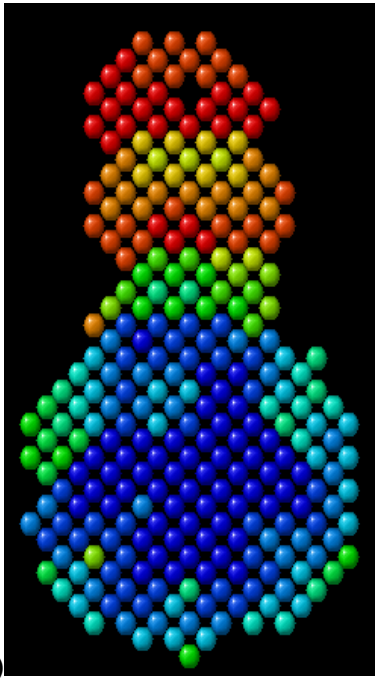


Figure 4.46: Analysis of SAXS data using GNOM algorithm. (A1)-(D1) fit to the experimental data (A2)-(D2) distance distribution functions for (A) GST, (B) GSThdMT, (C) GSTβhdMT and (D) GSTαhdMT respectively. $J(s)$ experimental data, s momentum transfer, $P(r)$ distance distribution function and r real space axis.

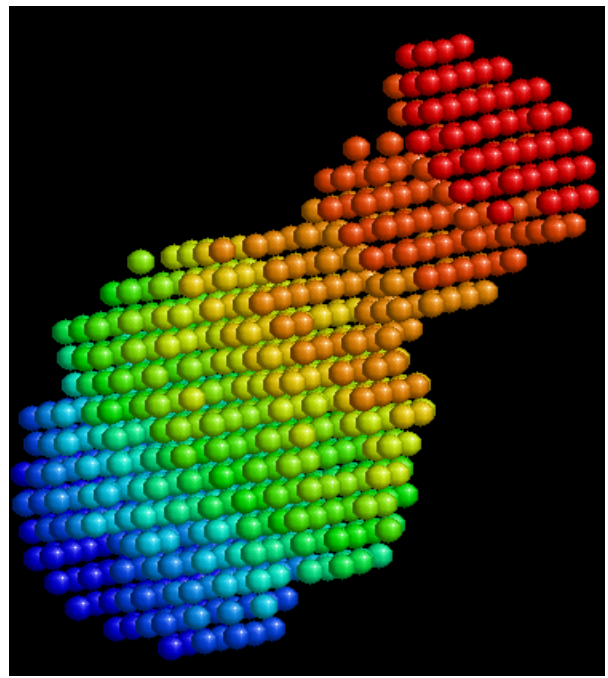
The differences in the shapes of the constructs are reflected in the shape of the $P(r)$ functions as shown in Figure 4.46. Although there is only 42 amino acids length difference between GST and GSThdMT, the D_{\max} values are 8 nm and 10.5 nm respectively. The shape of $P(r)$ function becomes more asymmetric as the molecules get more elongated. D_{\max} values for GST β hdMT and GST α hdMT are 14 nm and 12.5 nm respectively.

Modeling of the GSThdMT, GST β hdMT and GST α hdMT shapes were carried out by DAMMIN and DAMMIF algorithms. To have a more reliable solution DAMMIN was run ten times and the results were averaged using the DAMAVER averaging program. This program gives in pdb format the averaged structure (damaver) obtained from all runs, the filtered minimum structure (damfilt) that fits all results and statistical evaluation of the fits.

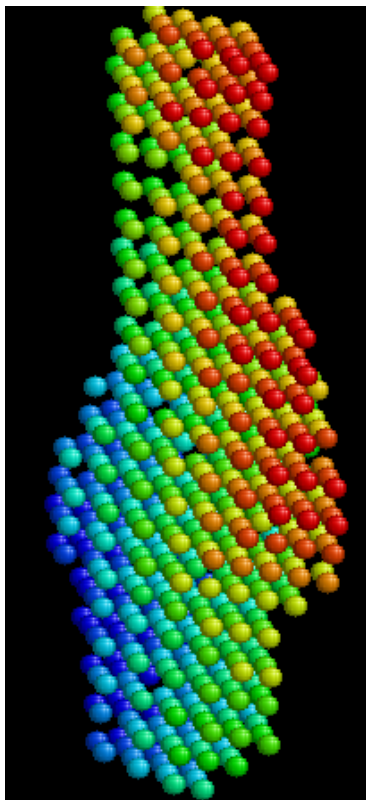
DAMMIF calculations of GSTdMT constructs converged to the models shown in Figure 4.47 A1, B1, and C1. Although it was known that the proteins form dimers in solution, initially no symmetry constraints were applied to the calculations (i.e. the calculations were done with P1 symmetry). Calculations were repeated with P2 symmetry (Figure 4.47 A2, B2, and C2). Independently of the symmetry constraints, the models of GSThdMT, GST β hdMT and GST α hdMT converged to elongated shapes with a globular region from which one broad tail extended.



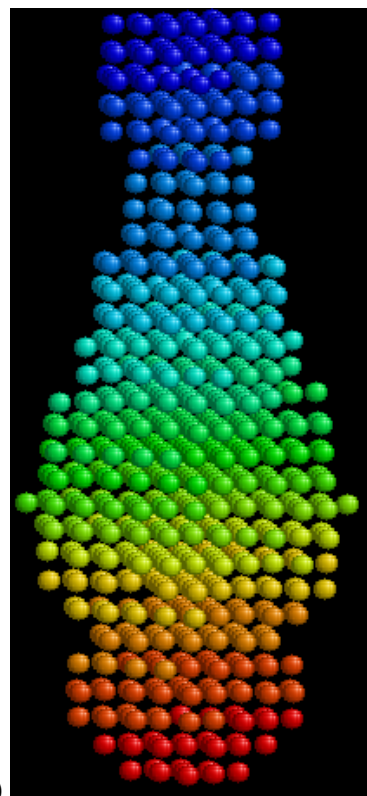
(A1)



(A2)



(B1)



(B2)

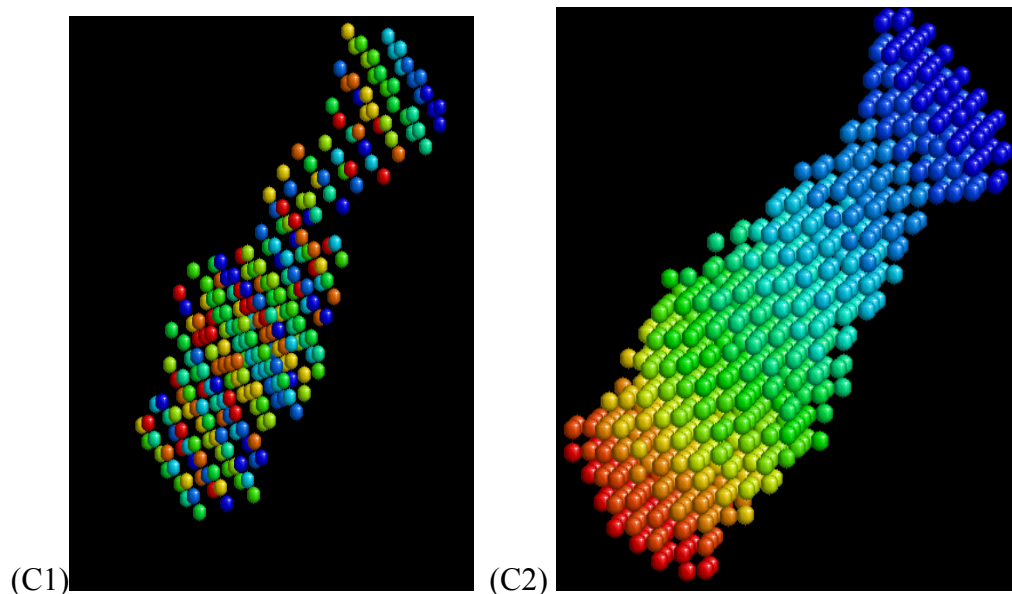
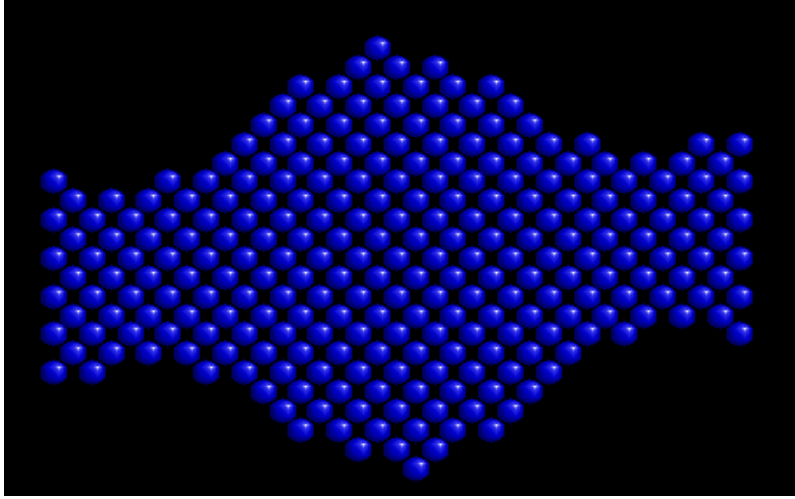
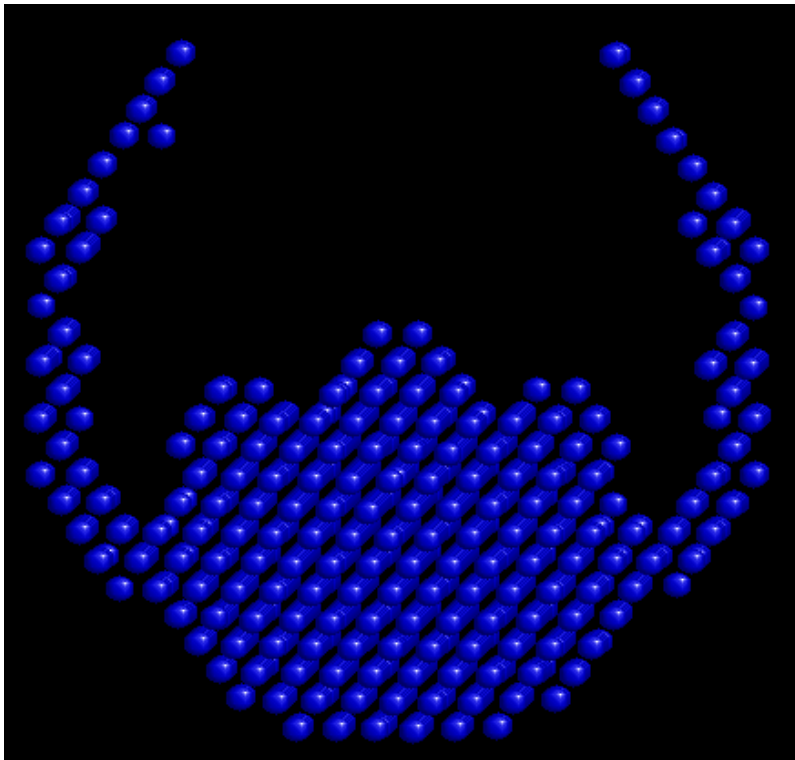


Figure 4.47: Shape models for GSThdMT, GSTβhdMT and GSTαhdMT with P1 symmetry; (A1), (B1) and (C1) and with P2 symmetry; (A2), (B2) and (C2) developed by DAMMIF.

Further models were generated by DAMMIN and DAMAVER using P2 symmetry and prolate particle shape; it was assumed that the particle is elongated across the horizontal twofold axis (Figure 4.48A, B and C). In all the models the central dense region corresponds to the GST dimer. In GSThdMT Figure 4.48A, the hinge region is observed as thin extensions from the central domain. The maximum distance measured from the model for this central region is about 7 nm. In GSTβhdMT (Figure 4.48B) and GSTαhdMT (Figure 4.48C) the central region is less compact (9-10 nm) than that of the hinge construct model. The Dmax values from the models are about 11-12 nm for both GSTβhdMT and GSTαhdMT constructs. These measurements from the models are basically in agreement with the values given in Table 4.3. In GSTβhdMT the extended regions appear more compact when compared to GSTαhdMT.

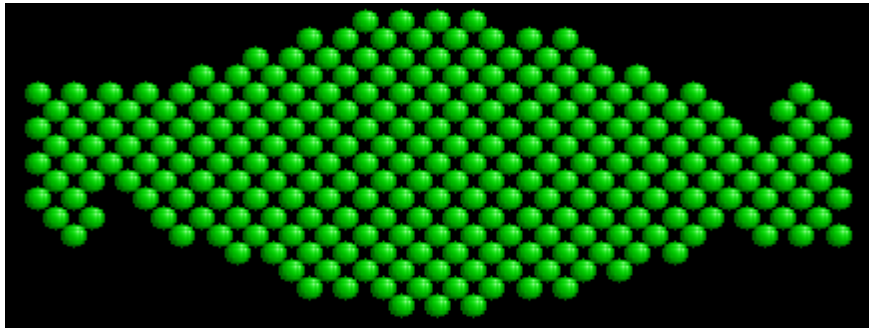


(A1)

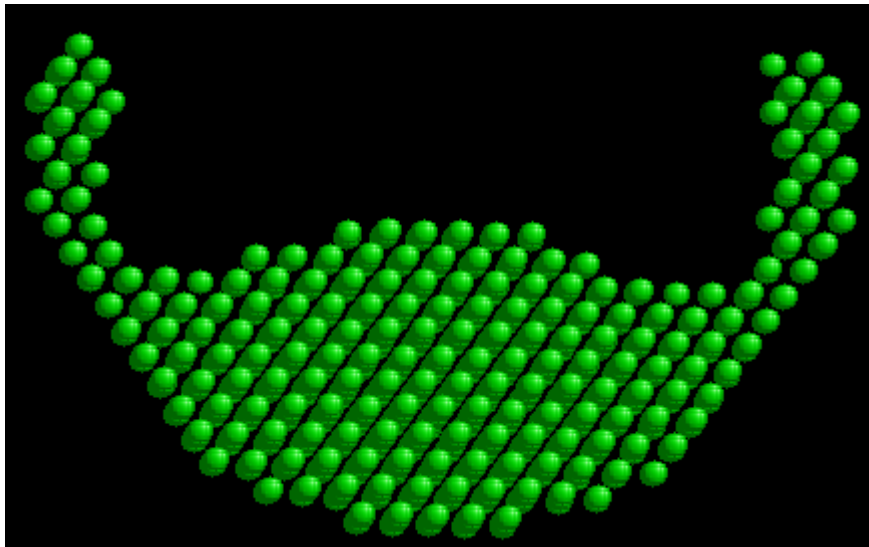


(A2)

(B1)



(B2)



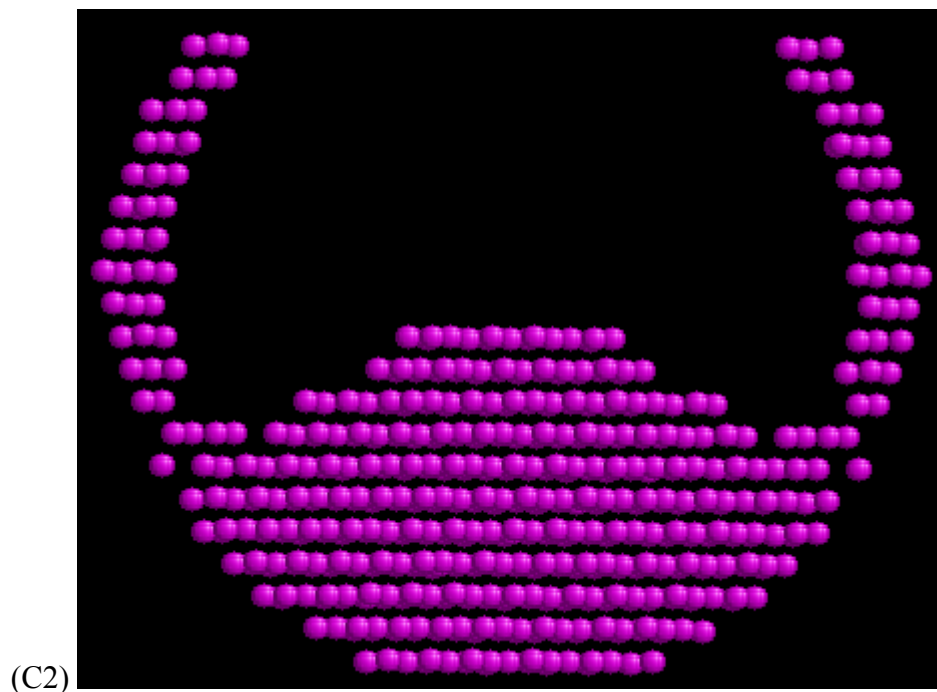
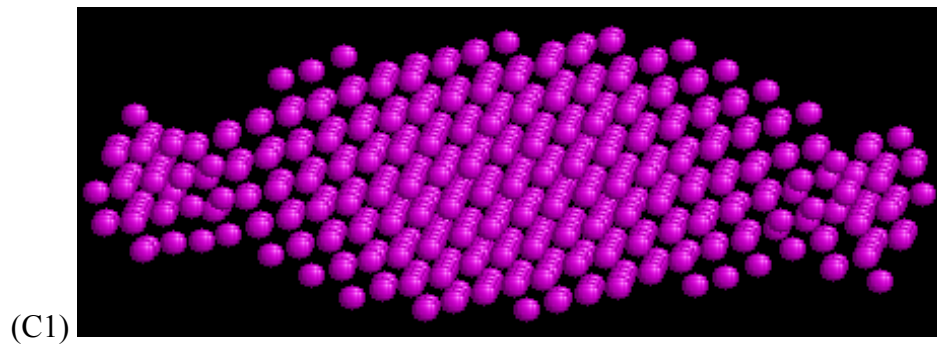
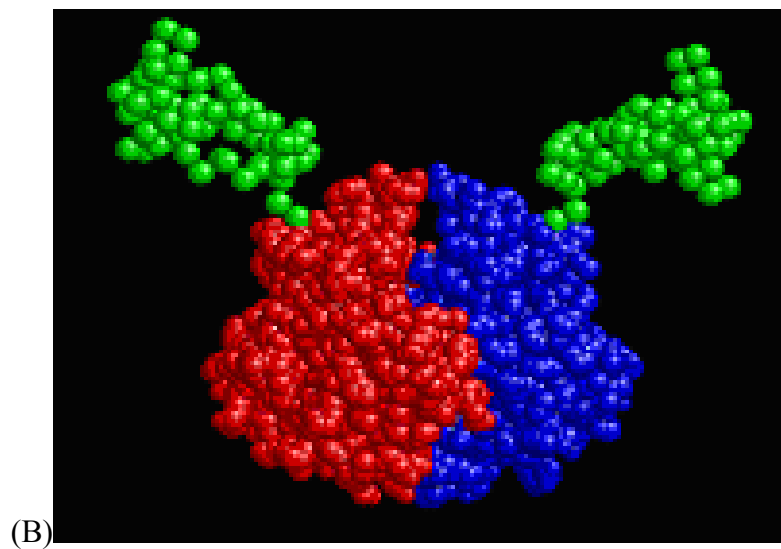
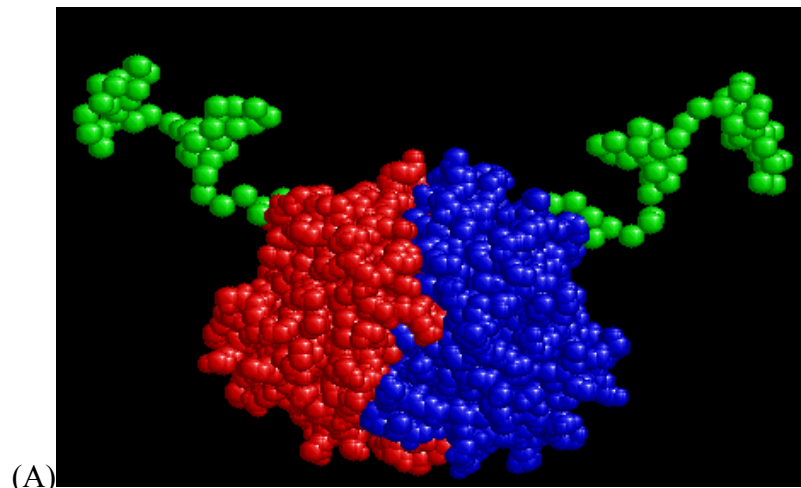


Figure 4.48: Shape models (DAMFILT) for (A1) GSThdMT, (B1) GSTβhdMT and (C1) GSTαhdMT developed by DAMMIN with P2 symmetry, prolate and across. (A2) (B2) and (C2) correspond to (A1) (B1) and (C1) rotated clockwise by 90° around the x-axis.

Rigid body modeling was also applied to the GSTdMT constructs using the BUNCH program. When the structures of individual domains of a protein are available, the program allows to model their three dimensional arrangement within the molecule based on the scattering data. The available crystallographic model of GST (1GTA) was used to model GSThdMT, GSTβhdMT and GSTαhdMT structures.

The program was run with P2 symmetry. The models obtained for GSTdMT constructs are shown in Figure 4.49 A, B and C. Several reconstructions yielded the similar models with of the dMT domain extensions sticking out in opposite directions. It has, however, not yet been possible to obtain a good fit to the experimental data when scattering patterns were calculated from the models (data not shown).



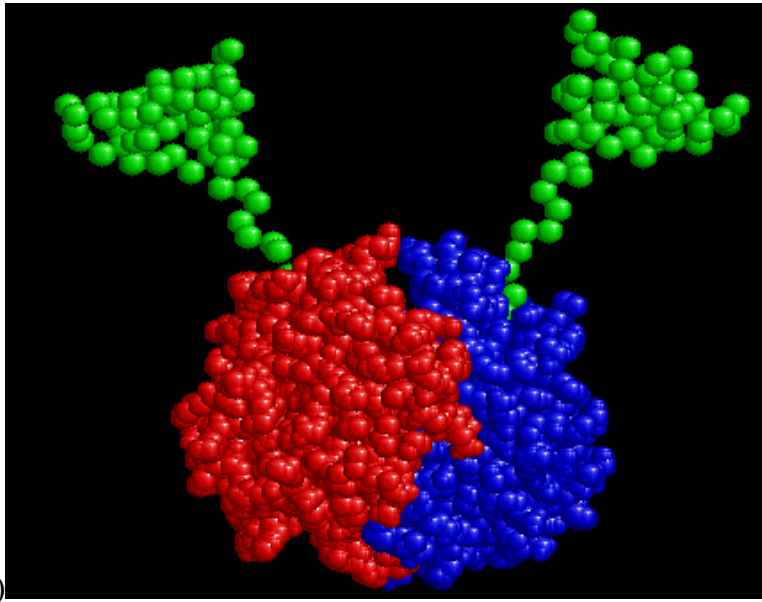


Figure 4.49: Shape models for (A) GST θ dMT (B) GST β dMT (C) GST α dMT developed by BUNCH.

Chapter 5

5. DISCUSSION

Information regarding plant MTs has been limited to spectroscopic characterization of the holoproteins. The function of the domains in plant MT is largely unknown and their structure and function have yet to be determined. dMT contains 75 amino acids (aa), 12 of which are Cys – 6 Cys are present in its β domain (N-terminal) with the remaining 6 in its α domain (C-terminal) – and a 42 aa long hinge (spacer) region (not containing any Cys) connecting the two domains.

The hinge region of plant MT is significantly longer than that of mammalian MTs. It is not clear whether the region takes part in the metal binding of the Cys-rich domains. The present study seeks to elucidate the role of the hinge region and the individual β hdMT and α hdMT in overall folding and in metal binding of dMT. The approach taken was to clone and express the type I MT hinge region (hdMT) and the Cys-rich N- and C-terminals with the hinge, β hdMT and α hdMT respectively, fused to Glutathione-S-transferase (GST) in *E. coli*.

5.1 Cloning, Expression and Purification of dMT constructs

There are only few reports of isolation of plant MTs directly from plant tissues in the literature and detailed studies are available only for Ec type wheat protein and Arabidopsis MTs (Lane *et al.*, 1987, Murphy *et al.*, 1997). The main reason for the

lack of direct isolation is that MTs are sensitive to oxidation and their long hinge region is targets for proteolytic cleavage (Tommey *et al.*, 1991).

To overcome the problems associated with direct isolation, recombinant expression of plant MTs in bacterial expression systems is preferred. GST as a fusion partner facilitates purification, quantification and detection. Another advantage of using GST is that, the thrombin cleavage site serves as a flexible linker between GST domain and the fused protein domains (Zhou *et al.*, 2001). This probably allows GST to retain its native structure and to have little interference with the structure of fused proteins (Zhan *et al.*, 2001). One drawback of utilizing GST as a fusion base is that it is prone to dimerization and aggregation (Schroeder and de Marco, 2005).

dMT cDNA sequences coding for the individual domains were cloned as C-terminal fusions to GST using the pGEX-4T-2 vector. Protease deficient BL21(DE3) bacterial cells were used for overexpression of the recombinant proteins. It was anticipated that expression of small dMT domains as a fusion to GST would provide protection from proteolytic cleavage and help proper folding. The possible dimerization of GST was taken into consideration during further characterization of the domains.

Different types of plant MTs have been cloned using pGEX-4T-2 to synthesize the encoded peptides fused to the C-terminal of GST. Examples include the work of Murphy *et al.*, 1997 on *Arabidopsis* MT1, MT2 and MT3 proteins, Abdullah *et al.*, 2002 on Type III MT3-A from oil palm, Bilecen *et al.*, 2005 on Type I durum wheat MT, Domenech *et al.*, 2005, on Type II *Quercus suber* MT. More recently, intein tags (protein self splicing elements) were also used for recombinant expression of an Ec Type MT from *Triticum aestivum*, Type III MT from *M. acuminata* and Type I MT from *Cicer arietinum* including a chitin binding domain (Peroza and Freisinger, 2007, Freisinger, 2007, Schicht and Freisinger, 2009).

Hitherto there is only a single reference on the cloning of individual plant MT domains (Domenech *et al.*, 2006). Individual N-terminal (N25) and C-terminal (C18) Cys-rich domains of type II *Quercus suber* metallothionein (QsMT) were cloned using pGEX4T-2 vector and expressed in *E.coli*. In the same study a chimera in which

the hinge region was replaced with a four glycine bridge (N25-C18) was also investigated.

Expression of GSThdMT was monitored by SDS-PAGE analysis which revealed that the recombinant protein was degraded and aggregated. The presence of GST was not sufficient to prevent proteolytic degradation. Under extreme conditions, such as overproduction of a recombinant protein in a cell, the chaperones which are the members of post-translational folding machinery cannot act normally to prevent or correct misfolding of the protein. To overcome this problem, following reports in the literature, the expression temperature was lowered, and osmolytes were included in growth medium (Diament *et al.*, 2003). GSThdMT was either expressed in the presence of benzyl alcohol, which is a chaperone inducer, at 20 °C for 20 hours or in the presence of betaine and NaCl at 37 °C. None of these conditions helped to reduce proteolytic cleavage of GSThdMT. In the final conditions, bacterial cells expressing GSThdMT were grown at 37 °C for 5.5 hours. GSTβhdMT and GSTαhdMT expression was conducted at 37 °C for 4 - 4.5 hours to reduce possible degradation during expression. In the final analysis, however, the purified proteins always contained some degradation products.

Proteolytic cleavage of plant MTs from the long hinge region is an unresolved problem, however, the N- and C- terminal domains are protected by the formation of metal thiolate clusters (Kille *et al.*, 1991). For proper folding and stabilization of GSTβhdMT and GSTαhdMT 0.1 mM CdCl₂ was included in the growth medium. Since GSTαhdMT appeared to be more susceptible to degradation, 0.3 mM CdCl₂ was also introduced during expression and purification.

Metals were also added during bacterial expression of metalloproteins in recent studies e.g. during expression of *Triticum aestivum* Ec-1MT, 0.1 mM ZnCl₂ or CdCl₂ were used in growth media (Freisinger, 2007). For the expression of holo *Quercus suber* MT (QsMT) 0.5 mM CuSO₄ or 0.3 mM ZnCl₂ was used (Domenech *et al.*, 2006). The authors also used 0.4 mM CdCl₂ and ZnCl₂ during the growth of bacterial cells expressing *C. arietinum* MT1 (Schicht and Freisinger, 2009).

dMT constructs were purified in two steps: this was accomplished first by affinity chromatography followed by size exclusion chromatography. The purification procedure of GST α hdMT was optimized by monitoring the effect of CdCl₂ concentration on the integrity of the purified protein. Purified GSTdMT constructs were monitored by controlling purity, integrity, monodispersity, and the oligomerization state. The Cd content of purified GST β hdMT and GST α hdMT was also monitored.

Purity was analyzed by SDS-PAGE and visualized by coomassie blue staining. Monodispersity and oligomerization states were monitored by native-PAGE analysis and DLS measurements and the Cd content was ascertained by ICP-OES measurements.

The GST tag in dMT constructs made it possible to bind the low molecular weight dMT domains to GSTrap® FF column (GE Healthcare), enabling a straightforward isolation from the crude cell extract.

All purification procedures were performed at 4 °C. Because of the susceptibility of sulfhydryl groups to both oxidation and disulfide formation, GST β hdMT and GST α hdMT were purified with extra caution, in the presence of CdCl₂ in an argon filled environmental bag or under a continuous flow of argon to avoid oxidation. All buffers used were degassed and argon saturated.

Affinity chromatography of GSTdMT constructs resulted in one peak with an eluate volume of 3 ml for GSThdMT, 4 ml for GST β hdMT and GST α hdMT (Figure 4.13 A, B and C). Protein yields of the constructs were 5-21 mg for GSThdMT, 14-22 mg for GST β hdMT and 9 to 12 mg for GST α hdMT. The yield of GSThdMT cannot be compared with the others because of its longer expression time. The differences in the yields of GST β hdMT and GST α hdMT may be due to differences in levels of recombinant protein expression in *E. coli*, as well as possibly reflect a difference in the solubility of the two proteins. When the cell masses and final OD₆₀₀ values after expression were compared similar results were obtained (data was not shown); therefore, a possible explanation for the lower protein yield of GST α hdMT could be a lower expression rate or degradation of protein after expression. It is more likely, however, that the protein degraded during expression and/or during purification. This

conclusion is also supported by the more prominent degradation observed in SDS PAGE analysis of GST α hdMT (Figure 4.14 B and C).

From this point on the procedures reported in the present work differ from those reported in the literature (e.g. Domenech *et al.*, 2006 and 2007). In our procedure we continue with the GST fusion constructs after elution from the affinity column. In contrast, in the literature plant MTs were cleaved from GST after the protein was bound to the affinity matrix. We chose, however, to continue working with GST fusion constructs in order to be able to carry out meaningful biochemical and biophysical characterization of the purified proteins.

Previous reports contained heterogeneous not well defined metal protein aggregates. This results in ambiguity in protein concentration determination and metal/protein determination (e.g. Domenech *et al.*, 2006). Heterogeneous starting material leads to ambiguities in interpretation of structural data such as those that come from CD as aggregation affects the patterns (e.g. Domenech *et al.*, 2007). Presence of inhomogeneous aggregates also makes it difficult to interpret tryptic digestion results (e.g. Peroza and Ferisinger, 2007).

The main disadvantage of our approach is that we are actually dealing with a different protein which consists of two major components; it is not clear if the constructs attached to GST fold in their native form. It is also not clear if metal binding would be the same as it is expected in the native protein. Dimeric forms due to presence of GST may affect behavior. These points were individually investigated. The Cd content of the constructs appears to agree with that expected from intact dMT. As shown in Table 4.2 the average Cd²⁺ to protein molar ratio was found to be 1.53 ± 0.6 for GST β hdMT and 1.5 ± 0.8 for GST α hdMT and this results agrees with the average Cd²⁺ to protein molar ratio 3.5 ± 0.5 for GSTdMT (unpublished results). ICP results were also confirmed by UV-vis spectroscopy.

GSTdMT constructs were further purified by size exclusion chromatography. Under optimized conditions size exclusion chromatography of GSTdMT constructs resulted in two peaks for GSThdMT, two and three peaks for GST β hdMT and GST α hdMT as shown in Figures 4.16, 4.29 and 4.30. This result

depends on the amount of protein loaded to the size exclusion column; a total of 8.25 mg of total protein was recommended to be loaded for better separation. When amounts below 8.25 mg were loaded, two well separated peaks were observed for GSThdMT. Three further, distanced peaks were seen for GSTβhdMT and GSTαhdMT. According to the calibration of the column, peak II for GSThdMT and III for GSTβhdMT and GSTαhdMT corresponded to dimeric forms of the constructs. The total yield was approximately 7 mg for GSTβhdMT and 5.5-6 mg for GSTαhdMT.

Monodispersity of fractions in peak II and peak III was monitored by dynamic light scattering (DLS), which is a sensitive method for detecting large aggregates in solution. Although hmw bands corresponding to aggregated forms of the proteins were more apparent in native-PAGE analysis, small amounts of aggregation were observed according to the size distribution of particles by intensity. Measurements of the different fractions resulted in a main peak centered around 10 nm in the intensity distribution, indicating that the major species in solution was dimeric (Figures 4.19 and 4.33).

The storage conditions were analyzed for GSThdMT monitoring the higher and lower oligomeric forms of the protein by native-PAGE analysis and DLS measurements after the storage at 4 °C, -20 °C and -80 °C with and without additives. The best storage condition was found to be 4 °C without any additives, rather than freezing at -20 °C and -80 °C (Figures 4.21-24). The same storage conditions were applied to the other constructs as well. Although, generally, MTs are stored at -70 °C and -80 °C until further use, effect of storage conditions on quality or oligomeric state does not seem to have been investigated (Freisinger, 2007, Domenech *et al.*, 2006).

5.2 Biophysical Characterization of GSTdMT constructs

It was shown that both GSTαhdMT and GSTβhdMT were capable of Cd-binding and that the presence of GST does not inhibit interactions with the metal. As shown in Table 4.2 the average Cd²⁺ to protein molar ratio was 1.53 ± 0.6 for GSTβhdMT and 1.5 ± 0.8 for GSTαhdMT, when 0.1 mM Cd was included in the growth medium of the expression cultures and in the lysis buffer. With 0.3 mM Cd in the growth medium and lysis buffer, however, the Cd²⁺/ protein molar ratio was 3.78 for

GST β hdMT (single determination) and 2.1 ± 0.68 for GST α hdMT. Since Cd was included only at the very early stages of the purification procedure it can be concluded that all the determined metal is associated with the recombinant proteins and that the metal content of the constructs saturates only when it is present at several fold excess when the recombinant proteins are synthesized. Variable metal content was also observed with the single domain constructs from QsMT, however, because the oligomeric forms of the constructs are not well characterized it is not possible to make direct comparisons (Domenech *et al.*, 2006). Recently it was reported that recombinant *C. arietinum* MT1 could be purified with varying amounts of Cd²⁺ (3, 4 or 5 Cd²⁺/protein) (Schicht and Freisinger, 2008). It is noteworthy that this property is observed also with single domain constructs of dMT in fusion with GST and points to similarity between the GST-fusions and the native proteins.

T. durum type I MT was reported to coordinate 4 ± 1 Cd²⁺ in the presence of 0.05 mM CdSO₄ (Bilecen *et al.*, 2005).

GSTdMT constructs were characterized by UV-vis spectroscopy, a commonly used technique for the characterization of MTs. While the shoulder at 280 nm arising from aromatic residues of GST was observed in the spectra of all three constructs, the charge transfer bands at 250 nm, due to the bound Cd were observed only in GST β hdMT and GST α hdMT (Figure 4.35). Charge transfer bands have been observed in other plant MTs, such as *M. acuminata* MTIII and wheat seed MT (Freisinger, 2007, Peroza and Freisinger, 2007).

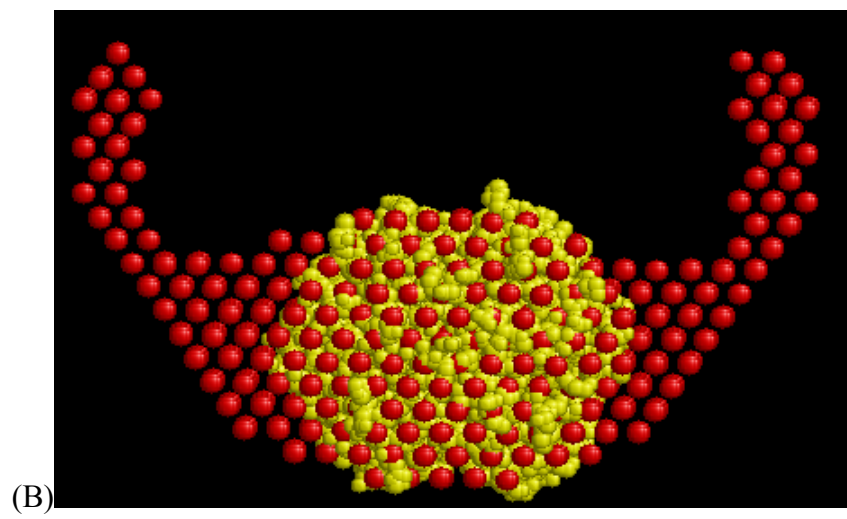
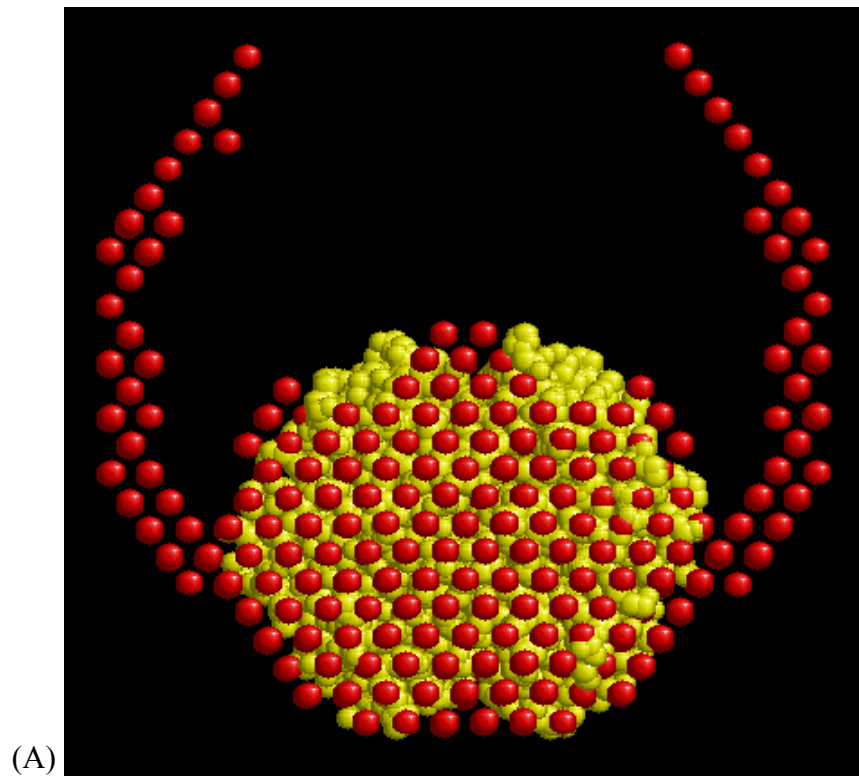
5.3 Structural Analysis of GSTdMT constructs

SAXS was used for determination of structural parameters and calculation of shape models for the GSTdMT constructs. X-ray scattering patterns and structural parameters are consistent with those expected from dimeric molecules. The experimental molecular masses were calculated from the excluded volume of the hydrated particle or Porod volume (Porod, 1982), which is computed from the shape of the scattering curve without model assumptions and independently of normalization. This procedure was used instead of calculation of the molecular mass relative to that of a reference protein (BSA or GST) because of the errors introduced by concentration

determinations. The molecular masses calculated were in agreement with the theoretical molecular masses of dimers of GSTdMT constructs (Table 4.3).

Shape models of the GSTdMT constructs were calculated from the scattering curves and results with P1 and P2 symmetry constraints were similar, which further confirmed the dimerization of the recombinant proteins. Models obtained for all constructs (Figure 4.48) could be interpreted in terms of the structure of the GST dimer and the dMT domain extensions at the C-termini of the GST molecules.

For all constructs central regions of the models represent the GST dimer and the domains of dMT appear as extensions from this central mass without any apparent contact points. Figure 5.1 A-C shows the fit of GST dimer structure (1GTA) to the calculated models. Comparison of the models highlights the structural features expected from each construct. In the model for GSThdMT (Figure 5.1 A) the exact overlap between the central region and the GST dimer (1GTA) shows the accuracy of the model. The thin extensions are the cause of the differences observed in the scattering patterns and the Dmax values for GST and GSThdMT. The superimposition of the GST dimer to the central regions of the models for GST β hdMT and GST α hdMT (Figure 5.1B and C respectively) reflect the fusion of larger masses to the dimer. The model for GST β hdMT in general gives more stubby extensions compared to GST α hdMT. The model for GST α hdMT also shows the extensions, however, wide regions connect the extensions to GST α hdMT.



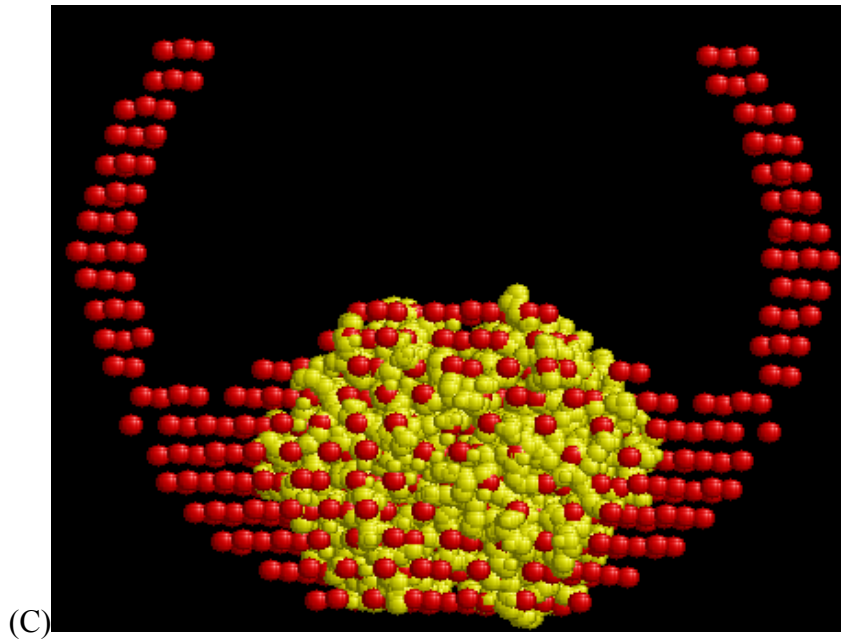


Figure 5.1: Superposition of GST dimer (1GTA) with (A) GSThdMT, (B) GSTβhdMT and (C) GSTαhdMT *ab initio* shape models. GST dimer (1GTA) is shown in yellow.

The models agree with the results from tryptic cleavage experiments given in section 4.6.2 GSThdMT and GSTαhdMT are first cleaved from the K47 in the center of the hinge region and then most probably from the R224 in GST C terminal. This showed that the hinge regions in the two constructs are available for tryptic cleavage due to an extended structure. These results are in agreement with the previous reports on susceptibility of plant MTs to proteolytic degradation (Kille *et al.*, 1991). The resistance of GSTβhdMT to tryptic cleavage, on the other hand, is in contrast to the behaviour observed with the other two constructs. It is in agreement with the SAXS models which show a compact structure. This compact structure impedes the approach of the trypsin molecule to the K47 cleavage site in the hinge region. This finding is further supported by the results of native PAGE analysis given in Figure 4.36. These results show that the mobility of GSTβhdMT is higher than that of GSTαhdMT and GSThdMT and this can be explained by a more compact structure.

SAXS measurements, low resolution by nature, do not allow for distinction of individual domains in the constructs. All models however point to an elongated shape for individual domains. Furthermore it appears that the hinge region folds into a more

compact structure in the presence of the β domain as compared to that observed in the presence of α domain. The extended structures of the individual domains point to an extended structure for the complete dMT. The observation that the individual domains bind Cd^{2+} may be used as evidence for a similar mechanism in the native dMT as suggested by Bilecen *et al.*, 2005. In other words the findings presented in this thesis also suggest a dumbbell shape with two metal binding domains separated by the hinge region. The real proof for this model, however, can only be obtained through usage of high resolution techniques such as NMR.

Chapter 6

6. CONCLUSION

Contrary to the extensive amount of information on mammalian MTs, structure- function investigations on plant MTs is limited in the literature. The structure of the metal binding domains and especially the structure of the long hinge region is largely unknown. The general aim of the work presented in this thesis was to investigate the role of the hinge region and the individual β hdMT and α hdMT domains in the overall folding and in metal binding of dMT. The findings and conclusions are summarized below:

- 1- Individual hinge, β - and α - domains of durum wheat Type I Metallothionein dMT can be synthesized as recombinant GST fusion constructs in E.coli. Biochemical and biophysical analyses show that each protein can be purified in dimeric form.
- 2- Recombinant GST β hdMT and GST α hdMT maintain metal binding properties and under the purification conditions given in this thesis it was shown that GST β hdMT and GST α hdMT bound 1.53 ± 0.6 and 1.5 ± 0.8 Cd²⁺ per protein respectively.
- 3- Preservation of metal binding property of the constructs indicates that interference of GST in the structure of the domains is minimum.

- 4- Evidence from the tryptic cleavage experiments shows that the hinge region in the GST α hdMT construct has a similar structure to that observed in the GST hdMT construct. In other words the presence of the α domain does not significantly influence folding of the hinge region. In both cases the hinge is readily accessible to protease attack. The hinge region in the GST β hdMT construct, on the other hand, has a different more compact structure which impedes protease action.
- 5- SAXS shape models confirm the above findings. Both GSThdMT and GST α hdMT appear as elongated extended structures. GST β hdMT models, in contrast show more compact extensions. Although the resolution of the present data does not allow clear distinction between the metal binding domains and the associated hinge regions it appears that the β hinge folds into a more compact structure. It may be speculated that the presence of the β domain has a stronger affect on the folding of the hinge region.
- 6- Extrapolating from the shape of the individual metal binding domains and the hinge region, it appears that the dMT molecule has an extended shape.

The results obtained from the analysis of *ab initio* models along with the limited tryptic cleavage are preliminary in nature. Based on these findings future work is needed for:

- Extending modelling work for GSTdMT constructs using the existing SAXS data for comparison with models for GSTdMT and dMT.
- Investigation of the structure of individual domains cleaved from GST with techniques that yield better resolution than SAXS. NMR measurements would be suitable for this purpose. These small structures can also be analyzed by CD for investigating the affect of metal binding on folding.
- Expression of β - and α - domains separately without the hinge to determine the effect of the hinge on the folding of separate domains.

- Expression of β - and α - domains in the absence of hinge to observe, if any, the contribution of hinge to overall folding of dMT.

Chapter 7

7. REFERENCES

1. Abdullah, S.N.A., Cheah, S.C., Murphy, D.J. (2002). Isolation and characterization of two divergent type 3 metallothioneins from the oil palm, *Elaeis guineensis*. *Plant Physiology and Biochemistry*, 40(3):255-263.
2. Akashi, K., Noriyuki, N., Ishida, Y., Yokota, A. (2004). Potent hydroxyl radical-scavenging activity of drought-induced type-2 metallothionein in wild water melon. *Biochemical and Biophysical Research Communications*, 323: 72-78.
3. Armitage, I. M. and Boulanger Y. (1983). Cadmium -113 NMR. *NMR Newly Accessible Nucl.*, 2: 337-365.
4. Arseniev, A., Schultze, P., Wörgötter, E., Braun, W., Wagner, G., Vasák, M., Kägi, J.H., Wüthrich, K. (1988). Three-dimensional structure of rabbit liver [Cd7]metallothionein-2a in aqueous solution determined by nuclear magnetic resonance. *Journal of Molecular Biology*, 201(3): 637-657.
5. Bilecen, K., Ozturk, U.H., Duru, A.D., Sutlu, T., Petoukhov, M., Svergun, D.I., Koch, M.H.J., Sezerman, U., Cakmak, I., and Sayers, Z. (2005). Triticum durum metallothionein. Isolation of the gene and structural characterization of the

- proteins using solution scattering and molecular modeling. *The Journal of Biological Chemistry*, 280(14): 13701-13711.
6. Binz, P.A. and Kagi, J. H.R. (2001). <http://www.biochem.unizh.ch/mtpage/html>.
 7. Binz, P.A. and Kagi, J.H.R. (1999). Metallothionein: molecular evolution and classification. In *Metallothionein*, vol. IV (ed. C. Klaassen), pp. 7-13. Basel: Birkhauser.
 8. Bertini, I., Hartmann, H.J., Klein, T., Liu, G., Luchinat, C., Weser, U. (2000). High resolution solution structure of the protein part of Cu7 metallothionein. *European Journal of Biochemistry*, 267: 1008-1018.
 9. Bogeat-Triboulot, MB., Brosche', M., Renaut, J., Jouve, L., Le Thiec, D., Fayyaz, P. (2007). Gradual soil waterdepletion results in irreversible changes of gene expression, protein profiles, ecophysiology, and growth performance in *Populus euphratica*, in arid regions. *Plant Physiology*, 143:876–92.
 10. Buchanan-Wollaston, V. (1994). Isolation of cDNA clones for genes that are expressed during leaf senescence in *Brassica napus*. *Plant Physiology*, 105: 839-846.
 11. Cai, B., Zheng, Q., Huang, Z.X., (2005). The properties of the metal-thiolate clusters in recombinant mouse metallothionein-4. *Protein J.*, 24: 327–336.
 12. Calderone, V., Dolderer, B., Hartmann, H.J., Echner, H., Luchinat, C., Del Bianco, C., Mangani, S., Weser, U. (2005). The crystal structure of yeast copper thionein: the solution of a long-lasting enigma. *Proc. Natl. Acad. Sci. USA*, 102 (1): 51-56.
 13. Capdevila, M., Cols, N., Romero-Isart, N., González-Duarte, R., Atrian, S., González-Duarte, P (1997). Recombinant synthesis of mouse Zn3-beta and Zn4-

alpha metallothionein 1 domains and characterization of their cadmium(II) binding capacity. *Cell Mol Life Sci.*, 53(8): 681-8.

14. Chan, J., Huang, Z., Watt, I., Kille, P., Stillman, M.J. (2007). Characterization of the conformational changes in recombinant human metallothioneins using ESI-MS and molecular modeling. *Can. J. Chem.*, 85:898–912.
15. Cherian, M.G., Howell, S.B., Imura, N., Klaassen, C.D., Koropatnick, J., Lazo, J.S., and Waalkes, M.P.(1994). Role of metallothionein in carcinogenesis. *Toxicol. Appl. Pharmacol*, 126:1-5.
16. Cherniak, M.L. & Huang, P.C. (1991) Differential effect of cysteine-to serine substitutions in metallothionein on cadmium resistance. *Proc. Natl Acad. Sci. USA*, 88: 3024-3028.
17. Choi, D., Kim, H.M., Yun, H.K., Park, J.A., Kim, W.T., Bok, S.H (1996). Molecular cloning of a metallothionein-like gene from *Nicotiana glutinosa* L. and its induction by wounding and tobacco mosaic virus infection. *Plant Physiology*, 112: 353-359.
18. Cismowski, M.J., Narula, S.S., Armitage, I.M., Cherniak, M.L. & Huang, P.C. (1991) Mutation of invariant cysteines of mammalian metallothionein alters metal binding capacity, cadmium resistance, and ¹¹³Cd NMR spectrum. *J. Biol. Chem.*, 266: 24390-24397.
19. Cobbett, C., Goldsbrough, P. (2002). Phytochelatins and metallothioneins: roles in heavy metal detoxification and homeostasis. *Annu Rev Plant Biology*, 53:159–182.
20. Cobine, P.A., McKay, R.T., Zangger, K., Dameron, C.T., Armitage, I.M. (2004). Solution structure of Cu₆ MT from the fungus *Neurospora crassa*. *Eur. J. Biochem*, 271: 4213-4221.

21. Cody, C.W. & Huang, P.C. (1993) Metallothionein detoxification function is impaired by replacement of both conserved lysines with glutamines in the hinge between the two domains. *Biochemistry*, 32: 5127-5131.
22. Cody, C.W. & Huang, P.C. (1994) Replacement of all a-domain lysines with glutamates reduces metallothionein detoxification function. *Biochem. Biophys. Res. Commun.*, 202: 954-959.
23. De Marco, A., Vigh, L., Diamant, S., Goloubinoff, P. (2005). Native folding of aggregation-prone recombinant proteins in *Escherichia coli* by osmolytes, plasmid- or benzyl alcohol-overexpressed molecular chaperones. *Cell Stress & Chaperones*, 10, 329-339
24. De Miranda J.R., Thomas M.A., Thurman D.A., Tomsett A.B. (1990). Metallothionein genes from the flowering plant *M.guttatus*. *FEBS Letters*, 260: 277-280.
25. Diamant, S., Rosenthal, D., Azem, A., Eliahu, N., Ben-Zvi, A.P., Goloubinoff, P. (2003). Dicarboxylic amino acids and glycine-betaine regulate chaperone-mediated protein disaggregation under stress. *Mol. Microbiol.*, 49:401–410.
26. Domènech, J., Mir, G., Huguet, G., Capdevila, M., Molinas, M., Atrian, S. (2006). Plant metallothionein domains: functional insight into physiological metal binding and protein folding. *Biochimie*, 88: 583-593.
27. Domènech, J., Orihuela, R., Mir, G., Molinas, M., Atrian, S., Capdevila, M. (2007). The Cd(II)-binding abilities of recombinant *Quercus suber* metallothionein: bridging the gap between phytochelatins and metallothioneins. *J. Biol. Inorg. Chem.*, 12(6): 867-82.
28. Domènech, J., Tinti, A., Capdevila, M., Atrian, S., Torreggiani, A. (2007). Structural study of the zinc and cadmium complexes of a type 2 plant (*Quercus suber*) metallothionein: insights by vibrational spectroscopy. *Biopolymers*, 86(3): 240-8.

29. Duncan, K.E.R., Stillman, M.J. (2006). Metal- dependent protein folding: Metallation of metallothionein. *Journal of Inorganic Biochemistry*, 100: 2101-2107.
30. Duncan, K.E.R., Stillman, M.J. (2007). Evidence for noncooperative metal binding to the α domain of human metallothionein. *FEBS Journal*, 274: 2253-2261.
31. Foley, R.C., Liang, Z.M., Singh, K.B. (1997). Analysis of type I metallothionein cDNAs in *Vicia faba*. *Plant Molecular Biology*, 33, 583-591.
32. Foley, R.C., Singh, K.B. (1994). Isolation of *Vicia faba* metallothionein –like gene: expression in foliar trichomes. *Plant Molecular Biology*, 26: 435-444.
33. Fowler, B.A., Hildebrand, C.E., Kojima, Y., Webb, M. (1987). Nomenclature of metallothionein. *Experientia Suppl*, 52:21.
34. Freisinger, E. (2007). Spectroscopic characterization of a fruit-specific metallothionein: *M. acuminata* MT3. *Inorganica Chimica Acta*, 360: 369–380.
35. Furey, W.F., Robbins, A.H., Clancy, L.L., Winge, D.R., Wang, B.C., Stout, C.D. (1986). Crystal structure of Cd,Zn metallothionein. *Science*, 231: 704-710.
36. Garcia-Hernandez, M., Murphy, A., and Taiz, L. (1998). Metallothioneins 1 and 2 have distinct but overlapping expression patterns in *Arabidopsis*. *Plant Physiology*, 118:387-397.
37. Gehrig, P.M., You, C., Dallinger, R., Gruber, C., Brouwer, M., Kagi, J.H.R., Hunziker, P.E. (2000). Electrospray ionization mass spectrometry of zinc, cadmium, and copper metallothioneins: evidence for metal-binding cooperativity. *Protein Sci.*, 9(2): 395-402.

38. Good, M., Hollenstein, R., Sadler, P.J., Vasak, M. (1988). 113 Cadmium NMR studies on metal-thiolate cluster formation in rabbit Cd(II)-metallothionein: evidence for a pH dependence. *Biochemistry*, 27: 7163–7166.
39. Guo, W.J., Bundithya, W., Goldsbrough, P.B. (2003). Characterization of the Arabidopsis metallothionein gene family: tissue-specific expression and induction during senescence and in response to copper. *New Phytologist*, 159: 369-381.
40. Hamer, DH. (1986). Metallothionein. *Annual Review of Biochemistry*, 55: 913–951.
41. Haq, F., Mahoney, M., Koropatnick, J. (2003). Signaling events for metallothionein induction. *Mutat. Res*, 533, 211–226.
42. Hidalgo, J., Aschner, M., Zatta, P., and Vasá'k, M. (2001). Roles of the metallothionein family of proteins in the central nervous system. *Brain Res. Bull.*, 55: 133–145.
43. Hozumi, I., Suzuki, J.S., Kanazawa, H., Hara, A., Saio, M., Inuzuka, T., Miyairi, S., Naganuma, A., Tohyama, C. (2008). Metallothionein-3 is expressed in the brain and various peripheral organs of the rat. *Neurosci Lett.*, 438(1): 54-8.
44. Hsieh, H.M., Liu, W.K., Chang, A., Huang, P.C. (1996). RNA expression patterns of a type 2 metallothionein-like gene from rice. *Plant Molecular Biology*, 32: 525–529.
45. Hsieh, H.M., Liu, W.K., Huang, P.C. (1995). A novel stress-inducible metallothionein-like gene from rice. *Plant Molecular Biology*, 28: 381–389.
46. Jin, S., Cheng, Y., Guan, Q., Liu, D., Takano, T., Liu, S.A. (2006). Metallothionein-like protein of rice (rgMT) functions in E. coli and its gene expression is induced by abiotic stresses. *Bio technolLett*, 28: 1749–53.

47. Kagi, J.H. and Kojima, Y. (1987). Chemistry and Biochemistry of metallothionein. *Experientia Suppl.*, 52: 25-61
48. Kagi, J. H. and Schaffer, A. (1988). Biochemistry of metallothionein. *Biochemistry*, 27: 8509-8515.
49. Kang, Y.J. (2006). Metallothionein redox cycle and function. *Exp. Biol. Med.*, 231: 1459–1467.
50. Kawashima, I., Kennedy, T.D., Chino, M., Lane, B.G. (1992). Wheat Ec metallothionein genes. *European Journal of Biochemistry*, 209: 971-976.
51. Kille, P., Winge, D.R., Harwood, J.L., Kay, J. (1991). A plant metallothionein produced in E.coli. *FEBS Letters*, 295: 171-175
52. Klaassen, C.D., Liu, J., Choudhuri, S. (1999). Metallothionein: an intracellular protein to protect against cadmium toxicity. *Annu. Rev. Pharmacol. Toxicol.*, 39: 267–294.
53. Koch, M.H., Vachette, P., Svergun, D.I. (2003). Small-angle scattering: a view on the properties, structures and structural changes of biological macromolecules in solution. *Q Rev Biophys.*, 36(2):147-227
54. Konarev, P. V., Volkov, V.V., Sokolova, A. V., Koch, M.H.J., Svergun, D. I. (2003). PRIMUS: a Windows PC-based system for small angle scattering data analysis. *Journal of Applied Crystallography*, 36: 1277-1282.
55. Konarev, P. V., Petoukhov, M. V., Volkov, V. V., Svergun, D. I. (2006). ATSAS 2.1, a program package for small-angle scattering data analysis. *J. Appl. Cryst.*, 39, 277-286.
56. Kojima, Y., Binz, P.A., Kägi, J.H.R. (1999). In: Klaassen C (ed) Metallothionein IV. Birkhäuser, Basel, pp 3-6.

57. Krezel, A., Maret, W. (2008). Thionein/metallothionein control Zn (II) availability and the activity of enzymes. *J. Biol. Inorg. Chem.*, 13: 401–409.
58. Lane, B., Kajioka, R., Kennedy, T. (1987). The wheat germ Ec protein is a zinc-containing metallothionein. *Biochemistry Cell Biology*, 65: 1001-1005.
59. Ledger, S.E., Gardner, R.C. (1994). Cloning and characterization of five cDNAs for genes differentially expressed during fruit development of kiwifruit (*Actinidia deliciosa* var. *deliciosa*). *Plant Molecular Biology*, 25: 877–886.
60. Lee, J., Shim, D., Song, W.Y., Hwang, I., Lee, Y. (2004). Arabidopsis metallothioneins 2a and 3 enhance resistance to cadmium when expressed in *Vicia faba* guard cells. *Plant Mol. Biol.*, 54: 805-815.
61. Leszczyszyn O., I., Schmid, R., Blindauer, C.A. (2007). Toward a property/function relationship for metallothioneins: Histidine coordination and unusual cluster composition in a zinc-metallothionein from plants. *Proteins*, 68: 922-935.
62. Liu, J.R., Suh, M.C., Choi, D. (2000). Phytoremediation of cadmium contamination: overexpression of metallothionein in transgenic tobacco plants. *Bunde Ges Gesu.*, 43(2): 126-130.
63. Margoshes, M., Vallee, B.L. (1957). A cadmium protein from equine kidney cortex. *J. Am. Chem. Soc.*, 79: 4813-4814.
64. Merrifield, M.E., Chaseley, J., Kille, P., Stillman, M. (2006). Determination of the Cd/S cluster stoichiometry in *Fucus vesiculosus* metallothionein. *J. Chem. Res. Toxicol.*, 19:365-375.
65. Messerle, B. A., Schäffer, A., Vasak, M., Kägi, J. H. R., Wüthrich, K. (1990). Three-dimensional structure of human [113Cd7]metallothionein-2 in solution determined by nuclear magnetic resonance spectroscopy. *Journal of Molecular Biology*, 214 (3): 765-769.

66. Miles, A. T., Hawksworth, G. M., Beattie, J. H., and Rodilla, V. (2000). Induction, regulation, degradation, and biological significance of mammalian metallothioneins. *Crit. Rev. Biochem. Mol. Biol.*, 35: 35–70
67. Mocchegiani, E. (2004). Zinc, immune plasticity, aging, and successful aging: role of metallothionein. *Ann. N. Y. Acad. Sci.*, 1019: 127–134.
68. Murphy, A., Taiz, L. (1995). Comparison of metallothionein gene expression and nonprotein thiols in ten *Arabidopsis* ecotypes. Correlation with copper tolerance. *Plant Physiol.*, 109(3): 945-54.
69. Murphy, A., Zhou, J.M., Goldsbrough, P.B., Taiz, L. (1997). Purification and immunological identification of metallothioneins 1 and 2 from *Arabidopsis thaliana*. *Plant Physiology*, 113: 1293-1301.
70. Narula, S.S., Brouwer, M., Hua, Y., Armitage, I.M. (1995). Three-dimensional solution structure of *Callinectes sapidus* metallothionein-1 determined by homonuclear and heteronuclear magnetic resonance spectroscopy. *Biochemistry*, 34: 620-631.
71. Navabpour, S., Morris, K., Allen, R., Harrison, E., A-H-Mackerness, S., Buchanon Wollaston, V. (2003). Expression of Senescence Enhanced Genes in Response to Oxidative stress. *Journal of Experimental Botany*, 54(391):2285-2292.
72. Nemer, M., Wilkinson, D.G., Travaglini, E.C., Sternberg, E.J. and Butt, T.R. (1985). Sea urchin metallothionein sequence: key to an evolutionary diversity *Proc.Natl Acad. Sci.*, 82: 4992-4994.
73. Nettesheim, D.G., Engeseth, H.R., Otvos, J.D. (1985). Products of metal exchange reactions of metallothionein. *Biochemistry*, 24: 6744-51.
74. Nordberg M. & Kojima Y. (1979). *Experientia. Suppl.* 34, 48-55

75. Okumura, N., Nishizawa, N.K., Umehara, Y., Mori, S. (1991). An iron deficiency-specific cDNA from barley roots having two homologous cysteine-rich MT domains. *Plant Mol. Biol.*, 17: 531–533.
76. Otvos, J.D., Armitage, I.M.(1980). Structure of the metal clusters in rabbit liver metallothionein. *Proc. Natl. Acad. Sci.*, 77:7094–7098.
77. Palmiter, R. D. (1998). The elusive function of metallothionein. *Proc. Natl. Acad. Sci.*, 95: 8428–8430
78. Palmiter, R. D. (1987) Molecular biology of metallothionein gene expression. *Experientia Suppl.*, 52: 63–80.
79. Penkowa, M. (2006). Metallothioneins are multipurpose neuroprotectants during brain pathology. *FEBS Journal*, 273: 1857–1870.
80. Peroza, E., Freisinger, E. (2007). Metal ion binding properties of Tricium aestivum Ec-1 metallothionein: evidence supporting two separate metal thiolate clusters. *J. Biol. Inorg. Chem.*, 12: 377–391.
81. Peterson, C.W., Narula, S.S., Armitage, I.M.(1996). 3D solution structure of copper and silver-substituted yeast metallothioneins. *FEBS Lett.*, 379: 89-93.
82. Porod, G. (1982) in *Small-angle X-ray Scattering* (Glatter, O., and Kratky, O., eds) pp. 17–51, Academic Press, London.
83. Rauser, W.E. (1999). Structure and function of metal chelators produced by plants: the case for organic acids, amino acids, phytin and metallothioneins. *Cell Biochem Biophysics*, 31: 19–48.
84. Richards, M.. (1989). Recent developments in trace element metabolism and function: role of metallothionein in copper and zinc metabolism. *J. Nutr.*, 19:1062–1070.

85. Riek, R., Precheur, B., Wang, Y., MacKay, E.A., Wider, G., Güntert, P., Liu, A., Kägi, J.H.R., Wütrich, K. (1999). NMR structure of the sea urchin (*Strongylocentrotus purpuratus*) metallothionein MTA. *Journal of Molecular Biology*, 291: 417-428.
86. Robbins, A. H., McRee, D. E., Williamson, M., Collett, S. A., Xuong, N. H., Furey, W. F., Wang, B. C., Stout, C. D. (1991). Refined crystal structure of Cd, Zn metallothionein at 2.0 Å resolution. *Journal of Molecular Biology*, 221 (4): 1269-93.
87. Romero-Isart, N., Vasak, M. (2002). Advances in the structure and chemistry of metallothioneins. *J. Inorg Biochem.*, 88 (3-4): 388-96.
88. Salgado, M.T., Stillman, M.J. (2004). Cu⁺ distribution in metallothionein fragments. Cu⁺ distribution in metallothionein fragments. *Biochem. Biophys. Res. Commun.*, 318(1): 73-80.
89. Sambrook, J., Manniatis, T., Fritsh, E.F., (1989). *Molecular cloning; A laboratory manual*. Cold Spring Harbor Laboratory Press. 2nd edition.
90. Schicht, O., Freisinger, E. (2009). Spectroscopic characterization of *Cicer arietinum* metallothionein 1. *Inorganica Chimica Acta*, in press.
91. Schroedel, A., de Marco, A. (2005). Characterization of the aggregates formed during recombinant protein expression in bacteria. *BMC Biochem.*, 31: 6-10.
92. Schultze, P., Wörgötter, E., Braun, W., Wagner, G., Vasak, M., Kägi, J. H. R.; Wü thrich, K. (1988). Conformation of [Cd⁷⁵]-metallothionein-2 from rat liver in aqueous solution determined by nuclear magnetic resonance spectroscopy. *Journal of Molecular Biology*, 203(1): 251-68.
93. Snowden, K.C. and Gardner, R.C.(1993). Five genes induced by aluminum in wheat (*Triticum aestivum* L.) roots. *Plant Physiology*, 103: 855-861.

94. Stillman, M.J. (1995). Metallothioneins. *Coord. Chem. Rev.*, 144: 461-511
95. Stillman, M.J., Thomas, D., Trevithick, C., Guo, X., Siu, M. (2000). Circular dichroism, kinetic and mass spectrometric studies of copper(I) and mercury(II) binding to metallothionein. *J. Inorg. Biochem.*, 79 (1-4): 11-9.
96. Street, N.R., Skogström, O., Sjödin, A., Tucker, J., Rodríguez-Acosta, M., Nilsson, P.(2006). The genetics and genomics of the drought response in *Populus*. *Plant J.*, 48: 321–41.
97. Sutherland, D.E.K., Stillman, M.J. (2008). Noncooperative cadmium (II) binding to human metallothionein 1a. *Biochemical and Biophysical Research Communications*, 372: 840-844.
98. Svergun, D.I. and Koch, M.H.J. (2003). Small-angle scattering studies of biological macromolecules in solution. *Rep. Prog. Phys.*, 66:1735–1782.
99. Svergun, D.I. and Koch, M.H.J. (2002). Advances in structure analysis using small-angle scattering in solution. *Cur. Opin. Struct. Biol.*, 12: 654-660
100. Tommey, A.M., Shi, J.G., Lindsay, W.P., Urwin, P.E., Robinson, N.J. (1991). Expression of the pea gene PsMTA. *E.coli*: Metal binding properties of the expressed protein. *FEBS Letters*, 292: 48-52.
101. Uchida, Y., Takio, K., Titani, K., Ihara, Y., and Tomonaga, M. (1991). The growth inhibitory factor that is deficient in the Alzheimer's disease brain is a 68 amino acid metallothionein-like protein. *Neuro.*, 7: 337-347.
102. Van Hoof, N.A., Hassinen, V.H., Hakvoort, H.W., Ballintijn, K.F., Schat, H., Verkleij, J.A., Ernst, W.H., Karenlampi, S.O., Tervahauta, A.I. (2001). Enhanced copper tolerance in *Silene vulgaris* (Moench) Garcke populations from copper mines is associated with increased transcript levels of a 2b-type metallothionein gene. *Plant Physiol.*, 126(4): 1519-26.

103. Vasak, M., Kägi, J.H.R. (1981). Metal thiolate clusters in cobalt (II)-metallothionein. *Proc. Natl. Acad. Sci.*, 78: 6709-6713.
104. Vasak, M., Kägi, J.H.R. (1994). In: Metallothioneins Encyclopedia of Inorganic Chemistry (King, R.B.,Ed.) 4:2229-2241, *J.Wiley and Sons*, New York.
105. Vasak, M. (2005). Advances in metallothionein structure and functions. *Journal of Trace Elements in Medicine and Biology*, 19: 13-17
106. Vasak, M., Hasler, D.W. (2000). Metallothioneins: new functional and structural insights. *Current Opinion in Chemical Biology*, 4: 177-183.
107. Wang, Y.C., Mackay, E.A., Zerbe, O., Hess, D., Hunziker, P.E., Vasak, M., Kägi, J. (1995). Characterization and sequential localization of the metal clusters in sea urchin metallothionein. *Biochemistry*, 34: 7460-7467.
108. White, C.N., Rivin, C.J. (1995). Characterization and expression of a cDNA encoding a seed-specific metallothionein in maize. *Plant Physiology*, 108: 831-832.
109. Willner, H., Vasak, M., Kägi, J.H.R. (1987). Cadmium-thiolate clusters in metallothionein: spectrophotometric and spectropolarimetric features. *Biochemistry*, 26: 6287-6292.
110. Winge, D.R., Miklossy, K.A. (1982). Domain nature of metallothionein. *J. Biol. Chem.*, 257(7): 3471-6.
111. Wong, H.L., Sakamoto, T., Kawasaki, T., Umemura, K., Shimamoto, K. (2004). Down-regulation of metallothionein, a reactive oxygen scavenger, by the small GTPase OsRac1 in rice. *Plant Physiology*, 135: 1447-1456.
112. Yesilirmak, F. (2008). Biophysical and Functional Characterization of Wheat Metallothionein at Molecular Level. P.hD. Thesis, Sabanci University

113. Yu, L.H., Umeda, M., Liu, J.Y., Zhao, N.M., Uchimiya, H. (1998). A novel MT gene of rice plants is strongly expressed in the node portion of the stem. *Gene*, 206: 29-35.
114. Zangger, K., Öz, G., Otvos, J. D., Armitage, I. M. (1999). Three-dimensional solution structure of mouse [Cd7]-metallothionein-1 by homonuclear and heteronuclear NMR spectroscopy. *Protein Sci.*, 8: 2630-8.
115. Zhan, Y., Song, X., Zhou, G.W. (2001). Structural analysis of regulatory protein domains using GST-fusion proteins. *Gene*, 281:1-9.
116. Zhou, J.M., Goldsbrough, P.B. (1994). Functional homologs of fungal metallothionein genes from Arabidopsis. *Plant Cell*, 6: 875–884.
117. Zhou, J.M., Goldsbrough P.B. (1995). Structure, organization and expression of the metallothionein gene family in Arabidopsis. *Molecular and General Genetics*, 248: 318-328.
118. Zhou, G.K., Xu, Y.F. and Liu, J.Y. (2005). Characterization of a rice class II metallothionein gene: Tissue expression patterns and induction inresponse to abiotic factors. *J.Plant Physiol*, 162: 686-696.
119. Zhu, C., Lü, T., Zhang, R., Zhao, N., Liu, J. (2000). Modeling of kiwi fruit metallothionein kiwi503. *Chinese Science Bulletin*, 45: 1413-1417.
120. Zimeri, A. M., Dhanker, O.P., McCaig, B., Meagher, R.B. (2005). The plant MT1 metallothioneins are stabilized by binding cadmium and are required for cadmium tolerance and accumulation. *Plant Molecular Biology*, 58: 839-855.

APPENDIX A

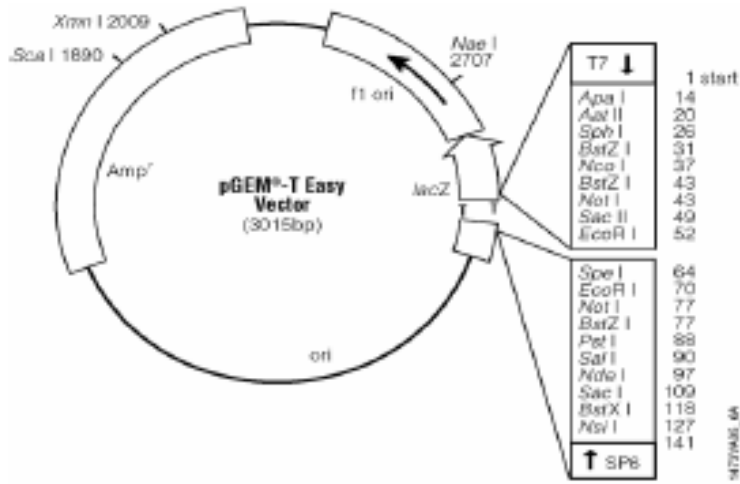
CHEMICALS

Acetic acid (glacial)	Riedel-de Häen, Germany	27225
30% Acrylamide-0.8% Biacrylamide	Sigma, Germany	A3699
Albumin (bovine serum)	Sigma, Germany	A7906
Bromophenol blue	Applichem, Germany	A3640
1-Butanol	Merck, Germany	100988
Cadmium (II) sulphate	Fluka, Switzerland	20920
Chloroform	Amresco, USA	3566B066
Coomassie Brilliant Blue R-250	Fluka, Switzerland	27816
Complete Protease Inhibitor	Roche	11 836 145 001
Cocktail Tablets		
DNaseI	Fermentas	EN0521
dNTP mix	Fermentas	R0241
1,4-Dithiothreitol	Fluka, Switzerland	43815
DryEase mini cellophane	Invitrogen, Germany	NC2380
<i>EcoRI</i>	Fermentas	ER0271
Ethanol	Riedel-de Häen, Germany	32221
Ethylenediaminetetraaceticacid	Riedel-de Häen, Germany	27248
Glycerol (87%)	Riedel-de Häen, Germany	15523
Glycine	Amresco, USA	0167
HEPES	Fluka	54461
Hybond-P PVDF membranes	GE-Healthcare, USA	RPN2020F
Hydrochloric acid (37%)	Merck, Germany	100314
IPTG	Fermentas	R0392
MassRuler DNA Ladder Mix	Fermentas	SM0403
MassRuler DNA Ladder Low Range	Fermentas	SM0383
2-Mercaptoethanol	Aldrich, Germany	M370-1
Methanol	Riedel-de Häen, Germany	24229

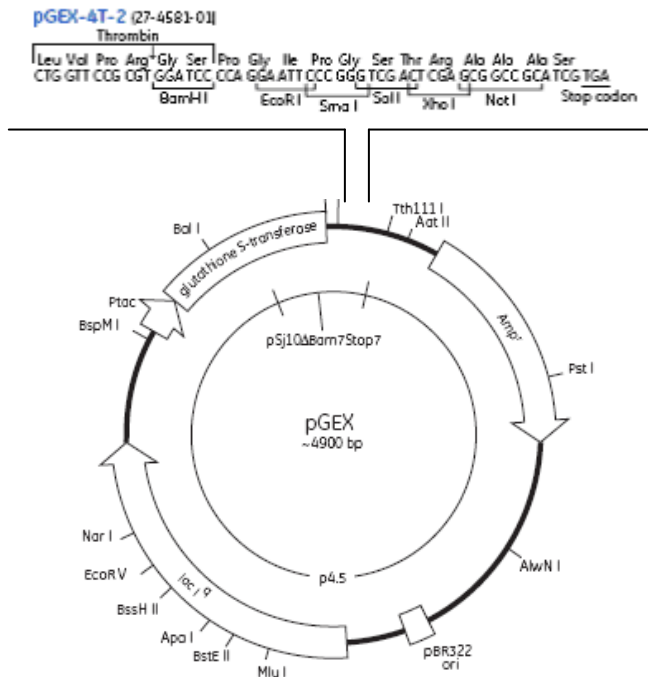
PageRuler protein ladder	Fermentas, Germany	SM0661
Phenylmethylsulphonylfluoride	Amresco, USA	0754
Prestained protein MW marker	Fermentas, Germany	SM0441
2-Propanol	Merck, Germany	100996
Protein Prestained Ladder	Fermentas	SM0671
Protein Molecular Weight Marker	Fermentas	SM0431
Reduced Glutathione	Merck	K33271590522
Silver staining plus kit	BioRad	161-0449
Sodium chloride	Riedel-de Häen, Germany	13423
Sodium dodecyl sulphate	Sigma, Germany	L-4390
T4 DNA ligase	Fermentas	EL0016
Taq polymerase	Fermentas	EP0401
Tetramethylethylenediamine	Sigma, Germany	T-7029
Thrombin	GE-Healthcare, Sweden	27-0846-01
Tris	Fluka, Switzerland	93349
Triton X-100	Applichem, Germany	A1388
DYEnamic™ ET Dye Terminator Kit	GE Healthcare, USA	US81090

APPENDIX B

A1. pGEMTeasy vector map with restriction enzyme sites



A2. pGEX-4T-2 vector map and multicloning site with available restriction enzyme sites



APPENDIX C

BUFFERS AND SOLUTIONS

Tris Borate EDTA Buffer (TBE) (5X): 54g Tris base, 27.5g Boric Acid, 20ml 0.5 M EDTA pH 8.0, completed to 500ml.

Tris Acetate EDTA Buffer (TAE) (50X): 121.1g Tris base, 28.55ml Glacial Acetic acid, 7.3g EDTA, completed to 500ml.

10 X Tris EDTA (TE) Buffer: 0.1M Tris-HCl, 10mM EDTA, pH adjusted to 7.5.

2x SDS Sample Buffer: 4% (w/v) SDS, 20% (v/v) Glycerol, 0.004% (w/v) Bromophenol blue, 10% (v/v) 2-mercaptoethanol, 0.125M Tris-HCl, pH 6.8 in ddH₂O.

2x Native Sample Buffer: 200mM Tris-HCl pH 7.5, 20% (v/v) Glycerol, 0.05% (w/v) Bromophenol blue in ddH₂O.

SDS-PAGE Running Buffer: 25mM Tris, 192mM Glycine, 0.1% (w/v) SDS in ddH₂O.

Native-PAGE Running Buffer: 25mM Tris, 192mM Glycine in ddH₂O.

Coomassie Staining Solution: 0.1% (w/v) Coomassie Brilliant Blue R-250, 40% (v/v) Methanol, 10% (v/v) Acetic acid in ddH₂O.

Destaining Solution: 4 % (v/v) Methanol, 7.5 % (v/v) Acetic acid completed to 1L.

Transfer Buffer: 96 mM Glycine, 12 mM Tris-base, and 20% Methanol in ddH₂O.

Blocking Solution: 5% Non-fat dry milk, in PBS-T (80 mM Na₂HPO₄, 20 mM NaH₂PO₄, 100 mM NaCl, 0.2% Tween-20, pH 7.4).

APPENDIX D

EQUIPMENTS

AKTA FPLC:	GE-Healthcare, SWEDEN
Autoclave:	Hirayama, Hiclave HV-110, JAPAN Certoclav, Table Top Autoclave CV-EL-12L, AUSTRIA
Balance:	Sartorius, BP211D, GERMANY Sartorius, BP221S, GERMANY Sartorius, BP610, GERMANY Schimadzu, Libror EB-3200 HU, JAPAN
Centrifuge:	Eppendorf, 5415C, GERMANY Eppendorf, 5415D, GERMANY Eppendorf, 5415R, GERMANY Kendro Lab. Prod., Heraeus Multifuge 3L, GERMANY Hitachi, Sorvall RC5C Plus, USA Hitachi, Sorvall Discovery 100 SE, USA
Dynamic Light Scattering:	Malvern, Zetasizer Nano-ZS, UK
Deepfreeze:	-80°C, Kendro Lab. Prod., Heraeus Hfu486, GERMANY -20°C, Bosch, TURKEY
Distilled Water:	Millipore, Elix-S, FRANCE Millipore, MilliQ Academic, FRANCE
Electrophoresis:	Biogen Inc., USA Biorad Inc., USA
Gel Documentation:	UVITEC, UVIdoc Gel Documentation System, UK Biorad, UV-Transilluminator 2000, USA
Ice Machine:	Scotsman Inc., AF20, USA

ICP-OES:	Varian, Vista-Pro CCD, AUSTRALIA
Incubator:	Memmert, Modell 300, GERMANY Memmert, Modell 600, GERMANY
Laminar Flow:	Kendro Lab. Prod., Heraeus, HeraSafe HS12, GERMANY
Magnetic Stirrer:	VELP Scientifica, ARE Heating Magnetic Stirrer, ITALY VELP Scientifica, Microstirrer, ITALY
Microliter Pipette:	Gilson, Pipetman, FRANCE Mettler Toledo, Volumate, USA
Microwave Oven:	Bosch, TURKEY
pH meter:	WTW, pH540 GLP MultiCal®, GERMANY
Power Supply:	Biorad, PowerPac 300, USA Wealtec, Elite 300, USA
Refrigerator:	+4°C, Bosch, TURKEY
Shaker:	Forma Scientific, Orbital Shaker 4520, USA GFL, Shaker 3011, USA New Brunswick Sci., Innova™ 4330, USA
Sonicator:	BioBlock Scientific, Vibracell 7504, FRANCE
Spectrophotometer:	Schimadzu, UV-1208, JAPAN Schimadzu, UV-3150, JAPAN Secoman, Anthelie Advanced, ITALY Nanodrop, ND-1000, USA.
Speed Vacuum:	Savant, Speed Vac® Plus Sc100A, USA Savant, Refrigerated Vapor Trap RVT 400, USA
Thermocycler:	Eppendorf, Mastercycler Gradient, GERMANY
Vacuum:	Heto, MasterJet Sue 300Q, DENMARK
Water bath:	Huber, Polystat cc1, GERMANY